



Available online at [www.sciencedirect.com](http://www.sciencedirect.com)

**ScienceDirect**

Energy Procedia 105 (2017) 4499 – 4512

Energy  
**Procedia**

The 8<sup>th</sup> International Conference on Applied Energy – ICAE2016

## **Effectiveness of CO<sub>2</sub> capture by calcium looping with regenerated calcium sorbents – last step calcination.**

Halina Pawlak-Kruczek<sup>a</sup>, Marcin Baranowski<sup>a</sup>,

*Mechanical Power Engineering Faculty, Wrocław University of Technology, W.Wyspianskiego 27, 50-370 Wrocław, PL*

### **Abstract**

The Ca looping process offers many advantages over the other CO<sub>2</sub> capture technologies, such as a relatively small decrease in power plant efficiency and a potential for further reduction. However, calcium sorbents in the consecutive cycles of adsorption and regeneration by calcination undergo deactivation, which is a considerable drawback of this technology. The depletion of sorbent reactivity is due to sintering, which causes changes in the sorbent's porous and crystal structure, whereby its reacting surface area decreases.

The approaches to reducing sorbent deactivation (sorption capacity loss) include thermal preactivation, reactivation by hydration and/or the production of synthetic sorbents and doping.

This paper studies three methods of regenerating deactivated sorbents. The sorbents underwent deactivation after working in the calcium looping of 10 calcination/carbonation cycles at respectively 900°C and 650°C. The first regeneration method consisted in hydration with water in controlled time and temperature conditions. The second regeneration method consisted in hydration with steam in controlled time and temperature conditions. The third method – 2-stage regeneration – besides water or steam hydration, included a second stage consisting in the controlled exposition of the sorbent to a CO<sub>2</sub> enriched atmosphere. In all the methods the regeneration of the spent sorbent was conducted after the final calcination process. After regeneration the sorbent was subjected to 24 calcination/carbonation cycles in similar conditions as before regeneration.

This study compares the three methods of regeneration in terms of the CO<sub>2</sub> capture efficiency of the regenerated sorbent. The sorbents collected after the looping tests and after each regeneration step were analysed by mercury porosimetry, X-ray diffraction and scanning electron microscopy to determine the interdependences between the sorbents' physicochemical properties and their CO<sub>2</sub> capture capacity.

The investigations showed that: 1) an improvement in CO<sub>2</sub> capture capacity in the calcium looping process was achieved by applying both water/steam hydration and 2-stage regeneration after 10 calcination/carbonation cycles), 2) the size of CaO crystallites increased during looping cycles and decreased as a result of the 2-stage regeneration, 3) the sorbent's pore and particle structure showed significant changes after the reactivation, which may explain the increase in its CO<sub>2</sub> capture capacity.

The regeneration and CO<sub>2</sub> sorption capacity of deactivated sorbent can be effected by radically changing the process temperature and simultaneously feeding saturated steam and then washing the sorbent with a gas with a high CO<sub>2</sub> content. The novelty of this idea consists in the fact that the desired

regeneration effects can be achieved by changing the regeneration parameters and only slight modifying the structure of the regenerators.

© 2017 Published by Elsevier Ltd. This is an open access article under the CC BY-NC-ND license (<http://creativecommons.org/licenses/by-nc-nd/4.0/>).

Peer-review under responsibility of the scientific committee of the 8th International Conference on Applied Energy.

**Keywords:** Calcium looping, regeneration, CO<sub>2</sub> capture

## Introduction

The calcium looping process is one of the promising CO<sub>2</sub> capture technologies based on cyclic calcination/carbonation reactions using calcium-based sorbents. Although the process is viable, CaO is a sorbent with a high, but limited CO<sub>2</sub> capture capacity. Furthermore, the CO<sub>2</sub> capture capacity of raw limestone rapidly decreases with each cycle of conversion, as reported by many authors [1, 2, 3, 4, 5, 6, and 7]. This is usually due to sintering accompanied by changes in the sorbent structure, including its porosity and the size of its crystallites [8-12].

The deactivation of the sorbent during multicycle Ca-looping results in reaction rates too low for a reasonably sized reactor because of the very large quantities of CaO needed for CO<sub>2</sub> removal.

An attractive alternative (from both the environmental and economic points of view) is the regeneration of CO<sub>2</sub> capture capacity by the water or steam hydration induced reactivation of the spent sorbent [10, 13]. The hydration induced reactivation of spent sorbents from calcium looping processes is a largely unexplored research topic which deserves investigation. The key issues involved are the changes in the sorbent physicochemical properties induced by hydration, the regeneration of CO<sub>2</sub> capture capacity, the influence of sorbent regeneration on the attrition tendency of the material once reused in the looping cycle. Nevertheless, the feasibility of the large-scale application of the hydration process to calcium looping has been demonstrated by Prof. Fan's team [14, 15] at the Ohio State University, who in their 120 kW facility used flue gas from coal combustion.

Various reactivation approaches have been tried to regenerate sorbent capacity for cyclic CO<sub>2</sub> capture. The approaches include: steam/water hydration or addition, thermal pre-treatment, using innovative sorbent precursors, doping, and incorporation with an inert matrix. The above reactivation schemes were comprehensively reviewed by Yu et al. [16].

Generally, steam is applied in three different ways: steam addition during carbonation [9, 17–23] steam addition during calcination, [24–28] and separate hydration after calcination. [10, 19, 29–31]. Steam addition during carbonation and/or calcination has different effects depending the sorbents and the conditions. In the case of severely sintered spent sorbents steam enhances solid-state diffusion in the slow diffusion-control reaction regime [17, 18], whereby it improves carbonation conversion. Also steam addition during calcination has been proven capable of enhancing the subsequent carbonation conversion [24, 25, 27, 28]. After calcination, steam can be easily separated by condensation, whereby a concentrated CO<sub>2</sub> stream is obtained. However, steam may promote sorbent sintering during the calcination process [26]. Therefore, the effect of steam on calcium sorbent reactivation during calcination needs to be investigated further.

Separate hydration after calcination at different temperatures, with excellent reactivation performance, has already been confirmed as a promising approach to regenerate the capture capacity and pore structure of the spent CaO-based sorbent [24, 29, 30]. The surface area and porosity of the sorbent were remarkably recovered by the hydration-dehydration process, i.e., CaO → Ca(OH)<sub>2</sub> → CaO. An enhanced cyclic CO<sub>2</sub> capture capacity of hydroxide-derived CaO, in comparison with carbonate-derived CaO, was reported by Wu et al. [10]. The reactivity of the spent sorbents was recovered from 20% to 65-

80% after hydration, but then the sorbent would rapidly deactivate in the subsequent cycles. A similar hydration performance is reported by Manovic and Anthony [29].

The effect of separate steam hydration is still temporary for multiple CO<sub>2</sub> capture cycles: sorbent reactivity decreases rapidly with an increasing number of cycles after hydration [10, 29]. From the practical point of view, the durability of the sorbent is much more important than its single-cycle reactivity. Therefore, more investigations should be dedicated to the maintenance of the durability of the CaO-based sorbent in cyclic carbonation/ calcination.

The optimal management of the Ca-looping cycle implies the continuous addition of fresh limestone in order to compensate for the deactivation and attrition of the spent sorbent. The landfilling of spent limestone is problematic because of the CaO-rich composition of this residue [32, 33]. The potential of the spent sorbent from Ca-looping as a source of raw material in cement manufacture is under investigation [13]. An attractive alternative (from both the environmental and economic points of view) is the regeneration of CO<sub>2</sub> capture capacity by the hydration induced reactivation of the spent sorbent [10, 13]. This process is based on CaO conversion to Ca(OH)<sub>2</sub>, which results in an increase in molar volume from 16.9 cm<sup>3</sup> mol<sup>-1</sup> (CaO) to 33.7 cm<sup>3</sup> mol<sup>-1</sup> (Ca(OH)<sub>2</sub>) and in a decrease in density from 3.32 g cm<sup>-3</sup> (CaO) to 2.20 g cm<sup>-3</sup> (Ca(OH)<sub>2</sub>). The swelling of CaO due to hydration is followed by the dehydration of Ca(OH)<sub>2</sub> as the reactivated material is re-injected into the calciner or carbonator. The resulting material (particularly CaO) is characterized by a large specific surface area and high porosity and so it is highly reactive towards acid gases (CO<sub>2</sub>/SO<sub>2</sub>). Hydration may also result in increased propensity of the reactivated material to attrition, but to date only a few results have been reported on this topic [34]. Typically, the spent CaO-rich sorbent retrieved from a calciner is hydrated without the limiting effect of the presence of the hard CaCO<sub>3</sub> shell. Eventually, the reactivated sorbent is re-injected into the carbonator, with a twofold benefit: the Ca(OH)<sub>2</sub> endothermic dehydration reaction occurs in parallel with exothermic carbonation and feeding the sorbent into the carbonator prevents attrition resulting from fast dehydration and sintering promoted by high temperatures which would otherwise predominate in the carbonator. Furthermore, the steam released during dehydration can have a positive effect on the concurrent, if any, SO<sub>2</sub> capture from the flue gas in the carbonator. As part of the present research, spent sorbents retrieved from calcination and carbonation cycles, and so CaO rich, would be regenerated and then re-injected into the calciner or carbonator.

The primary objective of this research was to investigate the influence of separate water and steam hydration after final calcination on the cyclic carbonation/calcination performance and durability of the CaO-based sorbent. Also a new two-stage regeneration method, consisting in hydration followed by feeding flue gas enriched with CO<sub>2</sub> at a temperature of 40–150°C, was studied.

The sorbent CO<sub>2</sub> capture capacity of each cycle was measured using a modified thermogravimetric analyser (TGA). Moreover, the morphology of the spent sorbent and that of the regenerated sorbent was examined using a special 3-stage tube reactor.

Finally, the effects of the reactivation methods on the CO<sub>2</sub> capture capacity, phase composition and size distribution of the regenerated sorbent were compared.

## Experimental

### 2.1. Samples

The raw sorbents used in this research were the German and Italian high-calcium limestone (EnBW, Xirorema) and the Polish high and relatively low calcium limestone (Tarnow Opolski and Czatkowice). Chemical analyses was performed using an XRF spectrometer. The chemical composition and mineralogical analysis of the samples are presented in tables 1 and 2 [35].

Table 1 Chemical composition.

Description	SiO <sub>2</sub>	Al <sub>2</sub> O <sub>3</sub>	Fe <sub>2</sub> O <sub>3</sub>	CaO	MgO	K <sub>2</sub> O	Na <sub>2</sub> O	TiO <sub>2</sub>
Tarnow Opolski	1.73	0.34	0.39	54.04	0.94	0.00	0.02	0.02
Czatkowice, Pl	3.91	0.39	0.31	52.88	0.99	0.00	0.02	0.03
EnBW	0.298	0.13	0.08	56.01	0.26	0.00	0.02	0.01
Xirorema Sand	0.83	0.26	0.36	55.13	0.56	0.00	0.01	0.02

The Czatkowice sample is the most “impure”, with an SiO<sub>2</sub> content exceeding 3.5%. The EnBW sample is the most pure calcareous sample with a minimal SiO<sub>2</sub> and MgO content

Table 2. Mineralogical analysis.

Description	Calcite (CaCO <sub>3</sub> )	Quartz (SiO <sub>2</sub> )	Dolomite (MgCa(CO <sub>3</sub> ) <sub>2</sub> )	Illite*	Chlinochlore **
Tarnow Opolski	93.9	2.7	3.4	—	—
Czatkowice, Pl	97.0	2.4	0.2	0.3	0.1
EnBW	99.2	0.3	0.5	—	—
Xirorema	3.9	0.5	95.6	—	0,1

\*Illite: (K<sub>0.6</sub>(H<sub>3</sub>O)<sub>0.4</sub>Al<sub>1.3</sub>Mg<sub>0.3</sub>Fe<sup>2+</sup><sub>0.1</sub>Si<sub>3.5</sub>O<sub>10</sub>(OH)<sub>2</sub>·(H<sub>2</sub>O)).

\*\* Chlinochlore: ((Mg,Fe<sup>2+</sup>)<sub>5</sub>Al(Si<sub>3</sub>Al)O<sub>10</sub>(OH)<sub>8</sub>).

## 2.2. Investigative apparatus and procedure.

The aim of this work was to demonstrate the potential of water/steam hydration as a means of reactivating the spent limestone-based sorbents used in the looping process for CO<sub>2</sub> capture. Spent sorbent regeneration by water at 95–100°C and by two other methods, namely either the online steam regeneration or 2-stage regeneration of the spent sorbent by steam hydration and then feeding gas with a high CO<sub>2</sub> concentration, was investigated using the TG apparatus. In addition, the online regeneration of the spent sorbent by steam hydration and steam hydration followed by feeding gas enriched with CO<sub>2</sub> was studied using a specially designed three-stage tube furnace. The sorbents collected after looping tests and after each regeneration step were analysed to determine the interdependences between the sorbent's physicochemical properties and its CO<sub>2</sub> capture capacity. The regeneration of the spent sorbent was carried out after the final calcination process.

Sorbent regeneration tests were conducted after 24 cycles of calcination and carbonation by the method of water hydration (close to 100°C) and also by lowering the temperature and feeding steam and then gas with a high CO<sub>2</sub> concentration (above 50%).

Preliminary cyclic carbonation and calcination tests were performed in a Perkin Elmer Diamond Thermogravimetric Analyser (TGA) specially adapted for long multicycle carbonation-calcination tests in different gas compositions. For each TGA run a batch of around 50 mg of sorbent was introduced into the sample holder. Calcination and carbonation reactions were conducted in the same atmosphere in subsequent cycles at 900°C and 650°C, respectively. Each cycle lasted 5 min. Then sorbent regeneration tests were run after 24 cycles of calcination and carbonation by the method of water hydration (~100°C) and also by lowering the temperature and feeding steam and then gas with a high carbon dioxide concentration of above 50% (the two-stage method). Investigations of the effect of hydration on the carbon capacity of calcium sorbents were carried out after 24 cycles where the final step was calcination. The goal of the hydration was to reactivate the deactivated CaO in the sorbent after many cycles of calcination and carbonation. The results for both cases are shown in Fig. 2b.

The two-stage regeneration procedure was as follows: the sorbent was inundated with boiling water and kept in hot water for 10 minutes; then the sample was placed in the TG analyser and heated at

40°C for 10 minutes; the heating atmosphere was CO<sub>2</sub> = 50% / N<sub>2</sub> = 50% by volume; subsequently the sample was rapidly heated (140°C/min) to 900°C and calcined.

Table 3. Denotations of samples.

## POST-CALCINATION SAMPLING

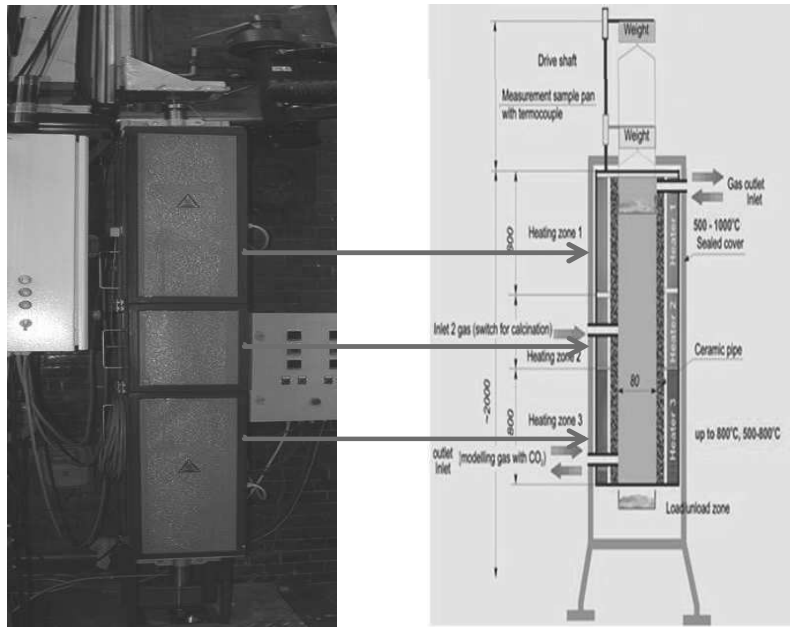
A	raw limestone sorbent
B	after 1 calcination step
C	after 10 calcination steps
D	after hydration by steam (30 min)
E	after hydration by steam (30 min) and after regeneration by CO <sub>2</sub> rich (50%) gas
F	after hydration by steam (30 min), CO <sub>2</sub> regeneration and 1 calcination step
G	after hydration by steam (30 min), CO <sub>2</sub> regeneration and 10 calcination steps

Table 4. Experimental conditions.

Calcination/Carbonation	Research program		Regeneration program		
	Condition 1	Condition 2	Condition 3	Condition 4	Condition 5
Duration [min]	10/5	10/5	30	30	10
Temperature [°C]	900/650	900/650	100	150	150
Inlet CO <sub>2</sub> [%v/v]	15	15	0	0	50
Inlet steam[%]	0	10	0	100	0
Inlet H <sub>2</sub> O [%]	0	0	100	0	0

The regeneration tests were carried out online by feeding saturated steam after 10 carbonation/calcination cycles and by the two-stage method consisting in subjecting the sorbent after the 10th calcination/calcination cycle to the action of steam and then gas with a high (50%) CO<sub>2</sub> content. Inlet H<sub>2</sub>O [%]

For this purpose a specially designed three-stage tube furnace (Fig. 1) was used. The apparatus makes it possible to study the different sorbent regeneration methods by varying the atmosphere, the temperature and the time. During the whole calcination/carbonation process the change in the sample mass was measured in each of the ten steps. The experimental conditions are shown in Table 3. For each of the sorbents the calcination/carbonation sequence in 15% CO<sub>2</sub> was repeated twice to obtain post-calcination and post-carbonation samples. After the regeneration of the selected sorbents multicycle tests were also performed in the TG analyser. The sorbents collected after the multicycle calcination/carbonation tests and after each regeneration step were analysed by mercury porosimetry, x-ray diffraction (XRD) and SEM. Mercury porosimetry was used to determine the bulk and absolute densities, pore diameter, total pore volume and surface area of the collected samples. The post-calcination sampling was carried out after 10 and 24 calcination/carbonation cycles (operating conditions 1 and 2).



**Figure 1.** Photo (left) and scheme (right) of experimental apparatus.

### 3. Results

The results obtained in the TG apparatus show an improvement in carbon dioxide capture by the regenerated calcium sorbent in comparison with the fresh sorbent, which was achieved through hydration. The reactivation of sorbent should take place when its CO<sub>2</sub> capture capacity approaches the minimum capture capacity acceptable in the process. Therefore in the considered case the sorbent after 24 calcination/carbonation cycles was deemed deactivated. The reactivation of the sorbent via hydration is a very promising technique owing to its simplicity and the fact that it can be quickly applied in practice. The results obtained by the authors and reported in [36] are positive and encourage further research. Although the results are encouraging, the challenge is to optimize the regeneration process conditions in order to avoid excessive particle fragmentation during hydration. For this reason as part of this study the more controllable hydration with steam instead of water was explored and then the regeneration by steam hydration followed by the injection of low-temperature gas enriched with CO<sub>2</sub> (the 2-stage regeneration process) was studied. After hydrating the sorbents for 24 cycles where the final step was carbonation a sorbent with improved mechanical properties, but with a slightly lower sorption capacity in the final cycles of carbonation, was obtained.

Figures 2 a,b,c show the carbonation conversion in the multicycle tests for the fresh sorbent and after hydration for respectively Tarnow Opolski, EnBW and Xirorema Sand sorbents. The CO<sub>2</sub> capture capacity is significantly higher for the hydrated EnBW sorbents up to the 8th cycle. However, from the 12th to the 15th cycle the CO<sub>2</sub> capture capacity of the hydrated sorbent declines below that of the fresh sorbent. After 15 cycles it recovers and is close to that of the fresh sorbent. This behaviour was observed for each of the investigated reactivated sorbents.

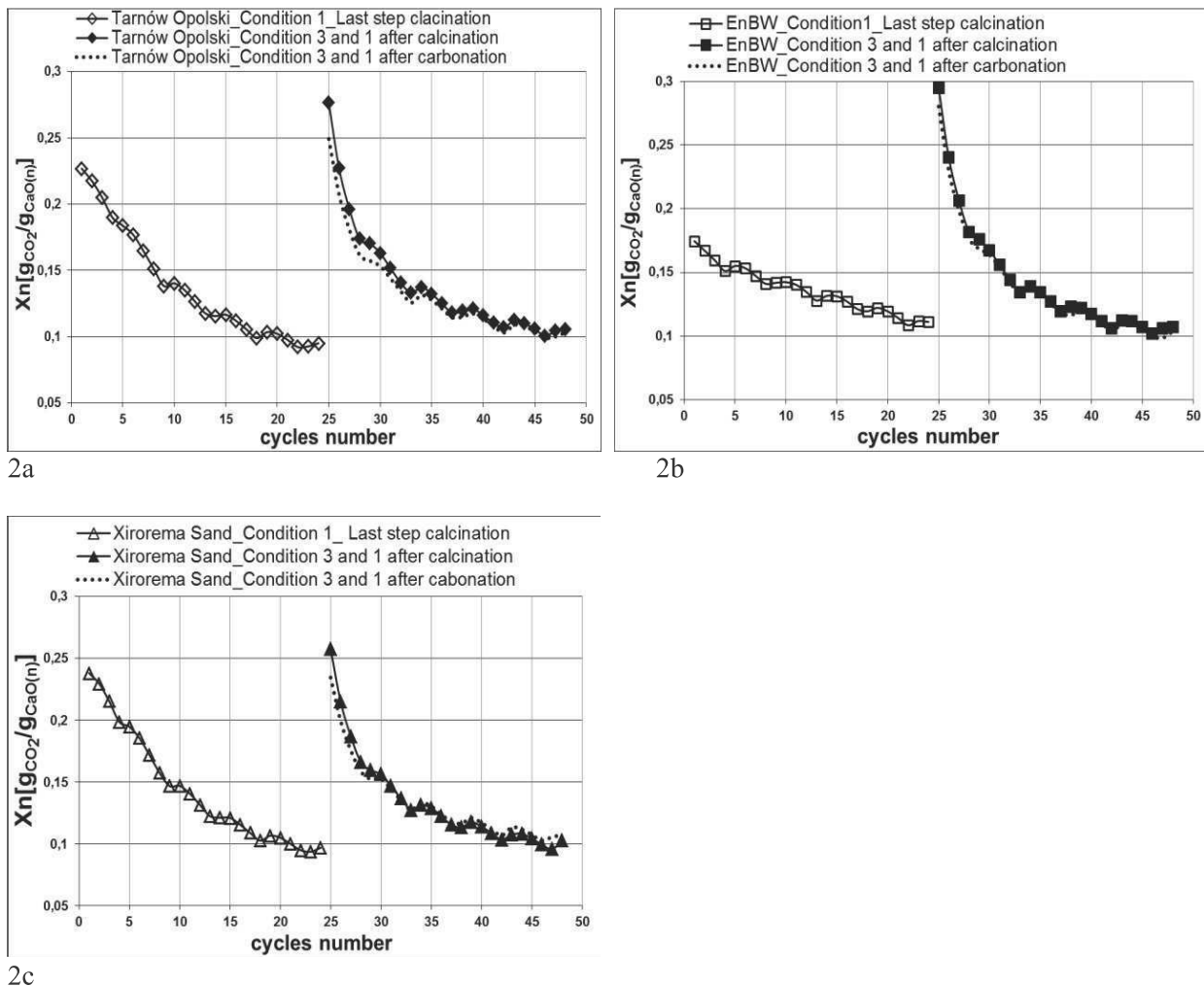
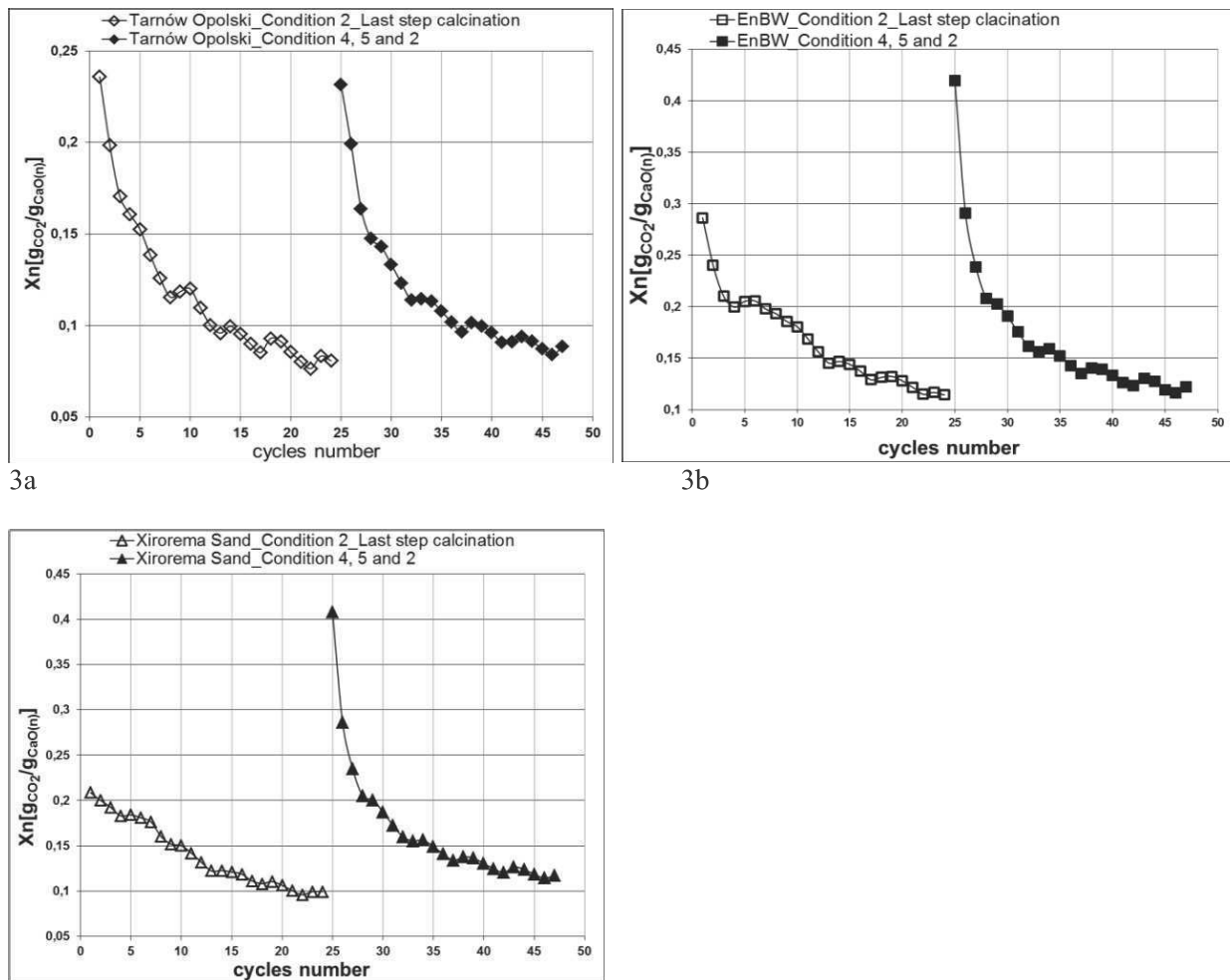


**Figure 2a,b,c.** CO<sub>2</sub> capture capacity for fresh sorbent (Condition 1, Table 4) and after hydration by hot water (Conditions 3 and 1, Table 4) in 24 cycles for Tarnow Opolski, EnBW and Xirorema Sand

The positive effect of water vapour on sorption capacity (Fig. 3 a, b, c) is the most significant for both the fresh and regenerated EnBW sorbent. In the case of the Xirorema Sand sorbent, higher sorption capacities were obtained for the regenerated sorbent than for the fresh sorbent. The sorption capacity of the regenerated Tarnow Opolski sorbent was similar as that of the fresh sorbent.



3c

**Figure 3a,b,c.** CO<sub>2</sub> capture capacity for fresh sorbent with steam in gas atmosphere (Condition 2, Table 4) and after hydration (Condition 5 and 2, Table 4) in 24 cycles for Tarnow Opolski, EnBW and Xirorema Sand.

Online hydration processes with steam instead of water and then hydration followed by CO<sub>2</sub> stream were explored. An improvement in CO<sub>2</sub> capture capacity in the calcium looping process was achieved by applying both steam hydration and 2-stage regeneration (after each 10 calcination/carbonation cycles with calcination in the final step). The effect of hydration on the CO<sub>2</sub> capture capacity of the calcium sorbents was examined after 10 cycles with calcination in the final step. The aim of steam hydration was to reactivate the deactivated (significantly high) CaO content in the sorbent particles. The 2-stage method turned out to be very effective in improving the reactivity of the spent sorbents and their mechanical properties.

Figures 4 a,b show CO<sub>2</sub> capture capacity in the multicycle tests for the fresh sorbent and after water hydration, steam hydration and 2-stage regeneration for the Czatkowice sorbent and the EnBW sorbents. Figures 5 a,b show the average rate of carbonation in the multicycle tests for the fresh sorbent and after water hydration, steam hydration and 2-stage regeneration for the Czatkowice sorbent and the EnBW sorbent. In both cases, the CO<sub>2</sub> capture capacity is high for the steam hydrated spent sorbents after calcination. However, after the 2-stage regeneration the EnBW sorbent shows the highest sorption capacity in the 8th cycle and then the sorption capacity of the sorbent regenerated by hydration with water or steam is similar to that of the fresh sorbent. Whereas the sorption capacity of the regenerated

Czatkowice sorbent is slightly lower in the first 12 cycles than that of the fresh sorbent. But in the case of the 2-stage regeneration the difference in the carbonation conversion between the regenerated spent sorbent after calcination and the one after carbonation is not significant. In the case of the EnBW sorbents, the average rate of  $\text{CO}_2$  capture for the regenerated spent calcined/carbonated sorbent is higher than that for the fresh sorbent. This is interesting because it means that the carbonation process is significantly faster for the regenerated sorbents than for the fresh sorbent. As a result, when steam hydration was applied to the sorbents after 10 cycles (with carbonation in the final step), a sorbent with improved mechanical properties (but with a slightly lower sorption capacity in the final cycles of carbonation) was obtained.

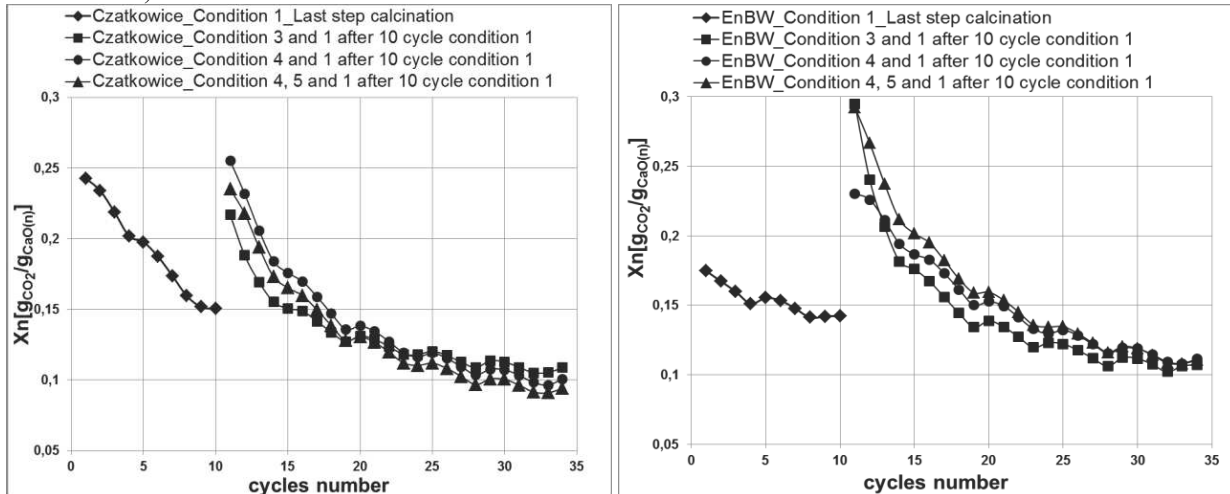


**Figure 4a,b.** Changes in  $\text{CO}_2$  capture capacity for Czatkowice (a), EnBW (b) and raw sorbent (Condition 1, Table 4) in consecutive calcination/carbonation cycles, after hydration by water (Condition 3, Table 4), hydration by steam (Condition 4, Table 4) and after 2-stage regeneration (Condition 5, Table 4).

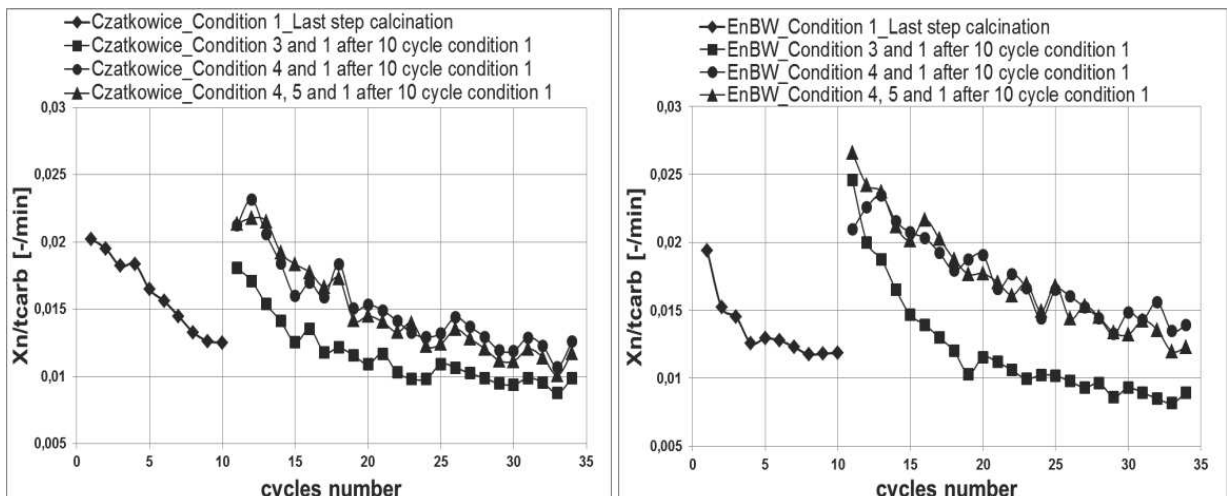


**Figure 5a,b.** Comparison of average rate of carbonation conversion for Czatkowice (a), EnBW (b) and raw sorbent (Condition 1, Table 4) in consecutive calcination/carbonation cycles, after hydration by water (Condition 3, Table 4), hydration by steam (Condition 4, Table 4) and after 2-stage regeneration (Condition 5, Table 4).

XRD, porosimetric and SEM analyses of the Czatkowice and EnBW sorbents after calcination, carbonation and regeneration showed that the size of  $\text{CaO}$  crystallite increased during both calcination and carbonation. The increase in  $\text{CaO}$  crystallite size for the EnBW sorbent after 10  $\text{Ca}$ -looping cycles amounts to about 52% (from 585.6 Å after 1 calcination to 892.2 Å after 10 calcinations). After the 2-

stage regeneration process the size of CaO crystallites decreases to 582 Å, which amounts to a ~44% decrease. After further calcination/carbonation cycles the CaO crystallite size increases again, though the increase is significantly smaller than in the case of the regenerated spent sorbent after the carbonation step (Fig. 6). Moreover, during the Ca-looping process with regeneration also the sorbent pore structure changes significantly (Fig. 7). SEM analyses of the post-calcination EnBW sorbent samples revealed more significant structural changes for the spent 2-stage regenerated raw sample after calcination than after carbonation. The SEM image of the EnBW sample A (Fig. 9a) shows a rather uniform surface of the raw sorbent sampled prior to the calcination/carbonation cycles. After calcination the sample shows traces of numerous fractures which developed during the calcination cycles. Where CO<sub>2</sub> was released during calcination the fractures form a dendritic network of connected channels. But the regenerated sorbent after calcination exhibits an even more nonuniform structure and numerous voids which developed during the cycles of calcination applied to the regenerated sorbent (Figs 8f,g). The increasing crystallite size can be responsible for sorbent deactivation, while the regeneration by steam and CO<sub>2</sub> rich gas improves the spent sorbent structure and so ameliorates the sorption capacity. The reactivated spent sorbents after 10 calcination steps were totally decomposed, whereby the CaCO<sub>3</sub> mass fraction is nearly zero for the samples (Fig. 9). The changes in the structure of the spent sorbents during regeneration bring about an improvement in reactivity, resulting in an increase in the sorption capacity of the reactivated spent sorbents. In comparison with the regeneration of the carbonated spent sorbents the regeneration of the calcined spent sorbents to a greater extent determines the improvement in CO<sub>2</sub> capture capacity, but it worsens the mechanical stability of the sorbent particles to a greater extent. A general comparison of the improvement in sorbent capacity for water hydration, steam hydration and 2-stage regeneration is presented in Figure 10.

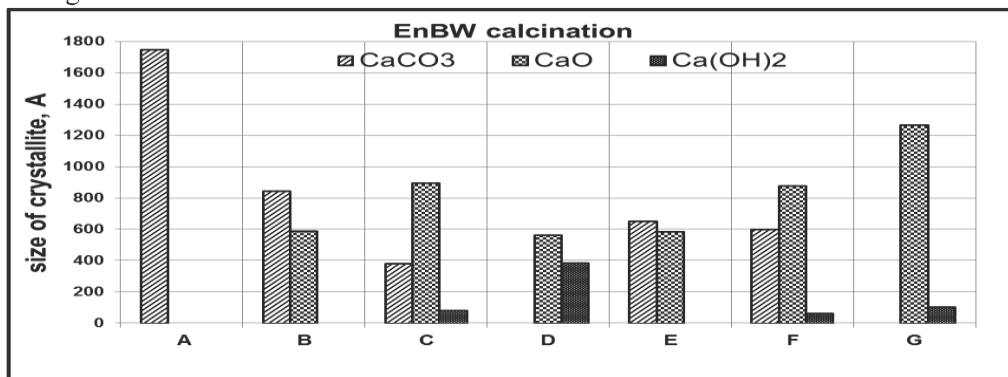


**Figure 6.** Change in EnBW CaO crystallite size during Ca-looping process with regeneration steps for calcined and carbonated spent sorbents (Table 3).

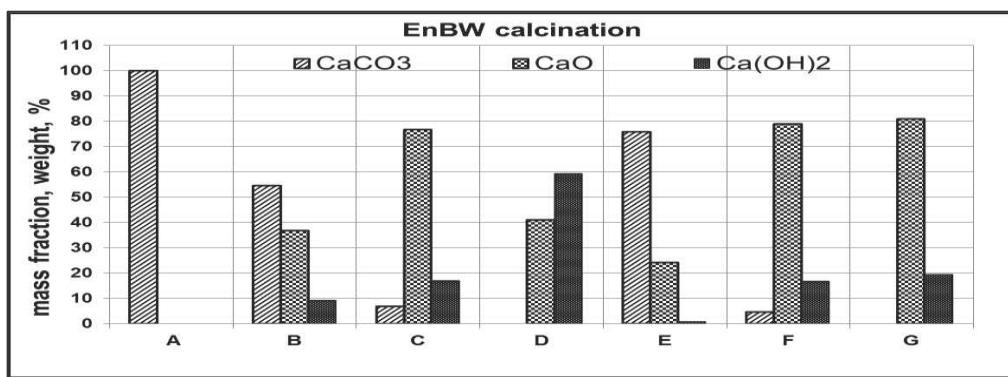


**Figure 7 .** Change in EnBW CaO mass fraction during Ca-looping process with regeneration steps for calcined and carbonated spent sorbents.

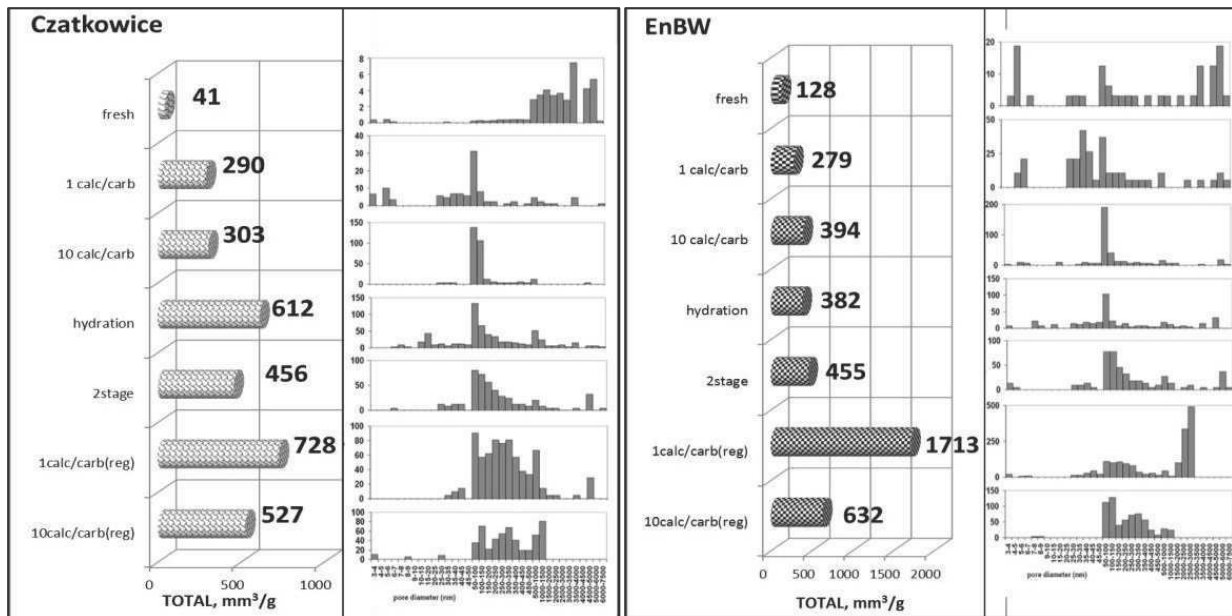


Figure 8. Distribution of specific pore volume (mm<sup>3</sup>/g) for diameter classes from 3-4 nm to 6000-7500 nm for calcined Czatkowice and EnBW sorbents.

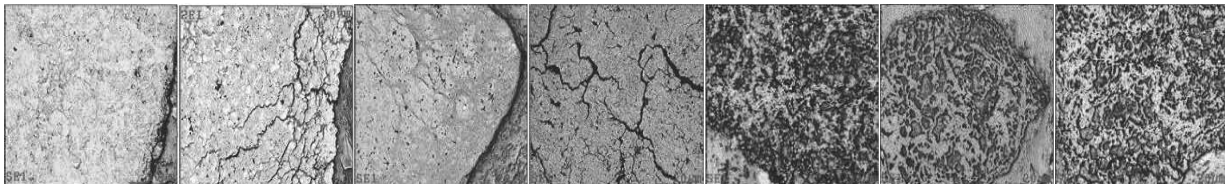


Figure 9. EnBW sorbent – SEM images for samples –A, –B, –C, –D (first row, from left to right), –E, –F, –G (second row, from left to right), (Table 3)

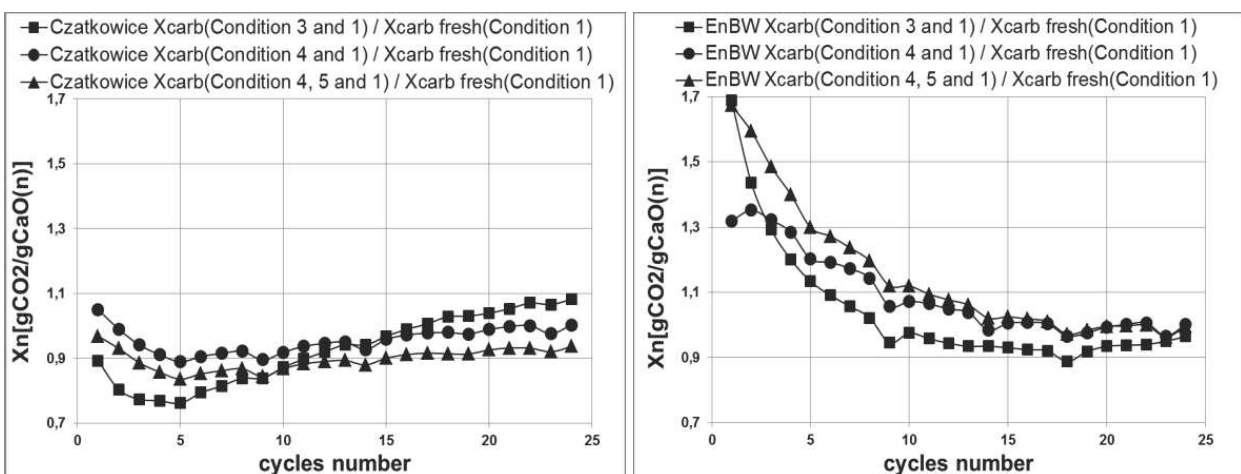


Figure 10. Comparison of changes in conversion (condition 1, Table 4) for Czatkowice (left), EnBW (right) sorbents, after hydration by water (Condition 3 and 1, Table 4), hydration by steam (Condition 4 and 1, Table 4) and after 2-stage regeneration (Condition 5 and 1, Table 4).

#### 4. Conclusions

The aim of this research was to demonstrate the potential of water/steam hydration as a means of reactivating spent limestone-based sorbents used in the looping process for CO<sub>2</sub> capture. The analysis of the results of the investigations into the regeneration by water and steam hydration as well as the 2-stage regeneration of the spent sorbents after 24 and 10 cycles of Ca-looping showed that:

- for each of the regeneration methods, i.e. hydration with respectively water and steam and the 2-stage regeneration, the sorption capacity of the regenerated sorbent was higher than that of the fresh sorbent.
- more rapid deactivation was observed in the initial sorbent regeneration Ca-looping cycles for the regenerated Czatkowice and EnBW sorbents,
- a sorbent with improved mechanical properties was obtained when steam hydration was applied to the spent carbonated material,
- 4) for each of the regeneration methods the sorbent morphology changes whereby a structure with a higher carbonation reactivity is obtained (probably due to an increase in the size of pores and changes in the size of CaO crystallites in the particular cycles),
- the pore size and the particle structure change significantly during regeneration whereby the sorbent becomes more porous, which means that its active surface increases and so does its CO<sub>2</sub> capture capacity.

It should be noted that the improvement in the capacity of the spent sorbents is the highest in the case of 2-stage regeneration, but it varies between the different sorbents, e.g. the Czatkowice sorbent containing some organic impurities showed similar regeneration effects for both steam hydration and 2-stage regeneration. This can be due to the different behaviour of the structure (including porosity, crystallite size and the various crystallite phases content) and the heavier sintering during the Ca-looping process. This in turn can be ascribed to the differences in the structure between the fresh sorbents and the more intensive sintering during both Ca-looping process and hydration with steam. The effect of hydration time on the textural changes in the spent sorbents, and so on the reactivity of the regenerated sorbents, is the subject of further research.

#### Acknowledgements

This work was funded by EU RFCS project CaL-Mod, Contract Number: RFR-CT-2010-00013. TITAN S.A. is acknowledged for the XRF analyses of sorbents

#### References:

- [1] Curran, G. P.; Fink, C. E.; Gorin, E. Carbon dioxide acceptor gasification process-studies of acceptor properties. *Adv. Chem. Ser.* 1967, 69, 141.
- [2] Baker, E. H. The calcium oxide-carbon dioxide system in the pressure range 1-300 atmospheres. *J. Chem. Soc.* 1962, 464.
- [3] Silaban, A.; Harrison, D. P. High-temperature capture of carbon dioxide: characteristics of the reversible reaction between CaO(s) and CO<sub>2</sub>(g). *Chem. Eng. Commun.* 1995, 137, 177.
- [4] Shimizu, T.; Hirama, T.; Hosoda, H.; Kitano, K.; Inagaki, M.; Tejima, K. A Twin Fluid-bed Reactor for Removal of CO<sub>2</sub> from Combustion Processes. *Trans IChemE* 1999, 77, 62.
- [5] Abanades, J. C.; Alvarez, D.; Anthony, E. J.; Lu, D. In-situ Capture of CO<sub>2</sub> in a Fluidized Bed Combustor. *Proceedings of the 17th FBC Conference*, Jacksonville, Florida, 2003.
- [6] Pawlak-Kruczek, H.; Wieckowska, K. *Chem. Process Eng.* 2010, 4, 889-903.
- [7] Coppola A., Scala F., Itskos G., Grammelis P., Pawlak-Kruczek H., Antiohos S., Salatino P., Montagnaro F., The Performance Of Natural Sorbents During Calcium Looping Cycles: A Comparison Between Fluidized Bed And Thermo-Gravimetric Tests. *Energy & Fuels* 2013, 27, 6048-6054.

- [8] Abanades, J. C.; Alvarez, D. Conversion limits in the reaction of CO<sub>2</sub> with lime. *Energy Fuels* 2003, 17 (2), 308-315.
- [9] Sun, P.; Grace, J. R.; Lim, C. J.; Anthony, E. J. Investigation of attempts to improve cyclic CO<sub>2</sub> capture by sorbent hydration and modification. *Ind. Eng. Chem. Res.* 2008, 47 (6), 2024-2032.
- [10] Wu, Y.; Blamey, J.; Anthony, E. J.; Fennell, P. S. Morphological changes of limestone sorbent particles during carbonation/calcination looping cycles in a thermogravimetric analyser (TGA) and reactivation with steam. *Energy Fuels* 2010, 24 (4), 2768-2776.
- [11] Grasa, G. S.; Abanades, J. C. CO<sub>2</sub> capture capacity of CaO in long series of carbonation/calcination cycles. *Ind. Eng. Chem. Res.* 2006, 45 (26), 8846-8851.
- [12] Sharat K. Pathi, Weigang Lin, Jytte B. Illerup,\* Kim Dam-Johansen, and Klaus Hjuler; CO<sub>2</sub> Capture by Cement Raw Meal; *Energy Fuels* 2013, 27, 5397-5406.
- [13] Hughes, R.W., Lu, D., Anthony, E.J., Wu, Y.: *Ind. Eng. Chem. Res.* 43 (2004), pp. 5529-5539.
- [14] Wang, W., Ramkumar, S., Li, S., Wong, D., Iyer, M., Sakadjian, B.B., Stanick, R.M., Fan, L.S.: *Ind. Eng. Chem. Res.* 49 (2010), pp. 5094-5101.
- [15] Wang, W., Ramkumar, S., Wong, D., Fan, L.S.: *Fuel* 92 (2012), pp. 94-106
- [16] Yu, F.-C.; Phalak, N.; Sun, Z.; Fan, L.-S. Activation strategies for calcium-based sorbents for CO<sub>2</sub> capture: A perspective. *Ind. Eng. Chem. Res.* 2011, 51 (4), 2133-2142.
- [17] Arias, B.; Grasa, G.; Abanades, J. C.; Manovic, V.; Anthony, E. J. The effect of steam on the fast carbonation reaction rates of CaO. *Ind. Eng. Chem. Res.* 2012, 51 (5), 2478-2482.
- [18] Manovic, V.; Anthony, E. J. Carbonation of CaO-based sorbents enhanced by steam addition. *Ind. Eng. Chem. Res.* 2010, 49 (19), 9105–9110.
- [19] Manovic, V.; Anthony, E. J. Steam reactivation of spent CaO based sorbent for multiple CO<sub>2</sub> capture cycles. *Environ. Sci. Technol.* 2007, 41 (4), 1420-1425.
- [20] Dobner, S.; Sterns, L.; Graff, R. A.; Squires, A. M. Cyclic calcination and recarbonation of calcined dolomite. *Ind. Eng. Chem. Process Des. Dev.* 1977, 16 (4), 479-486.
- [21] Lu, H.; Reddy, E. P.; Smirniotis, P. G. Calcium oxide based sorbents for capture of carbon dioxide at high temperatures. *Ind. Eng. Chem. Res.* 2006, 45 (11), 3944-3949.
- [22] Yang, S.; Xiao, Y. Steam catalysis in CaO carbonation under low steam partial pressure. *Ind. Eng. Chem. Res.* 2008, 47 (12), 4043-4048.
- [23] Wang, C. B.; Jia, L. F.; Tan, Y. W.; Anthony, E. J. Carbonation of fly ash in oxy-fuel CFB combustion. *Fuel* 2008, 87 (7), 1108-1114.
- [24] Wang, Y.; Lin, S.; Suzuki, Y. Limestone calcination with CO<sub>2</sub> capture (II): Decomposition in CO<sub>2</sub>/steam and CO<sub>2</sub>/N<sub>2</sub> atmospheres. *Energy Fuels* 2008, 22 (4), 2326-2331.
- [25] Ramkumar, S.; Fan, L. S. Thermodynamic and experimental analyses of the three-stage calcium looping process. *Ind. Eng. Chem. Res.* 2010, 49 (16), 7563-7573.
- [26] Borgwardt, R. H. Calcium oxide sintering in atmospheres containing water and carbon dioxide. *Ind. Eng. Chem. Res.* 1989, 28 (4), 493-500.
- [27] Champagne, S.; Lu, D. Y.; Macchi, A.; Symonds, R. T.; Anthony, E. J. Influence of steam injection during calcination on the reactivity of CaO-based sorbent for carbon capture. *Ind. Eng. Chem. Res.* 2012, 52 (6), 2241-2246.
- [28] Donat, F.; Florin, N. H.; Anthony, E. J.; Fennell, P. S. Influence of high-temperature steam on the reactivity of CaO sorbent for CO<sub>2</sub> capture. *Environ. Sci. Technol.* 2012, 46 (2), 1262-1269.
- [29] Nai Rong, Qinhu Wang,\* Mengxiang Fang, Leming Cheng, Zhongyang Luo, and Kefa Cen Steam Hydration Reactivation of CaO-Based Sorbent in Cyclic Carbonation/Calcination for CO<sub>2</sub> Capture ; *Energy Fuels* 2013, 27, 5332-5340.
- [30] Materić, B. V.; Sheppard, C.; Smedley, S. I. Effect of repeated steam hydration reactivation on CaO-based sorbents for CO<sub>2</sub> capture. *Environ. Sci. Technol.* 2010, 44 (24), 9496-9501.

- [31] Fennell, P. S.; Davidson, J. F.; Dennis, J. S.; Hayhurst, A. Regeneration of sintered limestone sorbents for the sequestration of CO<sub>2</sub> from combustion and other systems. *J. Energy Inst.* 2007, 80 (2), 116-119.
- [32] Montagnaro, F., Salatino, P., Scala, F., Bernardo, G., Valenti, G.L.: *Fuel* 82 (2003), pp. 2299-2307.
- [33] Montagnaro, F., Nobili, M., Telesca, A., Valenti, G.L., Anthony, E.J., Salatino, P.: *Fuel* 88 (2009), pp. 1092-1098.
- [34] Materić, V., Edwards, S., Smedley, S.I., Holt, R.: *Ind. Eng. Chem. Res.* 49 (2010), pp. 12429-12434.
- [35] Grigoris Itskos , Panagiotis Grammelis , Fabrizio Scala , Halina Pawlak-Kruczek, Antonio Coppola Piero Salatino b, Emmanuel Kakaras, A comparative characterization study of Ca-looping natural sorbents; *Applied Energy* 108 (2013) 373-382.
- [36] Blamey, J., Paterson, N.P.M, Dugwell, D.R., Stevenson, P., Fennell, P.S.: *Proc. Combust. Inst.* 33 (2011), pp. 2673-2681.

## FULL PAPER

# Alkali carbonate molten salt-coated CaO with highly improved CO<sub>2</sub> capture capacity

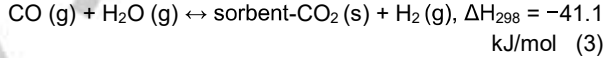
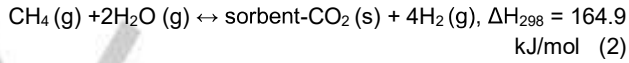
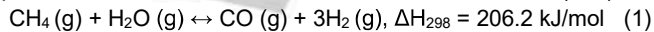
Liang Huang,<sup>[a]</sup> Yu Zhang,<sup>[a]</sup> Wanlin Gao,<sup>[a]</sup> Takuya Harada,<sup>[b]</sup> Qingqing Qin,<sup>[a]</sup> Qianwen Zheng,<sup>[a]</sup> T. Alan Hatton,<sup>[b]</sup> and Qiang Wang\*<sup>[a]</sup>

**Abstract:** CO<sub>2</sub> reduction is crucial if the effects of this gas on global warming are to be alleviated. We report an alkali carbonate molten salt promoted CaO-based CO<sub>2</sub> sorbent with superior CO<sub>2</sub> capture performance over that of neat CaO for the first time. The influence of chemical composition, loading, and melting temperature of (Li-Na-K)<sub>2</sub>CO<sub>3</sub> molten salts, and of the calcination and adsorption temperatures on CO<sub>2</sub> capture was evaluated systematically. The microstructural and morphological evolution of samples during CO<sub>2</sub> adsorption was studied by XRD, SEM, and FTIR. The (Li-K)<sub>2</sub>CO<sub>3</sub> molten salt coating not only promotes CO<sub>2</sub> uptake, but also facilitates the CO<sub>2</sub> desorption from CaO. In particular, at low temperatures of 500 and 600 °C, the CO<sub>2</sub> capture capacity increased significantly from 1.19 and 3.26 mmol g<sup>-1</sup> to 6.93 and 10.38 mmol g<sup>-1</sup>, respectively. The melting point of molten salts is also a crucial factor in the improvement of CO<sub>2</sub> uptake. Kinetic studies based on fractal-like models indicate that the rate coefficients for (Li-K)<sub>2</sub>CO<sub>3</sub>/CaO were about 3.3 to 3.8 times larger than those for neat CaO. The coating of alkali carbonate molten salts was believed to prevent the formation of a rigid CaCO<sub>3</sub> layer on the surface of CaO particles and provide a continuous delivery of CO<sub>3</sub><sup>2-</sup> to promote CO<sub>2</sub> capture. During the CO<sub>2</sub> adsorption/desorption cycling tests, (Li-K)<sub>2</sub>CO<sub>3</sub>/CaO resulted in a stable and reversible CO<sub>2</sub> uptake of 6.0–6.3 mmol g<sup>-1</sup>, which is much higher than that of neat CaO (2.0 mmol g<sup>-1</sup>).

## Introduction

The increasing demands for energy and natural resources lead to a tremendous growth in anthropogenic CO<sub>2</sub> emissions. As a major greenhouse gas, CO<sub>2</sub> traps and re-emits long-wave radiation, which warms the earth and leads to global warming.<sup>[1]</sup> According to reports by the Intergovernmental Panel on Climate Change (IPCC), the total anthropogenic greenhouse gas emissions were the highest in human history from 2000 to 2010 and reached 49 (±4.5) gigatonnes of CO<sub>2</sub> in 2010.<sup>[2]</sup> Hence, it is essential to cut down on the emission of CO<sub>2</sub> to reduce the risk of future devastating effects on our planet.<sup>[3]</sup> Although alternative energy sources (e.g. nuclear and solar energy) are being considered for

the mitigation of CO<sub>2</sub> emissions, it is still predicted that fossil fuels will remain the dominant energy source over the next several decades.<sup>[4]</sup> New technologies for CO<sub>2</sub> emissions reduction (e.g. capture, storage, and conversion) to reduce overall energy penalties and capital expenditures are under active study; the removal and recovery of CO<sub>2</sub> from hot gas streams has been identified as an important approach to solve these environmental issues.<sup>[5]</sup> Among the different technologies that have been developed, the sorption-enhanced steam reforming (SESR) reaction represents a promising technology for hydrogen production and CO<sub>2</sub> removal,<sup>[6]</sup> as described in reaction (1–3).<sup>[7]</sup>



The principle of SESR is to shift the equilibrium of reversible reactions through reliance on Le Chatelier's principle. For instance, the adsorption of CO<sub>2</sub> from the gas phase of the reversible reactions (2) and (3) on solid sorbents allows the production of highly pure hydrogen in a single step. A hydrogen conversion of as much as 95% (dry basis) can be achieved, which is much higher than that of a conventional reformer (maximum 80%, dry basis),<sup>[8]</sup> and the reaction temperature can be reduced from 800 °C to around 500–600 °C.<sup>[9]</sup> Particularly for a distributed reactor system, a relatively lower operating temperature is desired to improve safety, reduce material cost, and minimize preheating energy requirements.<sup>[10]</sup> Since the process is operated at an elevated temperature, separation of CO<sub>2</sub> from the process streams without first cooling the flue gases to room temperature seems to be a desirable and more economical approach to mitigating its emission to the environment; the key factor for such a process is the selection of a suitable CO<sub>2</sub> capture material.<sup>[11]</sup> To date, the three primary classes of high-temperature CO<sub>2</sub> sorbents are CaO,<sup>[12]</sup> alkali zirconates,<sup>[13]</sup> and alkali silicates,<sup>[14]</sup> among which CaO represents one of the most promising candidates for practical applications due to its low cost and high CO<sub>2</sub> capture capacity.<sup>[5f, 12a, b, 15]</sup>

The calcium looping process is a promising technique for CO<sub>2</sub> removal,<sup>[16]</sup> which is based on the reversible gas solid reaction between CaO and CO<sub>2</sub>. CaO exhibits high CO<sub>2</sub> capture capacity under stoichiometric conditions (17.86 mmol g<sup>-1</sup>), and has attracted tremendous attention owing to a number of advantages over other sorbents, although the low reversibility of the carbonation reaction due to the sintering of CaO sorbent particles is still a problem for practical applications.<sup>[17]</sup> To date, significant effort has been devoted to the improvement of the sintering-resistant properties of CaO particles, including (1) improvements in the synthesis method, (2) changes in the morphology and microstructure, (3) surface modification,<sup>[18]</sup> (4)

[a] L. Huang, Y. Zhang, W. Gao, Q. Qin, Q. Zheng, Prof. Q. Wang  
College of Environmental Science and Engineering  
Beijing Forestry University  
35 Qinghua East Road, Haidian District, Beijing 100083, P. R. China  
E-mail: qiang.wang.ox@gmail.com; qiangwang@bjfu.edu.cn

[b] T. Harada, Prof. T. A. Hatton  
Department of Chemical Engineering,  
Massachusetts Institute of Technology  
Massachusetts Avenue, Cambridge, Massachusetts, U.S.A

## FULL PAPER

synthesis of CaO based mixed oxides, (5) increasing attrition resistance, (6) reactivation of the degraded sorbents, and (7) influence of SO<sub>2</sub>, etc.<sup>[15]</sup> The primary goal of these efforts was to increase the CO<sub>2</sub> capture capacity and to improve the stability of the sorbents during CO<sub>2</sub> adsorption/desorption cycles.

In 2015, Harada et al.<sup>[19]</sup> reported that the CO<sub>2</sub> uptake of MgO can be improved significantly by coating MgO particles with molten alkali metal nitrates, from less than 1 mmol g<sup>-1</sup> for uncoated MgO to 10.2 mmol g<sup>-1</sup> at 300 °C. They also demonstrated that the peculiar effects of alkali metal nitrates could be attributed to the presence of a high concentration of oxide ions in the molten salt that restricted the formation of rigid surface layers of unideterminate carbonates and facilitated the generation of carbonate ions (CO<sub>3</sub><sup>2-</sup>), resulting in the rapid formation of MgCO<sub>3</sub> and ease of regeneration of the particles at moderate temperatures.<sup>[20]</sup> Inspired by this work, we were interested to determine whether this principle could be extended to CaO based CO<sub>2</sub> sorbent. In this contribution, the effects of molten coatings of alkali carbonate salts on the CO<sub>2</sub> adsorption capacity of commercial CaO particles at high-temperatures (400–700 °C) are studied. All prepared samples were characterized by XRD, ATR-FTIR, and SEM analyses. The CO<sub>2</sub> uptake and the CO<sub>2</sub> adsorption/desorption cycling stability of neat CaO and the alkali carbonate molten salts promoted CaO samples were examined with thermogravimetric analysis (TGA). Finally, the CO<sub>2</sub> adsorption kinetics were investigated with appropriate kinetic models.

## Results and Discussion

Figure 1 (a) shows the uptake of CO<sub>2</sub> by neat (uncoated) CaO particles and CaO particles coated with 10 mol% alkali metal carbonates (0.1R<sub>2</sub>CO<sub>3</sub>/CaO; R = Li, Na, K, Na-K, Li-K, Li-Na, Li-Na-K) when exposed at 600 °C to 100% dry CO<sub>2</sub> at ambient pressure (1 bar) for 1 h. Here, (Li-K)<sub>2</sub>CO<sub>3</sub>, (Li-Na)<sub>2</sub>CO<sub>3</sub>, and (Na-K)<sub>2</sub>CO<sub>3</sub> represent binary ([Li]:[K] = 0.428:0.572, mp = 498 °C; [Na]:[Li] = 0.52:0.48, mp = 500 °C; [Na]:[K] = 0.555:0.445, mp = 710 °C) and (Li-Na-K)<sub>2</sub>CO<sub>3</sub> represents ternary ([Li]:[Na]:[K] = 1:1:1) mixtures of alkali carbonates, respectively. It is apparent that the alkali carbonate molten salt coating can improve the CO<sub>2</sub> capture performance of CaO significantly.

For neat CaO, both the CO<sub>2</sub> adsorption capacity and the adsorption kinetics were relatively poor, after 1 h of adsorption, the CO<sub>2</sub> uptake was still less than 3.26 mmol g<sup>-1</sup>, while within the first minute, only 31.81% of its maximum CO<sub>2</sub> uptake was achieved. The CO<sub>2</sub> uptake of CaO increased when the particles were coated with single alkali salts Li<sub>2</sub>CO<sub>3</sub>, Na<sub>2</sub>CO<sub>3</sub>, or K<sub>2</sub>CO<sub>3</sub>, to reach 3.59, 6.27, and 7.65 mmol g<sup>-1</sup>, respectively. The promoting effect follows the sequence K<sub>2</sub>CO<sub>3</sub> > Na<sub>2</sub>CO<sub>3</sub> > Li<sub>2</sub>CO<sub>3</sub>. The binary and ternary alkali carbonates, however, showed much better performance enhancement than did the single carbonates. After coating with (Li-Na)<sub>2</sub>CO<sub>3</sub>, (Na-K)<sub>2</sub>CO<sub>3</sub>, and (Li-K)<sub>2</sub>CO<sub>3</sub>, the CO<sub>2</sub> uptake by the CaO particles was increased significantly to 10.27, 8.55, and 10.38 mmol g<sup>-1</sup>, respectively, indicating that a mixture which has low melting point can lead to a better CO<sub>2</sub> capture performance. In particular, for (Li-K)<sub>2</sub>CO<sub>3</sub>/CaO, the adsorption

kinetics was also much faster, with 57.33% of the maximum CO<sub>2</sub> uptake by CaO achieved within the first minute of exposure to CO<sub>2</sub>. With particles coated with the ternary carbonate (Li-Na-K)<sub>2</sub>CO<sub>3</sub>, the CO<sub>2</sub> uptake (10.09 mmol g<sup>-1</sup>) and adsorption kinetics (64.28% of its maximum uptake within 1 min) of CaO were also obviously improved.

Figure 1 (b) shows the influence of the Li<sub>2</sub>CO<sub>3</sub>/(Li-K)<sub>2</sub>CO<sub>3</sub> molar ratio on the CO<sub>2</sub> capture capacities of 10 mol% (Li-K)<sub>2</sub>CO<sub>3</sub>/CaO sorbents. To determine the optimal Li/K ratio for the promoted CaO sorbents, the Li<sub>2</sub>CO<sub>3</sub>/(Li-K)<sub>2</sub>CO<sub>3</sub> molar ratio ranging from 0.328 to 0.72 was studied. It can be seen clearly that the CO<sub>2</sub> uptake first increased with an increase in Li<sub>2</sub>CO<sub>3</sub>/(Li-K)<sub>2</sub>CO<sub>3</sub> ratio from 0.328 to 0.428, and that when the Li<sub>2</sub>CO<sub>3</sub>/(Li-K)<sub>2</sub>CO<sub>3</sub> ratio was higher than 0.62, the CO<sub>2</sub> uptake started to decrease with increasing Li<sub>2</sub>CO<sub>3</sub>/(Li-K)<sub>2</sub>CO<sub>3</sub> ratio. At Li<sub>2</sub>CO<sub>3</sub>/(Li-K)<sub>2</sub>CO<sub>3</sub> ratios of 0.328 and 0.72, the CO<sub>2</sub> capture capacity was only 8.38 and 6.56 mmol g<sup>-1</sup>, respectively, while with the Li<sub>2</sub>CO<sub>3</sub>/(Li-K)<sub>2</sub>CO<sub>3</sub> ratio in the range 0.428–0.62, the CO<sub>2</sub> capture capacity reached 10.03–10.38 mmol g<sup>-1</sup>.

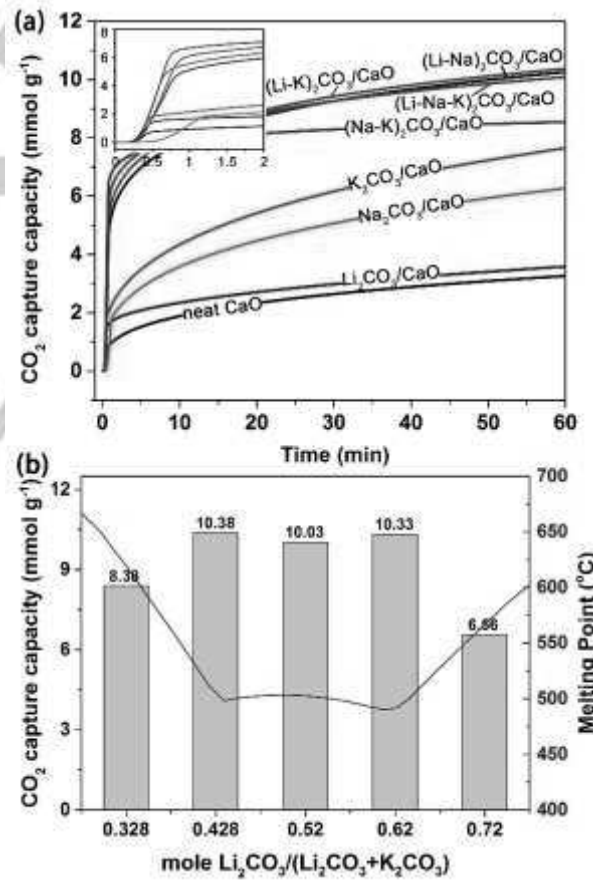
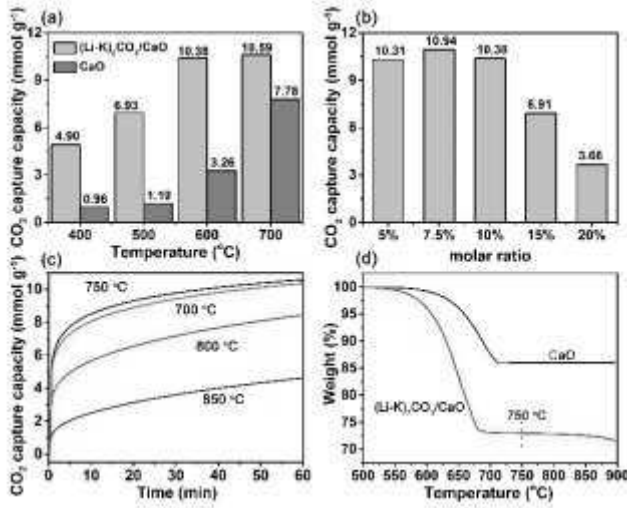


Figure 1. (a) CO<sub>2</sub> uptake by 10 mol% alkali metal carbonate-coated CaO samples at 600 °C and atmospheric pressure. (b) Influence of Li<sub>2</sub>CO<sub>3</sub>/(Li-K)<sub>2</sub>CO<sub>3</sub> molar ratio on the CO<sub>2</sub> capture capacities of 10 mol% (Li-K)<sub>2</sub>CO<sub>3</sub>/CaO samples, and the melting points thereof.

## FULL PAPER



**Figure 2.** (a) The influence of adsorption temperature on the CO<sub>2</sub> capture capacities of neat CaO and 10 mol% (Li-K)<sub>2</sub>CO<sub>3</sub>/CaO sorbents. (b) The influence of the molar loading of alkali carbonates on the CO<sub>2</sub> capture capacity of (Li-K)<sub>2</sub>CO<sub>3</sub>/CaO carbonated at 600 °C. (c) The influence of calcination temperature on the CO<sub>2</sub> capture capacity of 10 mol% (Li-K)<sub>2</sub>CO<sub>3</sub>/CaO. (d) TGA curves of CO<sub>2</sub> adsorbed 10 mol% (Li-K)<sub>2</sub>CO<sub>3</sub>/CaO and CaO samples.

Thus, it can be concluded that the Li<sub>2</sub>CO<sub>3</sub>/(Li-K)<sub>2</sub>CO<sub>3</sub> ratio has a significant effect on the CO<sub>2</sub> uptake by the promoted CaO sorbents. The strong dependence of CO<sub>2</sub> uptake on the Li<sub>2</sub>CO<sub>3</sub>/(Li-K)<sub>2</sub>CO<sub>3</sub> ratio correlates well with the melting points of (Li-K)<sub>2</sub>CO<sub>3</sub> molten salts with different Li/K ratios, summarized in Figure 1 (b).<sup>[21]</sup> A perfect negative correlation between the CO<sub>2</sub> uptake and the melting point temperature was observed. For instance, for Li<sub>2</sub>CO<sub>3</sub>/(Li-K)<sub>2</sub>CO<sub>3</sub> ratios were between 0.428 and 0.62, the melting point of (Li-K)<sub>2</sub>CO<sub>3</sub> is relatively low (488 to 503 °C), and higher CO<sub>2</sub> uptakes (> 10 mmol g<sup>-1</sup>) were observed. However, for Li<sub>2</sub>CO<sub>3</sub>/(Li-K)<sub>2</sub>CO<sub>3</sub> ratios of 0.328 and 0.72, the melting points were much higher (617 and 569 °C), and lower CO<sub>2</sub> uptakes were recorded. Similar results were observed previously with molten salt promoted MgO samples.<sup>[19]</sup> It was suggested that the CO<sub>2</sub> uptake can only be facilitated when the adsorption temperature is above the melting points of the molten salts coating the particles. The melting point of the (Li-K)<sub>2</sub>CO<sub>3</sub> molten salts can be tuned by changing the Li<sub>2</sub>CO<sub>3</sub>/(Li-K)<sub>2</sub>CO<sub>3</sub> ratio to influence the CO<sub>2</sub> uptake by the promoted CaO sorbents.

The influence of adsorption temperature on the CO<sub>2</sub> uptake of both neat and 10 mol% (Li-K)<sub>2</sub>CO<sub>3</sub> -promoted CaO sorbents was evaluated at 400, 500, 600, and 700 °C. The results shown in Figure 2 (a) indicate that higher temperatures are favorable for CO<sub>2</sub> capture with both neat and promoted CaO samples, and that the CO<sub>2</sub> uptake increased with an increase in adsorption temperature. Over the full temperature range (400–700 °C) tested, the 10 mol% (Li-K)<sub>2</sub>CO<sub>3</sub> promoted CaO showed much higher CO<sub>2</sub> uptake than did neat CaO, particularly at the lower temperatures (400–600 °C). For instance, at 400, 500, and 600 °C, the CO<sub>2</sub> uptake for neat CaO was only 0.96, 1.19, and 3.26 mmol g<sup>-1</sup>, respectively; however, after coating with 10 mol% (Li-K)<sub>2</sub>CO<sub>3</sub>, the CO<sub>2</sub> uptake was markedly improved to 4.90, 6.93, and 10.38

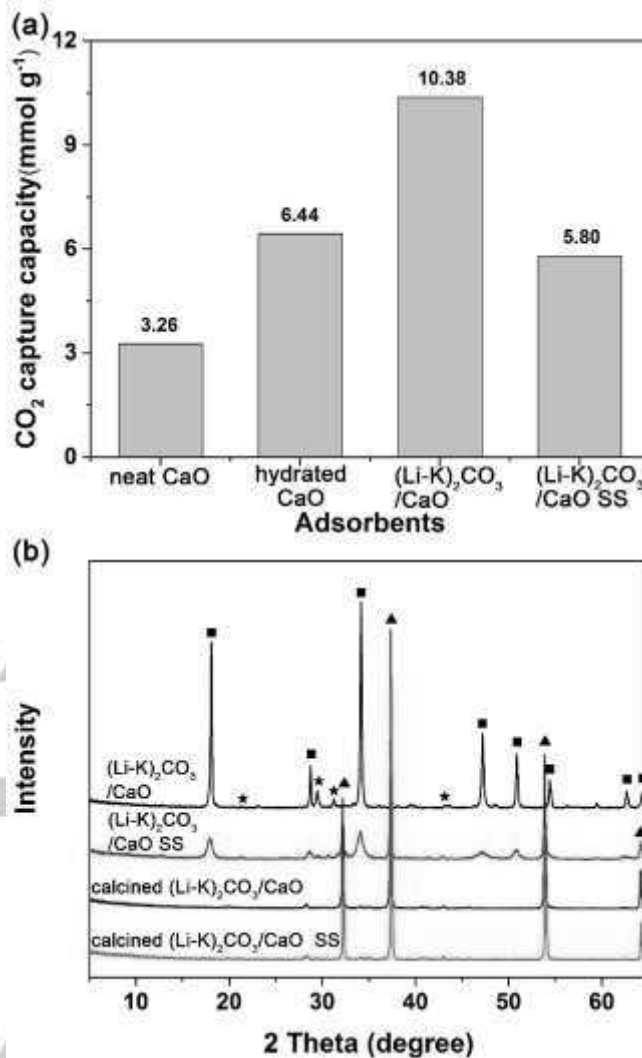


**Figure 3.** (a) CO<sub>2</sub> uptake by neat CaO, hydrated CaO, 10 mol% (Li-K)<sub>2</sub>CO<sub>3</sub>/CaO, and 10 mol% (Li-K)<sub>2</sub>CO<sub>3</sub>/CaO (SS) at 600 °C. (b) XRD patterns of 10 mol% (Li-K)<sub>2</sub>CO<sub>3</sub>/CaO, and 10 mol% (Li-K)<sub>2</sub>CO<sub>3</sub>/CaO (SS) before and after calcination. (■) Ca(OH)<sub>2</sub>, (▲) CaO, (★) (Li-K)<sub>2</sub>CO<sub>3</sub>.

mmol g<sup>-1</sup>, respectively. Even at 700 °C, the CO<sub>2</sub> uptake of 10 mol% (Li-K)<sub>2</sub>CO<sub>3</sub>/CaO (10.59 mmol g<sup>-1</sup>) was higher than that of neat CaO (7.78 mmol g<sup>-1</sup>). These data clearly demonstrate that the (Li-K)<sub>2</sub>CO<sub>3</sub> molten salt coating can promote the CO<sub>2</sub> capture capacity of CaO to a significant extent. More importantly, such a coating enables capture of CO<sub>2</sub> at lower temperatures than feasible with neat CaO, which is of great importance for practical applications.

Figure 2 (b) shows the influence of (Li-K)<sub>2</sub>CO<sub>3</sub> loading on the CO<sub>2</sub> uptake by (Li-K)<sub>2</sub>CO<sub>3</sub>/CaO. The CO<sub>2</sub> uptake first increased slightly from 10.31 to 10.94 mmol g<sup>-1</sup> as loading was changed from 5 to 7.5 mol%. However, when the (Li-K)<sub>2</sub>CO<sub>3</sub> loading was too high (ca. >10 mol%), the CO<sub>2</sub> uptake started to decrease. With 15 and 20 mol% (Li-K)<sub>2</sub>CO<sub>3</sub>, the CO<sub>2</sub> uptake by the (Li-K)<sub>2</sub>CO<sub>3</sub>/CaO samples decreased to 6.91 and 3.66 mmol g<sup>-1</sup>, respectively. These results suggest that for practical

## FULL PAPER

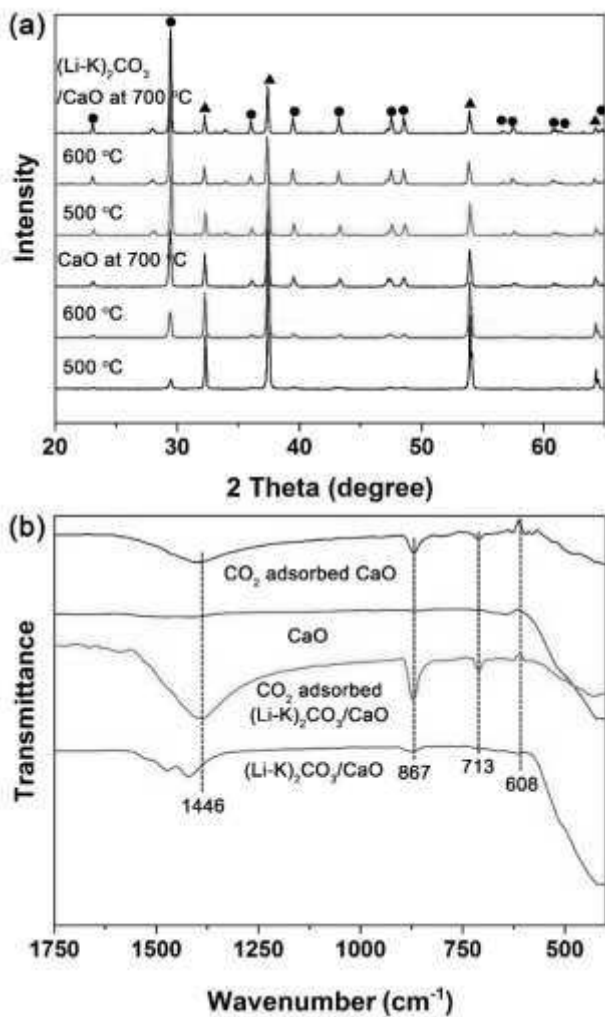


**Figure 4.** (a) XRD patterns of 10 mol% (Li-K)<sub>2</sub>CO<sub>3</sub>/CaO and CaO after adsorbing CO<sub>2</sub> at different temperatures (500–700 °C). (▲) CaO and (●) CaCO<sub>3</sub>. (b) FTIR analyses of neat CaO and 10 mol% (Li-K)<sub>2</sub>CO<sub>3</sub>/CaO before and after CO<sub>2</sub> adsorption at 600 °C.

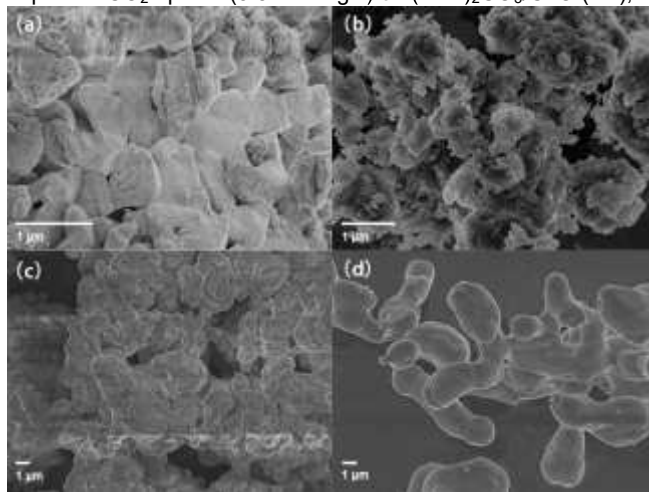
applications, the loading of (Li-K)<sub>2</sub>CO<sub>3</sub> molten salts should be no higher than 10 mol%, with an optimal loading of 7.5 mol%.

Figure 2(c) shows the influence of calcination temperature on CO<sub>2</sub> uptake by (Li-K)<sub>2</sub>CO<sub>3</sub>/CaO sorbents. It is clear that the sorbents calcined at 700–750 °C resulted in the largest uptake of CO<sub>2</sub> (10.34–10.38 mmol g<sup>-1</sup>), while at higher calcination temperatures (> 750 °C), the CO<sub>2</sub> uptake decreases with further increases in calcination temperature. This loss of capacity at these higher temperatures can be attributed to the decompositon of (Li-K)<sub>2</sub>CO<sub>3</sub> molten salts. These data demonstrated that the optimal calcination temperature for (Li-K)<sub>2</sub>CO<sub>3</sub>/CaO is 750 °C.<sup>[18]</sup>

While clearly the CO<sub>2</sub> capture performance of the sorbents is an important factor in their selection, the regeneration of these sorbents is also important for practical applications. The regenerability of the (Li-K)<sub>2</sub>CO<sub>3</sub>/CaO sorbents was investigated by evaluating the thermal stability of adsorbed CO<sub>2</sub> using TGA analyses. Figure 2(d) shows the weight loss of CO<sub>2</sub> adsorbed by 10 mol% (Li-K)<sub>2</sub>CO<sub>3</sub>/CaO and CaO at a temperature ramp of

10 °C/min, from which it can be concluded that the molten salt coating also facilitates CO<sub>2</sub> desorption. For the promoted CaO, both the starting and ending temperatures (510 and 680 °C) for CO<sub>2</sub> desorption were lower than those for neat CaO (530 and 710 °C). For neat CaO, the final weight loss was much less than that of 10 mol% (Li-K)<sub>2</sub>CO<sub>3</sub>/CaO owing to its worse CO<sub>2</sub> uptake. After 710 °C, no more weight loss was observed with CaO. However, for 10 mol% (Li-K)<sub>2</sub>CO<sub>3</sub>/CaO, a second weight loss was observed when the temperature was higher than 750 °C, indicating again that the (Li-K)<sub>2</sub>CO<sub>3</sub> molten salt started to decompose when the temperature is too high.<sup>[18]</sup> In summary, the data suggested that when the CaO is coated with (Li-K)<sub>2</sub>CO<sub>3</sub> molten salts, the regeneration of the sorbent is much easier and can be achieved at relatively lower temperatures. However, it should be noted that the regeneration temperature should be no higher than 750 °C to prevent the decompostion of the molten salts.

Previously it was reported that hydration also has a positive effect on the reactivation of CaO due to the improved morphology of the regenerated sorbent.<sup>[22]</sup> In order to confirm that the promotion of the CO<sub>2</sub> uptake by (Li-K)<sub>2</sub>CO<sub>3</sub> molten salts was not due to the hydration of CaO during preparation, two more samples were prepared. The first was hydrated CaO obtained by simple mixing of the particles with distilled water, and the other was 10 mol% (Li-K)<sub>2</sub>CO<sub>3</sub>/CaO (SS) prepared by the solid state mixing method with no water used to exclude any effects of hydration. All samples were pre-calcined at 750 °C for 5 h prior to the CO<sub>2</sub> capture tests. Figure 3 (a) shows that although the hydrated CaO possessed a higher CO<sub>2</sub> uptake (6.44 mmol g<sup>-1</sup>) than did neat CaO, its performance was still much poorer than that of 10 mol% (Li-K)<sub>2</sub>CO<sub>3</sub>/CaO (10.38 mmol g<sup>-1</sup>), confirming that the (Li-K)<sub>2</sub>CO<sub>3</sub> molten salt played a crucial role in promoting CO<sub>2</sub> capture. It was suggested that the hydration causes cracks to be formed in the CaO particles, creating channels that extend to the interior of the particles, with consequent improvement in the CO<sub>2</sub> capture capacity of CaO.<sup>[22–23]</sup> The CO<sub>2</sub> adsorption promotion by (Li-K)<sub>2</sub>CO<sub>3</sub> molten salt coatings was further confirmed by the improved CO<sub>2</sub> uptake (5.8 mmol g<sup>-1</sup>) of (Li-K)<sub>2</sub>CO<sub>3</sub>/CaO (SS).

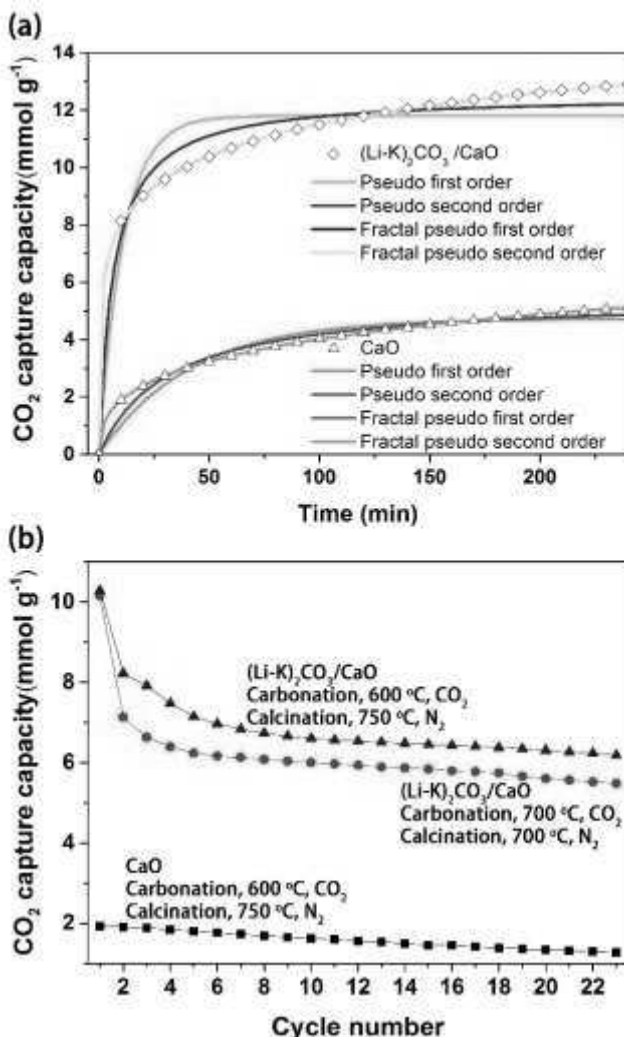
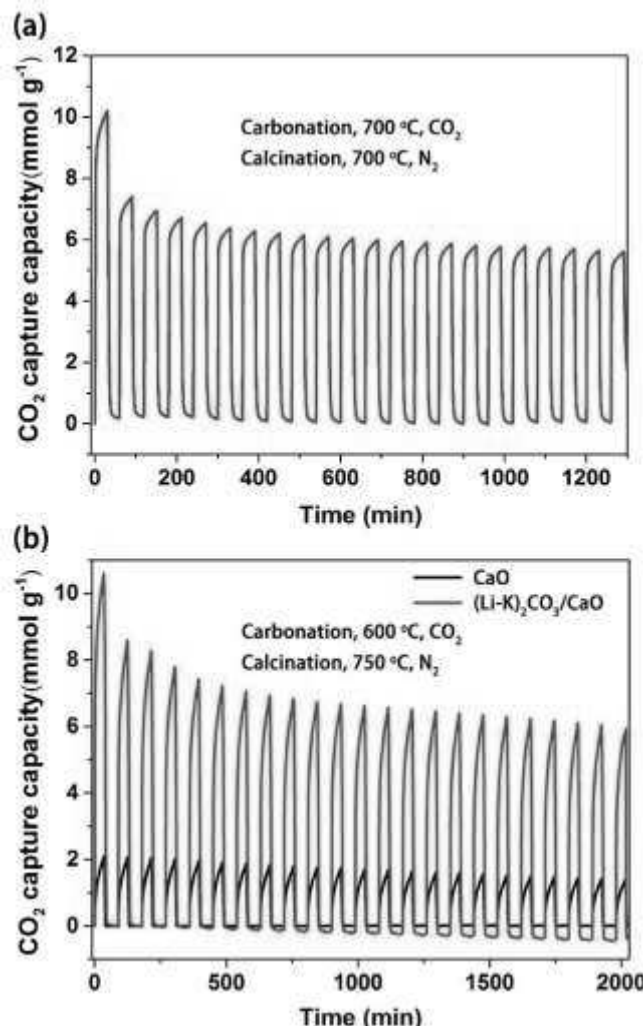


**Figure 5.** FE-SEM images of (a) CaO, (b) 10 mol% (Li-K)<sub>2</sub>CO<sub>3</sub>/CaO , (c) CaO after 10 cycles of CO<sub>2</sub> adsorption/desoriton, and (d) 10 mol% (Li-K)<sub>2</sub>CO<sub>3</sub>/CaO after 10 cycles of CO<sub>2</sub> adsorption/desoriton.

## FULL PAPER

**Table 1.** Fitted kinetic parameters for CO<sub>2</sub> adsorption on CaO and 10 mol% (Li-K)<sub>2</sub>CO<sub>3</sub>/CaO.

Kinetic model	formula	$k_l$ (min <sup>-1</sup> )	$q_e$ (mmol g <sup>-1</sup> )	$\alpha$	R <sup>2</sup>
<b>CaO</b>					
Pseudo-first order	$q_t = q_e(1 - e^{-k_1 t})$	0.020	4.73		0.886
Pseudo-second order	$q_t = \frac{q_e^2 k_2 t}{1 + q_e k_2 t}$	0.005	5.51		0.951
Fractal pseudo-first order	$q_t = q_e(1 - e^{-k_3 t^\alpha})$	0.089	9.52	0.392	0.999
Fractal pseudo-second order	$q_t = \frac{q_e^2 k_4 t^\alpha}{1 + q_e k_4 t^\alpha}$	0.003	14.86	0.403	0.999
<b>10 mol% (Li-K)<sub>2</sub>CO<sub>3</sub>/CaO</b>					
Pseudo-first order	$q_t = q_e(1 - e^{-k_1 t})$	0.09	11.81		0.544
Pseudo-second order	$q_t = \frac{q_e^2 k_2 t}{1 + q_e k_2 t}$	0.01	12.54		0.815
Fractal pseudo-first order	$q_t = q_e(1 - e^{-k_3 t^\alpha})$	0.34	18.36	0.234	0.987
Fractal pseudo-second order	$q_t = \frac{q_e^2 k_4 t^\alpha}{1 + q_e k_4 t^\alpha}$	0.01	23.70	0.260	0.988

**Figure 6.** (a) Experimental and predicted CO<sub>2</sub> adsorption curves for CaO and 10 mol% (Li-K)<sub>2</sub>CO<sub>3</sub>/CaO samples. (b) CO<sub>2</sub> adsorption/desorption cycling performance of neat CaO and 10 mol% (Li-K)<sub>2</sub>CO<sub>3</sub>/CaO.**Figure 7.** (a) CO<sub>2</sub> adsorption/desorption cycling performance of 10 mol% (Li-K)<sub>2</sub>CO<sub>3</sub>/CaO at 700 °C.. (b) CO<sub>2</sub> adsorption/desorption cycling performance of neat CaO and 10 mol% (Li-K)<sub>2</sub>CO<sub>3</sub>/CaO in a 750 °C calcination and 600 °C carbonation cycle.

## FULL PAPER

in which the influence by hydration was excluded. The XRD patterns in Figure 3 (b) revealed that for the  $(\text{Li}-\text{K})_2\text{CO}_3/\text{CaO}$  sample prepared by the wet impregnation method, the CaO phase changed to  $\text{Ca}(\text{OH})_2$  due to the presence of  $\text{H}_2\text{O}$  during preparation. The decomposition of this  $\text{Ca}(\text{OH})_2$  changed the morphology of CaO to render it more porous. For the  $(\text{Li}-\text{K})_2\text{CO}_3/\text{CaO}$  (SS) sample, the original CaO phase remained, with only a small amount of  $\text{Ca}(\text{OH})_2$  formed due to the contact with atmosphere vapour. In summary, the data demonstrated that the excellent  $\text{CO}_2$  capture capacity of 10 mol%  $(\text{Li}-\text{K})_2\text{CO}_3/\text{CaO}$  can be attributed to the combined promotion effects of hydration and of the molten salt coating.

The phase evolution of neat CaO and 10 mol%  $(\text{Li}-\text{K})_2\text{CO}_3/\text{CaO}$  after adsorbing  $\text{CO}_2$  at different temperatures (500–700 °C) was monitored using XRD analyses, as shown in Figure 4 (a). For both neat and promoted CaO samples, the  $\text{CaCO}_3$  phase formed upon adsorption of  $\text{CO}_2$ . For neat CaO, the intensity of the formed  $\text{CaCO}_3$  peaks increased with an increase in adsorption temperature. At low adsorption temperatures (500–600 °C), the  $\text{CaCO}_3$  peaks were quite weak and the peaks for remaining CaO were still quite obvious. On the other hand, for the 10 mol%  $(\text{Li}-\text{K})_2\text{CO}_3/\text{CaO}$  sample the  $\text{CaCO}_3$  peaks were very strong even at 500 °C, and the peaks associated with the remaining CaO were very weak. These data clearly demonstrated that the  $(\text{Li}-\text{K})_2\text{CO}_3$  molten salt coating facilitates the formation of  $\text{CaCO}_3$ , particularly at lower temperatures.

The facilitated  $\text{CO}_2$  capture on promoted CaO was further demonstrated by ATR-FTIR analyses. Figure 4 (b) shows the ATR-FTIR spectra of neat and promoted CaO before and after  $\text{CO}_2$  capture. Before  $\text{CO}_2$  adsorption, no carbonate species were observed with these two sorbents, but after exposure to  $\text{CO}_2$ , three carbonate peaks were detected at 713, 867, and 1446  $\text{cm}^{-1}$ , which can be attributed to the asymmetric stretch, out-of-plane bending vibration stretch, and antisymmetric stretch of carbonates. However, for the promoted CaO sample, the intensities of these three characteristic carbonate peaks were much stronger than those observed for the neat CaO sample, again suggesting that more  $\text{CaCO}_3$  is formed on coating the particles with  $(\text{Li}-\text{K})_2\text{CO}_3$  molten salts.

The morphologies and microstructures of CaO and 10 mol%  $(\text{Li}-\text{K})_2\text{CO}_3/\text{CaO}$  before and after  $\text{CO}_2$  capture were studied by FE-SEM imaging, as shown in Figure 5 (a-d) and Figure S1. It is clear that the CaO grains were composed of small particles with smooth surfaces and an average size of 0.5 to 4  $\mu\text{m}$  with a specific

surface area (SSA) of  $7.96 \text{ m}^2 \text{ g}^{-1}$ . (Table S1) When stirred in an alkali carbonate solution and reacted with  $\text{H}_2\text{O}$ , the CaO particles became more porous, and many pores and channels extending to the interior of the particles were created, SSA was increased to  $23.88 \text{ m}^2 \text{ g}^{-1}$ . After 10 cycles of  $\text{CO}_2$  adsorption and desorption, the CaO particles were partly coalesced and expanded to form larger particles corresponding to a decrease in SSA ( $3.20 \text{ m}^2 \text{ g}^{-1}$ ), due to the relatively low Tammann temperature of  $\text{CaCO}_3$  (561 °C).<sup>[24]</sup> However, the 10 mol%  $(\text{Li}-\text{K})_2\text{CO}_3/\text{CaO}$  particles were still well dispersed and formed individual units that were quite small relative to the large aggregated granules after 10 cycles, which is a clear benefit for  $\text{CO}_2$  uptake. With the cover of molten salts, the coated CaO shows a smooth surface comparing to the uncoated one, which resulted in a relatively low SSA of  $0.57 \text{ m}^2 \text{ g}^{-1}$ . Figure S2–5 show the nitrogen adsorption-desorption isotherms of CaO and 10 mol%  $(\text{Li}-\text{K})_2\text{CO}_3/\text{CaO}$  before and after 10 cycles, which exhibited a classical IV-type isotherm, a characteristic of mesoporous materials.<sup>[25]</sup> The pore size and pore volume obtained using the Barrett–Joyner–Halenda (BJH) model are also summarized in Table S1.

To understand the detailed reaction process for  $\text{CO}_2$  capture on neat and promoted CaO samples, the dynamic variations during the reaction of the particles with  $\text{CO}_2$  were further examined. According to literature reports, there is a large number of kinetic models used to describe the adsorption processes over different sorbents. Among these, the most widely used are the pseudo first-order and pseudo second-order adsorption models, as described in equations (1) and (2) below,<sup>[26]</sup> where  $q_e$  ( $\text{mmol g}^{-1}$ ) and  $q_t$  ( $\text{mmol g}^{-1}$ ) are the adsorption capacities at equilibrium and at a certain time  $t$ , respectively,  $k_1$  ( $\text{min}^{-1}$ ) is the first order kinetic constant, and  $k_2$  ( $\text{min}^{-1}$ ) is the second order kinetic constant.

$$q_t = q_e (1 - e^{-k_1 t}) \quad (1)$$

$$q_t = \frac{q_e^2 k_2 t}{1 + q_e k_2 t} \quad (2)$$

In these models, it is assumed that the rate coefficients  $k_1$  and  $k_2$  are constant, with no time dependence. Consequently, Kopelman et al.<sup>[27]</sup> proposed a fractal-like approach for the models with rate equations that have a time dependent rate coefficient  $k$ , as shown in equation (3),<sup>[27–28]</sup> where  $h$  is a constant. By introducing the time dependent rate coefficient to the previous kinetic models, fractal like-pseudo first order and fractal like-pseudo second order models could be improved to capture the experimentally observed trends in adsorption kinetic data. According to the fractal-like approach, the fractal pseudo-first order model and the fractal pseudo-second order model can be expressed as equation (4) and (5), where  $\alpha$  is a constant,  $\alpha = 1 - h$ , respectively.

$$k = k^* t^{-h} \quad 0 \leq h \leq 1 \quad (t \geq 1) \quad (3)$$

$$q_t = q_e (1 - e^{-k_3 t^\alpha}) \quad (4)$$

$$q_t = \frac{q_e^2 k_4 t^\alpha}{1 + q_e k_4 t^\alpha} \quad (5)$$

The mechanism of the  $\text{CO}_2$  adsorption process was probed through application of the above kinetic models to fit the  $\text{CO}_2$  uptake curves as a function of time, as shown in Figure 6 (a). The kinetic parameters for  $\text{CO}_2$  adsorption on CaO and 10 mol%  $(\text{Li}-\text{K})_2\text{CO}_3/\text{CaO}$  extracted from these model fits are summarized in Table 1. According to the kinetic data and the correlation

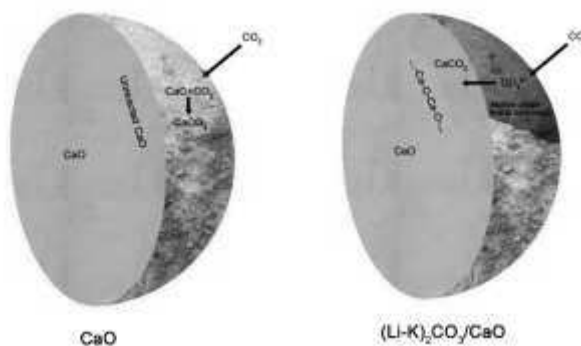


**Figure 8.** Schematic diagrams of the possible reaction for  $\text{CO}_2$  with  $(\text{Li}-\text{K})_2\text{CO}_3/\text{CaO}$  and CaO particles.

## FULL PAPER

coefficient ( $R^2$ ), the fractal-like pseudo kinetic models were more suitable for both CaO and 10 mol% (Li–K)<sub>2</sub>CO<sub>3</sub>/CaO than the traditional first- and second-order models. In addition, the models suggested that the CO<sub>2</sub> adsorption was chemisorption for both sorbents. During the very initial stages of the CaO carbonation reaction where the conversion is low enough to be neglected, the reaction rate is dependent on  $k$ , indicating that  $k$  can be regarded as an intrinsic chemical reaction rate constant.<sup>[26c]</sup> The rate constants  $k_3$  and  $k_4$  for 10 mol% (Li–K)<sub>2</sub>CO<sub>3</sub>/CaO were about 3.3 to 3.8 times higher than those for CaO, indicating that the CO<sub>2</sub> uptake was promoted significantly by the coating of alkali carbonate molten salts on the CaO particles.

For practical applications, the stability of the sorbents during CO<sub>2</sub> adsorption/desorption cycles is also very important. Thus, both neat CaO and 10 mol% (K–Li)<sub>2</sub>CO<sub>3</sub>/CaO sorbents were evaluated in a typical temperature swing adsorption (TSA) process. The adsorption was performed with pure CO<sub>2</sub> at 600 °C, while the desorption was with pure N<sub>2</sub> at 750 °C, both for 30 min. Figure 6 (b) shows the CO<sub>2</sub> adsorption and desorption performance for the two sorbents over 23 cycles. The CO<sub>2</sub> adsorption capacity showed an unobtrusive decrease during the cycles which was due to irreversible chemisorption. For neat CaO, its capture capacity was decreased to ca. 1.5 mmol g<sup>-1</sup> during the rest 22 cycles. While for the 10 mol% (K–Li)<sub>2</sub>CO<sub>3</sub>/CaO, its CO<sub>2</sub> capture capacity shows a ca. 6.3 mmol g<sup>-1</sup> uptake capacity during rest 16 cycles in TSA cycle.

The cycling performance of 10 mol% (K–Li)<sub>2</sub>CO<sub>3</sub>/CaO was also evaluated in a balance gas swing adsorption process. Both the adsorption and desorption were performed at 700 °C for 30 min, by a simple switching of the gas between pure CO<sub>2</sub> and pure N<sub>2</sub>, as shown in Figure 6 (b). The results indicated that CO<sub>2</sub> adsorption/desorption can also be achieved with the gas swing scheme, and the trend is similar to that observed with the TSA process. The CO<sub>2</sub> capture capacity stabilized after 8 cycles at ca. 6 mmol g<sup>-1</sup> for the rest of the 15 cycles. The actual CO<sub>2</sub> adsorption-desorption profiles for CaO and 10 mol% (Li–K)<sub>2</sub>CO<sub>3</sub>/CaO during balance gas swing adsorption process and the TSA process are presented in Figure 7(a) and (b). The results clearly demonstrated that the molten salt coated CaO has much better CO<sub>2</sub> capture performance during 23 cycles. The stable adsorption capacity was 3 times higher than that for the uncoated CaO, which provides a better opportunity for use of these coated particles in practical applications.<sup>[29]</sup>

In general, the reaction between the solid materials and gas molecules is restricted by the impermeable product layer that forms on the surfaces of the particles, as illustrated schematically in Figure 8. For neat CaO, CO<sub>2</sub> molecules are quickly adsorbed on the surface of the particles, forming a predominantly carbonate layer which retards the generation of CO<sub>3</sub><sup>2-</sup> ions required for the formation of CaCO<sub>3</sub>.<sup>[30]</sup> Due to this obstruction, the reaction between CaO and CO<sub>2</sub> is significantly inhibited when CaO particles are fully covered by CaCO<sub>3</sub> which was characterised by a very slow reaction rate attributable to diffusive limitations.<sup>[30]</sup> However, with the alkali metal carbonate coating on the CaO particle, CO<sub>2</sub> and CaO are both dissolved in the liquid molten salts. The reaction to form the carbonate occurs, and the CaCO<sub>3</sub> accumulates until saturation within the solution, at which point it precipitates out to form a permeable CaCO<sub>3</sub> layer to make the reaction not to become diffusion limited.<sup>[31]</sup> The molten salts can

permeate this layer and dissolve further CaO to ensure a persistent generation of dissolved CaCO<sub>3</sub>, and thereby improve the CO<sub>2</sub> capture capacity. Similar phenomena have also been observed with molten salt-promoted MgO sorbents.

## Conclusions

We have demonstrated that the CO<sub>2</sub> capture capacity of CaO sorbents can be improved significantly by coating the particles with an alkali carbonate molten salt, particularly in the lower temperature ranges. The chemical composition of the alkali carbonates has a great effect on the CO<sub>2</sub> uptake by the promoted CaO sorbents, with a performance that follows the order of (Li–K)<sub>2</sub>CO<sub>3</sub> > (Li–Na–K)<sub>2</sub>CO<sub>3</sub> > (Na–K)<sub>2</sub>CO<sub>3</sub> > (Li–Na)<sub>2</sub>CO<sub>3</sub> > K<sub>2</sub>CO<sub>3</sub> > Na<sub>2</sub>CO<sub>3</sub> > Li<sub>2</sub>CO<sub>3</sub>. With 7.5 mol% (Li–K)<sub>2</sub>CO<sub>3</sub>, the CO<sub>2</sub> uptake by CaO at 600 °C was markedly improved from 3.26 to 10.94 mmol g<sup>-1</sup>. We also demonstrated that by coating the particles with (Li–K)<sub>2</sub>CO<sub>3</sub> molten salt, the regeneration of CaO sorbent becomes easier and can be achieved at relatively low temperatures. Kinetic studies with fractal-like models indicated that the rate coefficients for 10 mol% (Li–K)<sub>2</sub>CO<sub>3</sub>/CaO are about 3.3 to 3.8 times higher than those for neat CaO. CO<sub>2</sub> adsorption/desorption cycling tests under both TSA and gas swing adsorption processes demonstrated that the stable CO<sub>2</sub> uptake of this molten salt-promoted CaO sorbent was 3 times higher than that of the uncoated CaO, which provides a better opportunity for application of CaO sorbents in industrial processes. With the alkali carbonate coating, the formation of a rigid CaCO<sub>3</sub> layer on the surface of CaO can be prevented, and the dissolved CO<sub>2</sub> and O<sup>2-</sup> from CaO in the liquid molten salts persistently generate CO<sub>3</sub><sup>2-</sup> to accelerate the CO<sub>2</sub> capture process. This work represents a novel scheme for preventing the CaO sintering by shifting its operation temperatures to a lower temperature window.

## Experimental Section

## Preparation of sorbents

Alkali–metal carbonate (Li<sub>2</sub>CO<sub>3</sub>, Na<sub>2</sub>CO<sub>3</sub>, and K<sub>2</sub>CO<sub>3</sub>) -promoted CaO sorbents were prepared by the co-calcination of a mixed suspension of commercial CaO (Xilong Scientific) and alkali metal carbonates (Sinopharm Chemical Reagent Co. Ltd) in water. In brief, 2.8 g CaO (0.05 mol) and appropriate amounts (5, 10, 20 mol%) of alkali metal carbonates were mixed in 20 mL of water with constant stirring for 1 h at room temperature. The resulting mixtures were dried in an oven at 120 °C overnight. Dried powders were ground in a mortar, then calcined at 750 °C for 5 h in air. The ratio of Li/Na/K in the sorbent was controlled by adding appropriate amounts of Li<sub>2</sub>CO<sub>3</sub>, Na<sub>2</sub>CO<sub>3</sub>, and K<sub>2</sub>CO<sub>3</sub>. For comparison purposes, the alkali–metal carbonate-promoted CaO particles were also prepared using a solid state milling method recorded as (Li–K)<sub>2</sub>CO<sub>3</sub>/CaO (SS). In this case, 2.8 g CaO (0.05 mol) and appropriate amounts (5, 10, 20 mol%) of alkali metal carbonates were mixed in a mortar for a continuous milling for 2 h to prepare mixed precursors, then the mixtures were calcined at 750 °C for 5 h in air, and transferred to the TGA analyzer for subsequent testing.

## FULL PAPER

## Characterization of sorbents

Ex-situ XRD patterns of samples were recorded on a Shimadzu XRD-7000 instrument in reflection mode with Cu K $\alpha$  radiation. The accelerating voltage was set at 40 kV with 30 mA current ( $\lambda = 1.542 \text{ \AA}$ ) at  $0.1^\circ \text{ s}^{-1}$  from  $5^\circ$  to  $65^\circ$ . The weight loss of alkali metal carbonate-promoted CaO was measured with a Q50 TGA analyzer (TA Instruments, N<sub>2</sub> flow rate = 60 ml min $^{-1}$ ). ATR-FTIR experiments were performed on a Vertex 70 FTIR spectrophotometer (Bruker). The morphology of samples was characterized by SEM analysis (SU8010, Hitachi) with an accelerating voltage of 5.0 kV. Powder samples were spread on carbon tape adhered to an SEM stage. Before observation, the samples were sputter coated with a thin gold layer to prevent charging and to improve the image quality.

Evaluation of CO<sub>2</sub> adsorption capacity

Thermogravimetric adsorption of CO<sub>2</sub> on alkali metal carbonate-promoted CaO was measured on a TGA analyzer (Q50 TA Instrument). Sorbents were first calcined in a Muffle furnace at a temperature of 750 °C for 5 h before the samples were transferred to the TGA analyzer. To avoid the error caused by the atmosphere, all samples were tested immediately after the first calcination; the sorbents were then further calcined in situ at 750 °C for 1 h in N<sub>2</sub> before the adsorption runs were initiated. CO<sub>2</sub> adsorption experiments were carried out at temperatures ranging from 400 °C to 700 °C under a constant flow of CO<sub>2</sub> (40 ml min $^{-1}$ ) and at ambient pressure (1 bar). The CO<sub>2</sub> capture capacity of a sample was defined as the amount of CO<sub>2</sub> adsorbed by 1 g of sorbent (mmol g $^{-1}$ ) after 1 h of reaction with CO<sub>2</sub> under the above conditions. Cycling tests were performed with a TGA analyzer. About 10 mg of calcined sorbent was loaded in a platinum sample pan. Two CO<sub>2</sub> adsorption/desorption cycling test modes, namely temperature swing adsorption (TSA) and balance gas swing adsorption, were used in this work. For TSA, the sorbent sample was first pre-heated at 750 °C under an atmosphere of pure N<sub>2</sub> for 60 min. After that, the temperature decreased to 600 °C at the same conditions and kept for 40 min. When the temperature was stabilized, the N<sub>2</sub> was replaced by CO<sub>2</sub>. After adsorption of CO<sub>2</sub> for 30 min, the gas was switched to N<sub>2</sub>, and the TGA was heated to 750 °C at a rate of 10 °C min $^{-1}$  and maintained at 750 °C for 30 min. After desorption cycle, the temperature was decreased at 10 °C min $^{-1}$  to 600 °C for the next adsorption of CO<sub>2</sub>. For gas swing adsorption, the adsorption temperature was fixed, and the CO<sub>2</sub> adsorption-desorption was controlled by changing the sample gases. At first, the sorbent sample was heated to 700 °C at a rate of 10 °C min $^{-1}$  under an atmosphere of pure N<sub>2</sub> and kept at this temperature for 40 min. When the temperature was reached and stabilized, the N<sub>2</sub> was replaced by CO<sub>2</sub>. After adsorption of CO<sub>2</sub> for 30 min, the gas was switched back to N<sub>2</sub>, kept at 700 °C for 30 min. After desorption, the sample gas was changed again to CO<sub>2</sub> for the next adsorption cycle.

## Acknowledgements

This work was supported by the Fundamental Research Funds for the Central Universities (2016ZCQ03), the National Natural Science Foundation of China (51622801, 51572029, and

51308045), and Beijing Excellent Young Scholar (2015000026833ZK11).

**Keywords:** climate change • sorption enhanced hydrogen production • carbon dioxide • calcium oxide • sorbent

- [1] M. Maslin, *Global Warming - A Very Short Introduction*, Oxford University Press, 2004.
- [2] O. Edenhofer, R. Pichs-Madruga, Y. Sokona, E. Farahani, S. Kadner, K. Seyboth, A. Adler, I. Baum, S. Brunner, P. Eickemeier, B. Kriemann, J. Savolainen, S. Schlömer, C. von Stechow, T. Zwickel, J. C. Minx and (eds.), *IPCC, 2014: Climate Change 2014: Mitigation of Climate Change. Contribution of Working Group III to the Fifth Assessment Report of the Intergovernmental Panel on Climate Change*, Cambridge University Press, United Kingdom and New York, NY, USA., 2014.
- [3] S. Chu, *Science* **2009**, 325, 1599.
- [4] a) Q. Wang, H. H. Tay, D. J. Ng, L. Chen, Y. Liu, J. Chang, Z. Zhong, J. Luo and A. Borgna, *ChemSusChem* **2010**, 3, 965-973; b) A. L. Chaffee, G. P. Knowles, Z. Liang, J. Zhang, P. Xiao and P. A. Webley, *Int. J. Greenh. Gas Control* **2007**, 1, 11-18.
- [5] a) M. J. Ramírez-Moreno, I. C. Romero-Ibarra, M. A. Hernández-Pérez and H. Pfeiffer, *Ind. Eng. Chem. Res.* **2014**, 53, 8087-8094; b) J. Wang, X. Mei, L. Huang, Q. Zheng, Y. Qiao, K. Zang, S. Mao, R. Yang, Z. Zhang, Y. Gao, Z. Guo, Z. Huang and Q. Wang, *J. Energy Chem.* **2015**, 24, 127-137; c) L. Huang, J. Wang, Y. Gao, Y. Qiao, Q. Zheng, Z. Guo, Y. Zhao, D. O'Hare and Q. Wang, *J. Mater. Chem. A* **2014**, 2, 18454-18462; d) Q. Wang, H. H. Tay, Z. Zhong, J. Luo and A. Borgna, *Energy Environ. Sci.* **2012**, 5, 7526-7530; e) R. Quinn, R. J. Kitchoff, J. R. Hufton and T. C. Golden, *Ind. Eng. Chem. Res.* **2012**, 51, 9320-9327; f) Q. Wang, J. Luo, Z. Zhong and A. Borgna, *Energy Environ. Sci.* **2011**, 4, 42-55.
- [6] L. Barelli, G. Bidini and F. Gallorini, *Applied Energy* **2015**, 143, 110-118.
- [7] a) B. Dou, B. Jiang, Y. Song, C. Zhang, C. Wang, H. Chen, B. Du and Y. Xu, *Fuel* **2016**, 166, 340-346; b) G.-h. Xiu, P. Li and A. E. Rodriguesa, *Chem. Eng. Sci.* **2002**, 57 3893 - 3908.
- [8] a) M. Shokrollahi Yancheshmeh, H. R. Radfarnia and M. C. Iliuta, *Chem. Eng. J.* **2016**, 283, 420-444; b) D. P. Harrison, *Ind. Eng. Chem. Res.* **2008**, 47, 6486-6501.
- [9] a) C. Dang, H. Yu, H. Wang, F. Peng and Y. Yang, *Chem. Eng. J.* **2016**, 286, 329-338; b) B. Dou, C. Wang, H. Chen, Y. Song and B. Xie, *Int. J. Hydrogen Energy* **2013**, 38, 11902-11909.
- [10] D. M. Anderson, M. H. Nasr, T. M. Yun, P. Kottke and A. G. Fedorov, *Ind. Eng. Chem. Res.* **2015**, 54, 8422-8436.
- [11] a) P. D. Cobden, P. van Beurden, H. T. J. Reijers, G. D. Elzinga, S. C. A. Kluiters, J. W. Dijkstra, D. Jansen and R. W. van den Brink, *Int. J. Greenh. Gas Control* **2007**, 1, 170-179; b) M. G. Plaza, C. Pevida, B. Arias, M. D. Casal, C. F. Martí, J. Fermoso, F. Rubiera and J. J. Pis, *J. Environ. Eng.* **2009**, 135, 426-432.
- [12] a) J. Blamey, E. J. Anthony, J. Wang and P. S. Fennell, *Prog. Energy Combust. Sci.* **2010**, 36, 260-279; b) M. E. Boot-Handford, J. C. Abanades, E. J. Anthony, M. J. Blunt, S. Brandani, N. Mac Dowell, J. R. Fernández, M.-C. Ferrari, R. Gross and J. P. Hallett, *Energy Environ. Sci.* **2014**, 7, 130-189; c) M. Alonso, N. Rodríguez, B. González, B. Arias and J. C. Abanades, *Ind. Eng. Chem. Res.* **2011**, 50, 6982-6989; d) P. Xu, M. Xie, Z. Cheng and Z. Zhou, *Ind. Eng. Chem. Res.* **2013**, 52, 12161-12169; e) C. Luo, Y. Zheng, C. Zheng, J. Yin, C. Qin and B. Feng, *Int. J. Greenh. Gas Control* **2013**, 12, 193-199; f) F.-Q. Liu, W.-H. Li, B.-C. Liu and R.-X. Li, *J. Mater. Chem. A* **2013**, 1, 8037-8044; g) V. Manovic and E. J. Anthony, *Ind. Eng. Chem. Res.* **2010**, 49, 6916-6922; h) W. Liu, B. Feng, Y. Wu, G. Wang, J. Barry and J. C. D. Diniz da Costa, *Environ. Sci. Technol.* **2010**, 44, 3093-3097; i) N. J. Amos, M. Widywati, S. Kureti, D. Trimis, A. I. Minett, A. T. Harris and T. L. Church, *J. Mater. Chem. A* **2014**, 2, 4332-4339; j) C.-C. Li, U.-T. Wu and H.-P. Lin, *J. Mater. Chem. A* **2014**, 2, 8257-8257; k) M. Zhao, M. Bilton, A. P. Brown, A. M. Cunliffe, E. Dvininov, V. Dupont, T. P. Comyn and S. J. Milne, *Energy Fuels* **2014**, 28, 1275-1283; l) P. Sanchez-Jimenez, L. A. Perez-Maqueda and J. Valverde, *Appl. Energy* **2014**, 118, 92-99.
- [13] a) K. B. Yi and D. Ø. Eriksen, *Sep. Sci. Technol.* **2006**, 41, 283-296; b) E. Ochoa-Fernandez, M. Rønning, T. Grande and D. Chen, *Chem. Mater.* **2006**, 18, 1383-1385; c) Q. Xiao, Y. Liu, Y. Zhong and W. Zhu, *J. Mater. Chem.* **2011**, 21, 3838-3842; d) D. B. Jiménez, M. A. E. Bretado, D. L. Gutiérrez, J. M. S. Gutiérrez, A. L. Ortiz and V. Collins-Martínez, *Int. J. Hydrogen Energy* **2013**, 38, 2557-2564; e) Y. Duan, *Phys. Chem. Chem. Phys.* **2013**, 15, 9752-9760.
- [14] a) M. Seggiani, M. Puccini and S. Vitolo, *Int. J. Greenh. Gas Control* **2013**, 17, 25-31; b) M. Kato, S. Yoshikawa and K. Nakagawa, *J. Mater. Sci. Lett.* **2002**, 21, 485-487; c) K. Essaki, M. Kato and H. Uemoto, *J. Mater. Sci.* **2005**, 40, 5017-5019; d) E. Ochoa-Fernández, T. Zhao, M. Rønning and D. Chen, *J. Environ. Eng.* **2009**, 135, 397-403; e) R. Pacciani, J. Torres, P. Solsona, C. Coe, R. Quinn, J. Hufton, T. Golden and L. Vega, *Environ. Sci. Technol.* **2011**, 45, 7083-7088; f) V. L. Mejía-Trejo, E. Fregoso-Israel and H. Pfeiffer, *Chem. Mater.* **2008**, 20, 7171-7176; g) F. Durán-Muñoz, I. C.

## FULL PAPER

- Romero-Ibarra and H. Pfeiffer, *J. Mater. Chem. A* **2013**, *1*, 3919-3925; h) Y. Duan, H. Pfeiffer, B. Li, I. C. Romero-Ibarra, D. C. Sorescu, D. R. Luebke and J. W. Halley, *Phys. Chem. Chem. Phys.* **2013**, *15*, 13538-13558.
- [15] J. Wang, L. Huang, R. Yang, Z. Zhang, J. Wu, Y. Gao, Q. Wang, D. O'Hare and Z. Zhong, *Energy Environ. Sci.* **2014**, *7*, 3478-3518.
- [16] a) W. Zhang, Y. Li, L. Duan, X. Ma, Z. Wang and C. Lu, *Chemical Engineering Research and Design* **2016**, *109*, 806-815; b) J. M. Valverde, P. E. Sanchez-Jimenez and L. A. Perez-Maqueda, *Applied Energy* **2014**, *136*, 347-356.
- [17] A.-M. Cormos and A. Simon, *Applied Thermal Engineering* **2015**, *80*, 319-327.
- [18] V. Tomkute, A. Solheim, S. Sakirzanovas and E. Olsen, *Energy Science & Engineering* **2016**, *4*, 205-216.
- [19] T. Harada, F. Simeon, E. Z. Hamad and T. A. Hatton, *Chem. Mater.* **2015**, *27*, 1943-1949.
- [20] V. Tomkute, A. Solheim and E. Olsen, *Energy Fuels* **2014**, *28*, 5345-5353.
- [21] FactSage FTsalt Salt Database List of Systems and Phases,  
[http://www.factsage.cn/fact/documentation/FTsalt/FTsalt\\_list.htm](http://www.factsage.cn/fact/documentation/FTsalt/FTsalt_list.htm).
- [22] N. Phalak, N. Deshpande and L. S. Fan, *Energy Fuels* **2012**, *26*, 3903-3909.
- [23] Y. Wu, J. Blamey, E. J. Anthony and P. S. Fennell, *Energy Fuels* **2010**, *24*, 2768-2776.
- [24] J. W. Butler, C. J. Lim and J. R. Grace, *Chem. Eng. Res. Des.* **2011**, *89*, 1794-1804.
- [25] N. N. Hlaing, S. Sreekantan, R. Othman, H. Hinode, W. Kurniawan, A. A. Thant, A. R. Mohamed and C. Salim, *Materials Letters* **2014**, *133*, 204-207.
- [26] a) S. Dong and Y. Wang, *Water Res.* **2016**, *88*, 852-860; b) G. Song, X. Zhu, R. Chen, Q. Liao, Y.-D. Ding and L. Chen, *Chem. Eng. J.* **2016**, *283*, 175-183; c) D. Lee, *Chem. Eng. J.* **2004**, *100*, 71-77.
- [27] R. Kopelman, *Science* **1988**, *241*, 1620-1626.
- [28] M. Haerifai and S. Azizian, *J. Phys. Chem. C* **2014**, *118*, 1129-1134.
- [29] A. de la Calle Martos, J. M. Valverde, P. E. Sanchez-Jimenez, A. Perejon, C. Garcia-Garrido and L. A. Perez-Maqueda, *Phys Chem Chem Phys* **2016**, *18*, 16325-16336.
- [30] A. M. Kierzkowska, R. Pacciani and C. R. Muller, *ChemSusChem* **2013**, *6*, 1130-1148.
- [31] A. Kurlov, M. Broda, D. Hosseini, S. J. Mitchell, J. Perez-Ramirez and C. R. Muller, *ChemSusChem* **2016**, *9*, 2380-2390.

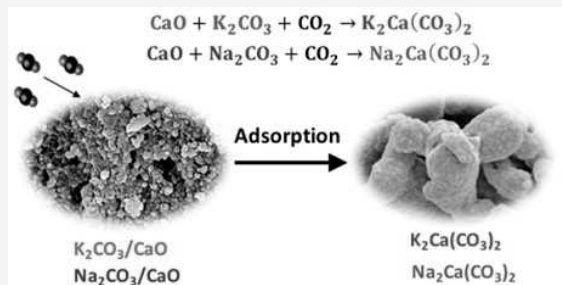
# Development of Potassium- and Sodium-Promoted CaO Adsorbents for CO<sub>2</sub> Capture at High Temperatures

Ahmed Al-Mamoori, Harshul Thakkar, Xin Li, Ali A. Rownaghi,<sup>ID</sup> and Fateme Rezaei\*<sup>ID</sup>

Department of Chemical & Biochemical Engineering, Missouri University of Science and Technology, 1101 N State Street, Rolla, Missouri 65409, United States

## Supporting Information

**ABSTRACT:** Development of highly efficient adsorbents for the high temperature CO<sub>2</sub> capture process is crucial for large scale implementation of this technology. In this work, development of novel potassium- and sodium-promoted CaO adsorbents (K–Ca and Na–Ca) is discussed, and their CO<sub>2</sub> capture performance at high temperatures is presented. A series of K–Ca and Na–Ca adsorbents with various K/Ca or Na/Ca molar ratios were developed and tested for CO<sub>2</sub> capture at high temperatures ranging from 300 to 400 °C. The structural, chemical, and morphological characteristics of the double salts were systematically evaluated before and after exposure to CO<sub>2</sub>. Our results indicated that CO<sub>2</sub> capacity is largely influenced by both K or Na concentration and adsorption temperature. Maximum capacities of 3.8 and 3.2 mmol/g were obtained for K–Ca and Na–Ca double salts, respectively, at 375 °C and 1 bar. Further investigation of the effect of temperature revealed that the window temperature for operation ranges from 300 to 650 °C, while beyond 650 °C, the double salts start to decompose and lose capacity. Moreover, it was found that both adsorption kinetics and capacity improve with temperature, with CO<sub>2</sub> uptake reaching a maximum at 10.7 mmol/g at 650 °C over K–Ca double salt. This study represents alkali metal-promoted CaO adsorbents as potential high-temperature adsorbents with similar performance to their MgO-based analogues.



## 1. INTRODUCTION

CO<sub>2</sub> emissions are continuously increasing due to ever increasing energy demand and population growth. Climate change that has recently affected various places around the world is a result of such excessive emissions which necessitates extensive effort to alleviate the greenhouse gas emissions. One of the most promising technologies to mitigate CO<sub>2</sub> emissions is adsorption due to its easy installation, relatively low cost, and low required energy, in comparison to the benchmark amine scrubbing process.<sup>1–3</sup> Recently, CO<sub>2</sub> adsorption at high temperature has attracted a great deal of attention since it offers various opportunities in processes such as sorption enhanced reaction (SER) and integrated gasification combined cycle (IGCC).<sup>4,5</sup> Additionally, there is no need to cool flue gas to ambient temperature and thus lose a lot of energy.<sup>6</sup> Furthermore, development of high temperature adsorbents for simultaneous CO<sub>2</sub> capture and conversion process in which CO<sub>2</sub> is first separated from flue gas and then is converted to commodity chemicals or fuels has recently gained interest among researchers worldwide.<sup>1,7</sup> However, selecting a suitable adsorbent is still challenging due to the high capacity, stability, selectivity, and fast adsorption/desorption kinetics requirements.<sup>8</sup> In addition to these criteria, the adsorbents are required to be practical, inexpensive, and regenerable.

To this end, there has been a wide variety of porous materials developed for CO<sub>2</sub> capture at both low and high temper-

atures.<sup>9–14</sup> Among solid adsorbents investigated so far, only a few materials such as calcium oxide (CaO), hydrotalcite (HT), calcium chabazite (CHA), alumina, and a few mixed-metal oxides have demonstrated favorable characteristics at elevated temperatures.<sup>8,15–18</sup> In large-scale CO<sub>2</sub> capture applications, CaO is advantageous compared to other adsorbents on account of higher capture capacity (~17.9 mmol/g at above 600 °C), low cost, and wide availability of precursors such as limestones or dolomites;<sup>15,19–21</sup> however, high temperature regeneration (i.e., above 800 °C) and low stability due to sintering could outweigh these benefits. Additionally, slow sorption kinetics due to the formation of CaCO<sub>3</sub> which results in limited CO<sub>2</sub> diffusion is another challenge associated with the practical use of CaO-based adsorbents.<sup>17</sup> The HTs, also known as layered double hydroxides (LDH), are composed of positively charged brucite-like layers with trivalent cations partially substituting divalent cations. This class of adsorbents shows good stability in the presence of water vapor and enhanced capacity when impregnated with alkali metals.<sup>19,22–25</sup> Despite these noticeable advantages, their relatively low capacity is still challenging for industrial applications.<sup>22</sup> Recently, Kim et al.<sup>26</sup> reported a high

Received: April 15, 2017

Revised: June 23, 2017

Accepted: July 7, 2017

Published: July 7, 2017

$\text{CO}_2$  uptake (ca. 9.27 mmol/g) over HT at 240 °C and 1 bar, but the capacity dropped dramatically to below 3.0 mmol/g after 16 cycles. CHA consists of double-six ring (D6R) units arranged in layers that are linked together by tilted 4-membered rings and is capable of yielding high  $\text{CO}_2$  selectivity due to the molecular sieving effect.<sup>8,27,28</sup> To enhance  $\text{CO}_2$  capacity of CHA, ion exchange can be done with Na, Ca, K, Mg, Li, and Ba ions.<sup>28,29</sup>

Development of more efficient adsorbents is needed for  $\text{CO}_2$  capture at high temperatures (i.e., 300–400 °C). Recent works have demonstrated the potential of double salts for effectively capturing  $\text{CO}_2$  with reasonable stability.<sup>18,26,30–34</sup> Harada and Hatton<sup>30</sup> prepared colloidal nanoclusters of  $\text{MgO}$  coated with Li, Na, and K nitrates/nitrites with various salts loadings and showed that both  $\text{CO}_2$  uptake and adsorbent regenerability can be enhanced by introduction of nitrite salts to the coating layer of  $\text{MgO}$  particles through the formation of magnesium nitro or nitrate species. In another investigation, Lee et al.<sup>18</sup> studied the effect of pH on double salt potassium based magnesium K–Mg by using different precursors for potassium (KOH/ $\text{K}_2\text{CO}_3$ ). The authors showed that  $\text{CO}_2$  capacity improves upon increasing pH of the potassium precursor. They also reported that K–Mg double salt has a rapid adsorption/desorption kinetics. Lee et al.<sup>33</sup> prepared a Na–Mg double salt by precipitation method and investigated for  $\text{CO}_2$  capture. The authors reported a relatively high  $\text{CO}_2$  uptake (3.48 mmol/g), good stability, and quick sorption kinetics at 375 °C and 1 bar.

Most of the double salts adsorbents investigated so far are based on  $\text{MgO}$  coated or doped with molten salts of alkali earth metals such as lithium, sodium, or potassium. Most recently, Huang et al.<sup>35</sup> reported development and evaluation of sorption performance of a series of alkali carbonate molten salt-coated  $\text{CaO}$  adsorbents. On the basis of their experimental results, the authors concluded that  $(\text{Li}-\text{K})_2\text{CO}_3$  molten salt coating not only enhances  $\text{CO}_2$  uptake, but also facilitates the  $\text{CO}_2$  desorption from  $\text{CaO}$ . They correlated this uptake enhancement to the role of coated molten salts in preventing the formation of a rigid  $\text{CaCO}_3$  layer on the surface of  $\text{CaO}$  particles and providing a continuous delivery of  $\text{CO}_3^{2-}$  to promote  $\text{CO}_2$  capture. Generally,  $\text{MgO}$ -based adsorbents exhibit much lower capacity at higher temperatures (>400 °C) than  $\text{CaO}$ -based double salts, and thus they are suitable for use at milder temperatures. On the other hand, although  $\text{CaO}$ -based adsorbents exhibit improved uptake with increasing temperature, they suffer from sintering during regeneration, as stated above, displaying reduction in their cyclic capacity. Significant efforts have been put forth to overcome this issue including the use of a porous support for  $\text{CaO}$  particles, the use of other naturally occurring precursors instead of limestone, or obtaining  $\text{CaO}$  from sintering-resistant precursors, among others.<sup>36,37</sup>

Motivated by the search for a better high-temperature  $\text{CO}_2$  adsorbent and the need for an active adsorbent as a catalyst support that could be used in simultaneous  $\text{CO}_2$  capture and conversion process, the objective of this study was to develop practical adsorbents that could be used in hybrid  $\text{CO}_2$  capture (from flue gas) and conversion process at high temperatures (i.e., 300–400 °C). More specifically, this work focused on development of a series of double salts such as potassium-promoted calcium (K–Ca) and sodium-promoted calcium (Na–Ca) adsorbents for  $\text{CO}_2$  capture that could later be used for development of hybrid adsorbent-catalyst materials.

## 2. EXPERIMENTAL SECTION

**2.1. Preparation of Double Salts.** **2.1.1. Double Salts K–Ca.** Potassium-promoted calcium oxide adsorbents were prepared according to the procedure described in the literature.<sup>18</sup> Briefly, a desired amount of potassium carbonate ( $\text{K}_2\text{CO}_3$ ) was added to the appropriate volume of distilled water. Potassium hydroxide (KOH) dissolved in distilled water was then added to the  $\text{K}_2\text{CO}_3$  solution. In the next step, the new solution was added dropwise to the calcium nitrate tetrahydrate ( $\text{Ca}(\text{NO}_3)_2 \cdot 4\text{H}_2\text{O}$ ) dissolved in distilled water. The final solution was stirred for 1 h at 700 rpm and allowed to settle down. After that, the precipitated particles were filtered using vacuum filtration, then dried in the oven overnight at 120 °C, and finally calcined at 700 °C for 5 h with ramping step of 10 °C/min. The molar ratios of the precursors are presented in Table 1. The samples were labeled as K–Ca-1, K–Ca-2, and K–Ca-3.

Table 1. K–Ca Double Salts Composition

name	K/Ca mol ratio	$\text{K}_2\text{CO}_3$ weight (g)	KOH weight (g)	$\text{Ca}(\text{NO}_3)_2 \cdot 4\text{H}_2\text{O}$ weight (g)
K–Ca-1	3.3	12.09	0.79	41.33
K–Ca-2	6.7	24.19	1.57	41.33
K–Ca-3	10	36.28	2.36	41.33

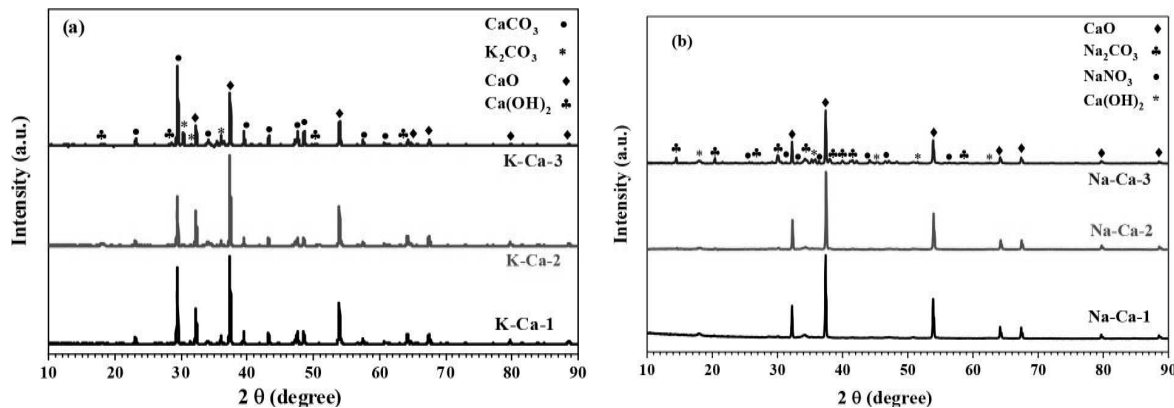
**2.1.2. Double Salts Na–Ca.** Sodium-promoted calcium oxide adsorbents were synthesized according to a previously reported procedure.<sup>33</sup> Briefly, 8.1 g of  $\text{Ca}(\text{NO}_3)_2 \cdot 4\text{H}_2\text{O}$  was dissolved in 100 mL of distilled water, and then the desired amounts of sodium carbonate ( $\text{Na}_2\text{CO}_3$ ) were added gradually to the solution and stirred for 1 h at 500 rpm. In the next step, the solution was allowed to precipitate and then dried at 110 °C overnight before calcination at 700 °C for 3 h with ramping step of 10 °C/min. The samples were labeled as Na–Ca-1, Na–Ca-2, and Na–Ca-3 with the compositions shown in Table 2.

Table 2. Na–Ca Double Salts Composition

name	Na/Ca mol ratio (%)	$\text{Na}_2\text{CO}_3$ weight (g)	$\text{Ca}(\text{NO}_3)_2 \cdot 4\text{H}_2\text{O}$ weight (g)
Na–Ca-1	2.8	10	8.1
Na–Ca-2	4.2	15	8.1
Na–Ca-3	5.6	20	8.1

**2.2. Characterization of Double Salts.** Phase analysis of adsorbents before and after  $\text{CO}_2$  exposure was performed by XRD experiments using PANalytical X'Pert multipurpose X-ray diffractometer with scan step size of 0.02°/step at the rate of 147.4 s/step. Surface area and total pore volume of the adsorbents were estimated from  $\text{N}_2$  physisorption data obtained by measurements performed on a Micromeritics 3Flex gas analyzer at 77 K. FT-IR experiments were carried out on a Nicolet Nexus 470 optical bench. For FT-IR measurements, around 1 mg of sample was mixed with 100 mg of KBr and pressed to pellets for analysis. Hitachi S4700 field emission scanning electron microscopy (SEM) was used to evaluate the structural morphology of double salt adsorbents before and after  $\text{CO}_2$  adsorption.

**2.3.  $\text{CO}_2$  Adsorption Isotherm Measurements.**  $\text{CO}_2$  adsorption isotherms were collected on the 3Flex at different temperatures. For the isotherm measurements, the samples



**Figure 1.** XRD patterns of (a) K–Ca double salts and (b) Na–Ca double salts.

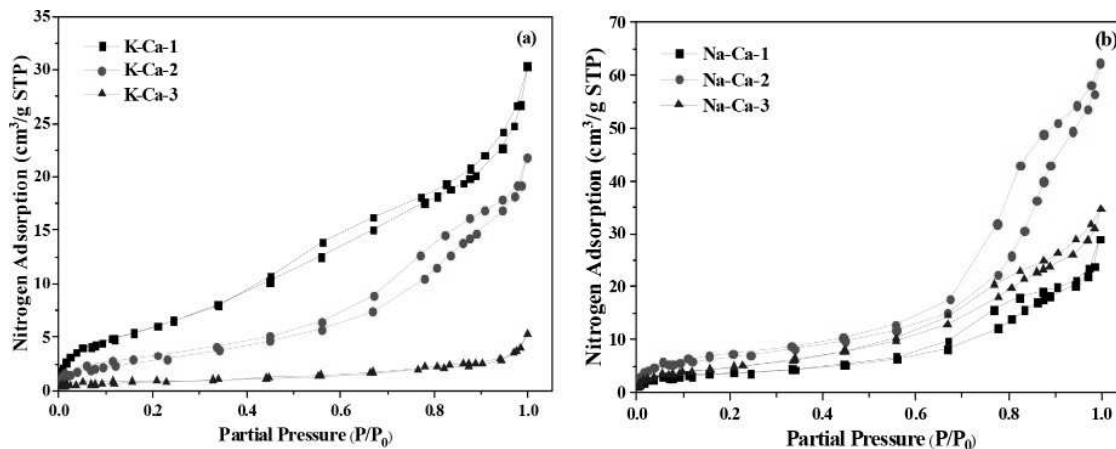


**Figure 2.**  $\text{N}_2$  physisorption isotherms for (a) K–Ca and (b) Na–Ca double salts.

were first degassed at 450 °C for 2 h under vacuum. The isotherms were collected at 300, 350, and 375 °C. In addition, TGA (Q500, TA Instruments) was utilized to analyze  $\text{CO}_2$  adsorption over time and to perform cyclic measurements. For the TGA measurements, the temperature was first ramped from ambient temperature to 450 °C at the rate of 10 °C/min under  $\text{N}_2$  flow to degas the samples before exposure to a gas mixture containing 10%  $\text{CO}_2$  in  $\text{N}_2$  at a desired adsorption temperature.

### 3. RESULTS AND DISCUSSION

**3.1. Characterization and Adsorption Performance of Double Salts.** Figure 1a,b shows the comparison of XRD spectra for three K–Ca and three Na–Ca double salts. It is clear from Figure 1a that the main components of K–Ca adsorbents are  $\text{CaO}$ ,  $\text{K}_2\text{CO}_3$ ,  $\text{CaCO}_3$ , and  $\text{Ca}(\text{OH})_2$ , whereas the XRD spectra in Figure 1b indicate that the main components of Na–Ca adsorbents are  $\text{CaO}$ ,  $\text{Na}_2\text{CO}_3$ ,  $\text{NaNO}_3$ , and  $\text{Ca}(\text{OH})_2$ . It should also be noted that by increasing the K/Ca molar ratio the intensity of  $\text{K}_2\text{CO}_3$  peaks increased, while similarly, a higher Na/Ca molar ratio resulted in higher intensity of  $\text{NaNO}_3$  and  $\text{Na}_2\text{CO}_3$  characteristic peaks. The components  $\text{CaCO}_3$  and  $\text{NaNO}_3$  were formed after the thermal treatment (calcination) of the samples at 700 °C. Also for both cases, a small amount of  $\text{Ca}(\text{OH})_2$  was formed at higher K/Ca or Na/Ca molar ratio. These XRD results confirm the successful formation of K–Ca and Na–Ca double salts.

The characteristic peaks of bare (unpromoted)  $\text{CaO}$  can also be observed in Figure S1 (Supporting Information).

Figure 2a,b shows  $\text{N}_2$  physisorption profiles of the K–Ca and Na–Ca double salts. These physisorption profiles show noticeable  $\text{N}_2$  uptake at partial pressures greater than 0.6 ( $P/P_0 > 0.6$ ), which indicates the presence of mesopores in the structure of the samples. Furthermore, the hysteresis loop confirms the presence of large void spaces between the crystals in double salts. For K–Ca materials, increasing the K concentration resulted in a decrease in  $\text{N}_2$  uptake, whereas for Na–Ca adsorbents, the  $\text{N}_2$  uptake first exhibited a sharp increase followed by a drop upon increasing the concentration of Na. These  $\text{N}_2$  physisorption isotherms obtained for K–Ca double salts are similar to the previously reported results for K–Mg materials which exhibited the decrease in porosity with increasing the K/Mg concentration ratio.<sup>38,39</sup>

Table 3 shows the BET surface area ( $\text{m}^2/\text{g}$ ), total pore volume ( $\text{cm}^3/\text{g}$ ) of the materials estimated at a partial pressure of 0.99, and pore size values obtained from  $\text{N}_2$  physisorption isotherms. It can be noted that, upon increasing the amount of K, the surface area and pore volume decreased from respectively, 24  $\text{m}^2/\text{g}$  and 0.04  $\text{cm}^3/\text{g}$  for K–Ca-1 to 3  $\text{m}^2/\text{g}$  and 0.01  $\text{cm}^3/\text{g}$  for K–Ca-3. On the contrary, upon increasing Na content, both surface area and pore volume increased respectively, from 12  $\text{m}^2/\text{g}$  and 0.04  $\text{cm}^3/\text{g}$  for Na–Ca-1 to 18  $\text{m}^2/\text{g}$  and 0.05  $\text{cm}^3/\text{g}$  for Na–Ca-3. K–Ca-2 and Na–Ca-2 exhibited respectively, a surface area of 11 and 24  $\text{m}^2/\text{g}$ , a pore

**Table 3.** N<sub>2</sub> Physisorption Data for K–Ca-2 and Na–Ca-2 Adsorbents

adsorbent	<i>S</i> <sub>BET</sub> (m <sup>2</sup> /g)	pore volume (cm <sup>3</sup> /g)	pore size (nm)
K–Ca-1	24	0.04	5
K–Ca-2	11	0.03	7
K–Ca-3	3	0.01	10
Na–Ca-1	12	0.04	8
Na–Ca-2	24	0.09	9
Na–Ca-3	18	0.05	7

volume of 0.03 and 0.09 cm<sup>3</sup>/g, and an average pore size of 7 and 9 nm. Moreover, for bare CaO, a BET surface area of 312 m<sup>2</sup>/g and a pore volume of 0.32 cm<sup>3</sup>/g were obtained, and as it is clear from the data in Table 3, upon CaO promotion with K and Na, both surface area and pore volume decreased drastically compared to unpromoted CaO. Similar behavior was reported for MgO-based double salts.<sup>38</sup>

The CO<sub>2</sub> adsorption isotherms obtained at 375 °C for three K–Ca and three Na–Ca double salts are presented in Figure 3a,b. In both cases, the double salt with the lowest amount of K or Na (K–Ca-1 and Na–Ca-1) exhibited the lowest CO<sub>2</sub> uptake. Also, it can be observed that, by increasing the K and Na composition, the CO<sub>2</sub> adsorption increased first (for K–Ca-2 and Na–Ca-2) and then experienced a decreasing trend upon further increase of the K and Na contents (for K–Ca-3 and Na–Ca-3). These results are in agreement with Zhang et al.<sup>32</sup> Moreover, Huang et al.<sup>35</sup> observed the same behavior and correlated the strong dependence of CO<sub>2</sub> uptake on the molar ratio of the (Li–K)<sub>2</sub>CO<sub>3</sub>/CaO salts to the dependency of melting points of (Li–K)<sub>2</sub>CO<sub>3</sub> on different Li/K ratios. Similarly, we can argue here that, for intermediate molar ratios (i.e., K–Ca-2 and Na–Ca-2), the melting point of K<sub>2</sub>CO<sub>3</sub> or Na<sub>2</sub>CO<sub>3</sub> was likely lower than that of samples with other molar ratios. According to Harada et al.,<sup>40</sup> for double salt adsorbents, CO<sub>2</sub> uptake can only be promoted at adsorption temperatures above the melting points of the molten salts coating the particles. This suggests that low and high K/Na content samples for each class (1 and 3) have melting points above 375 °C. It should also be mentioned here that, as a control experiment, we measured the CO<sub>2</sub> uptake over bare (unpromoted) CaO, and as Figure S2 (Supporting Information) shows, the adsorption capacity was very low compared

with the K- and Na-promoted CaO, reaching 0.4 mmol/g, as also shown by other researchers.<sup>35</sup>

Moreover, in both cases a general trend could be observed where the uptake increases sharply at lower pressures up to 0.02 bar followed by a gradual increase over higher pressures until 1 bar. For K–Ca-2, the CO<sub>2</sub> capacity reached 3.8 mmol/g, and for Na–Ca-2, the capacity was found to be 3.2 mmol/g at 1 bar. Lee et al.<sup>33</sup> reported a CO<sub>2</sub> uptake of 3.48 mmol/g over Na–Mg double salt at the same temperature and pressure. For the rest of analysis, we picked K–Ca-2 and Na–Ca-2 double salts that exhibited the highest adsorption uptake among their adsorbent counterparts.

### 3.2. Adsorption Performance of K–Ca-2 and Na–Ca-2.

The effect of adsorption temperature on CO<sub>2</sub> uptake over K–Ca-2 and Na–Ca-2 double salts is demonstrated in Figure 4a,b. It can be seen that, as the temperature increased from 300 to 375 °C, the uptake increased dramatically from 0.6 to 3.8 mmol/g for K–Ca-2 and from 1.1 to 3.2 mmol/g for Na–Ca-2 at 1 bar. The higher uptake at higher temperatures could be attributed to the formation of more carbonates that contribute more toward the adsorption of CO<sub>2</sub> molecules. Huang et al.<sup>35</sup> reported the same behavior for Li–K-promoted CaO, for which the capacity increased from 4.9 to 10.6 mmol/g upon temperature rise from 400 to 700 °C. For Mg-based materials, although a similar increasing trend has been reported,<sup>18</sup> the operating window is narrower and the uptake starts to decrease at temperatures above 400 °C.

Comparing the XRD patterns of the K–Ca-2 adsorbent before and after CO<sub>2</sub> adsorption at 375 °C in Figure 5a, it is apparent that no additional peaks were appeared after CO<sub>2</sub> capture; however, as can be clearly noted, the intensity of the calcium oxide (CaO) peaks decreased because of the reaction of calcium oxide with CO<sub>2</sub> while the intensity of the peaks corresponding to calcium hydroxide (Ca(OH)<sub>2</sub>) decreased. Further, the potassium calcium carbonate (K<sub>2</sub>Ca(CO<sub>3</sub>)<sub>2</sub>) phase formed after CO<sub>2</sub> exposure. For Na–Ca-2, investigating the XRD spectra presented in Figure 5b, it was found that the sodium calcium carbonate (Na<sub>2</sub>Ca(CO<sub>3</sub>)<sub>2</sub>) phase formed upon CO<sub>2</sub> adsorption, while like K–Ca-2, the remaining CaO peaks were weak. In addition, new peaks associated with CaCO<sub>3</sub> appeared confirming that the molten salts facilitate the formation of CaCO<sub>3</sub> during CO<sub>2</sub> adsorption. This however was not the case for K–Ca-2 mainly because the CaCO<sub>3</sub> phase

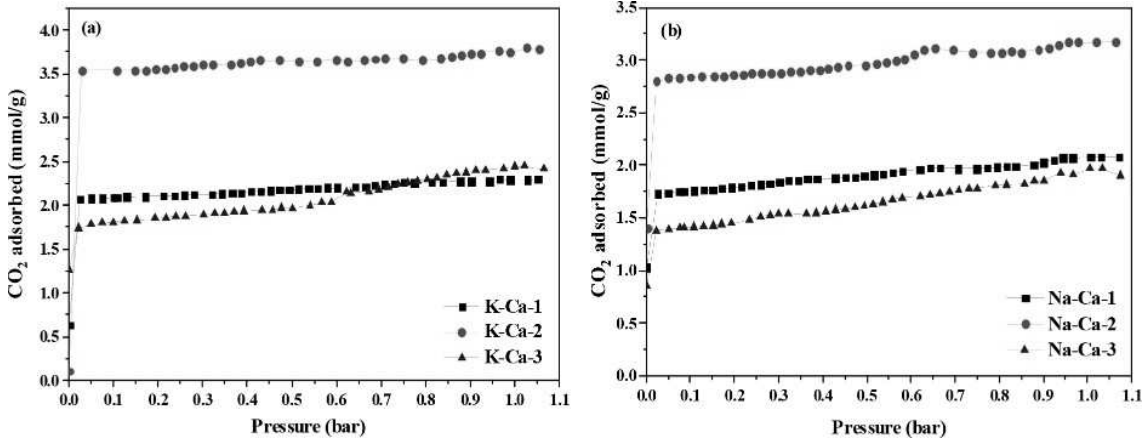


Figure 3. CO<sub>2</sub> adsorption isotherms for (a) K–Ca double salts and (b) Na–Ca double salts obtained at 375 °C.

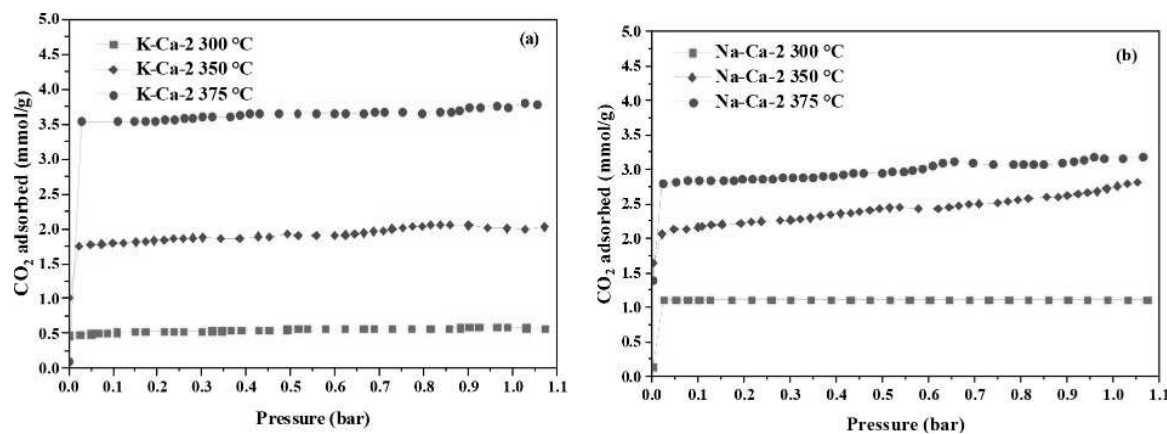


Figure 4. CO<sub>2</sub> adsorption isotherms for (a) K–Ca double salts and (b) Na–Ca double salts obtained at 375 °C.

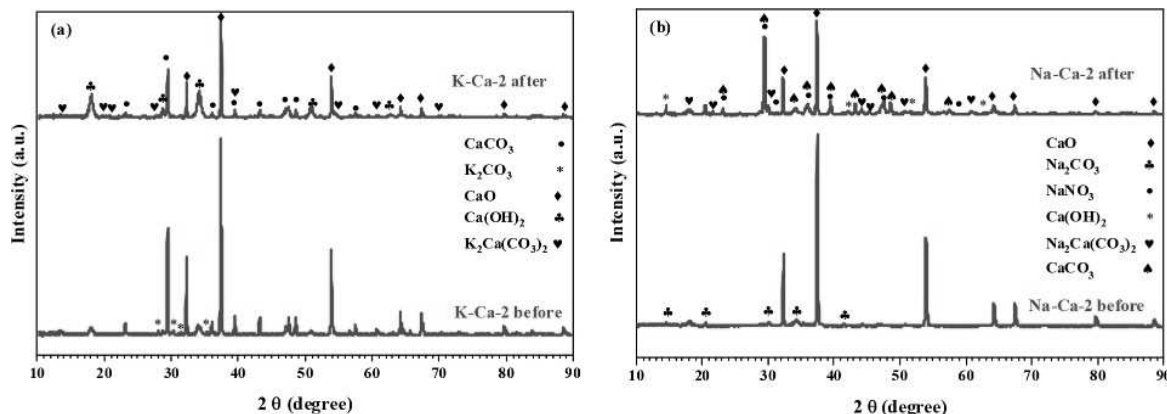


Figure 5. XRD patterns of (a) K–Ca-2 and (b) Na–Ca-2 before and after CO<sub>2</sub> exposure at 375 °C.

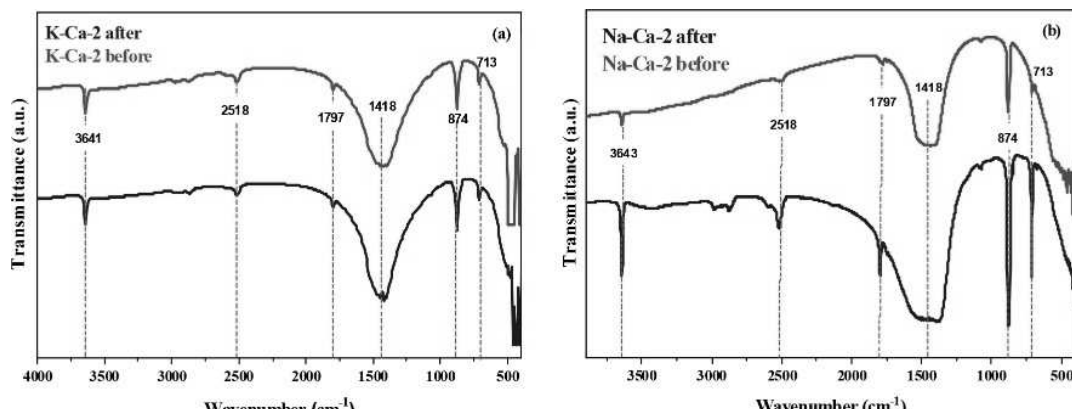


Figure 6. FT-IR spectra of (a) K–Ca-2 and (b) Na–Ca-2 before and after CO<sub>2</sub> exposure at 375 °C.

was present in the fresh material. The formation of K<sub>2</sub>Ca(CO<sub>3</sub>)<sub>2</sub> and Na<sub>2</sub>Ca(CO<sub>3</sub>)<sub>2</sub> is according to the following reactions on the K–Ca-2 and Na–Ca-2 double salts, respectively, as suggested by Lee et al.<sup>33</sup> for MgO-based materials:



The XRD spectra of unpromoted CaO before and after CO<sub>2</sub> adsorption are also presented in Figure S1 (Supporting Information). The appearance of several peaks related to CaCO<sub>3</sub> and Ca(OH)<sub>2</sub> was noticeable after CO<sub>2</sub> adsorption while the intensity of CaO characteristic peaks decreased in a similar fashion to the promoted samples.

To probe changes to the chemical properties of the double salts, the FT-IR spectra of the candidate double salts before and after CO<sub>2</sub> adsorption were compared. As Figure 6a,b demonstrates, both materials retained their chemical structure

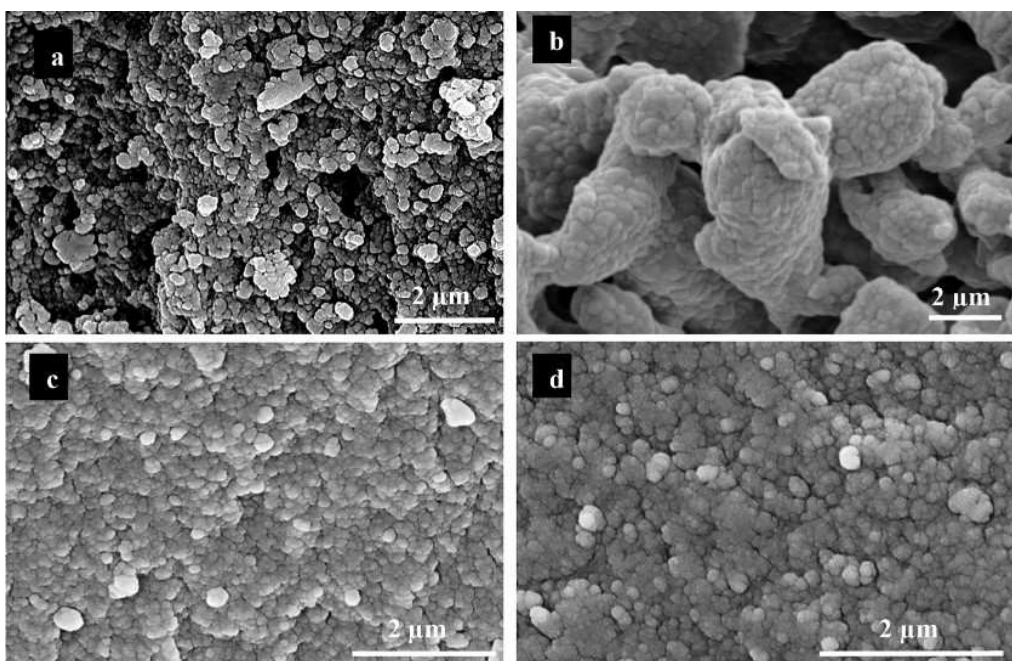


**Figure 7.** SEM images of (a and b) K–Ca-2 and (c and d) Na–Ca-2 before and after  $\text{CO}_2$  adsorption at 375 °C.

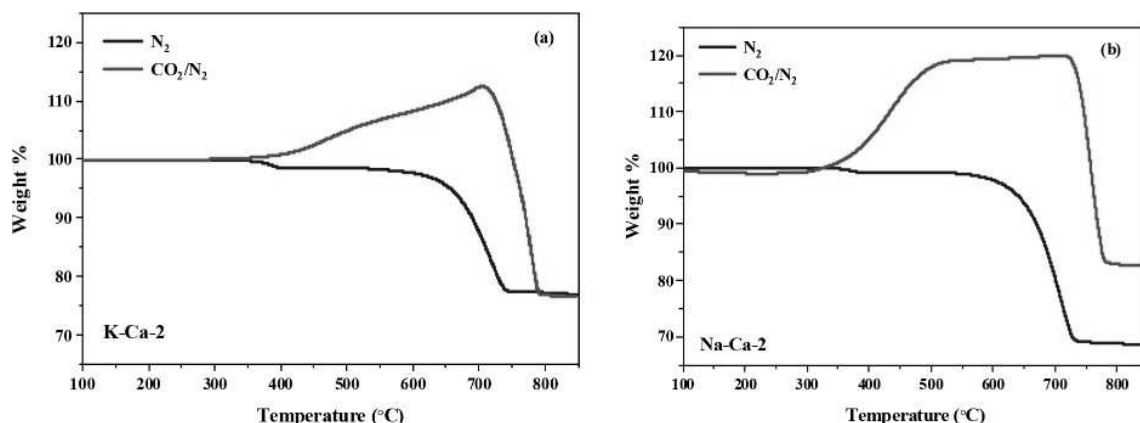


**Figure 8.** K–Ca-2 weight change of (a) K–Ca-2 and (b) Na–Ca-2 with increasing temperature under  $\text{N}_2$  and  $\text{CO}_2/\text{N}_2$  gas flow.

and displayed similar characteristic peaks before and after exposure to  $\text{CO}_2$ . The only noticeable change is the intensity of the characteristic peaks which was much stronger after  $\text{CO}_2$  adsorption confirming the formation of more  $\text{CaCO}_3$  on K- and Na-promoted double salts. Comparing the peak intensities of the K–Ca and Na–Ca after  $\text{CO}_2$  adsorption, it follows that the increase was more pronounced for Na–Ca-2 than for K–Ca-2, despite its lower uptake capacity. This could be explained by the fact that the fresh K–Ca-2 contains  $\text{CaCO}_3$  in its structure, as opposed to Na–Ca-2 (as confirmed by XRD results); hence, after  $\text{CO}_2$  adsorption, the intensity of the bands corresponding to the formation of carbonate is higher for Na–Ca-2.

The FT-IR spectra of K–Ca-2 and Na–Ca-2 after  $\text{CO}_2$  capture show clear peaks related to  $\text{CaCO}_3$  at 713, 874, 1484, 1797, and 2518  $\text{cm}^{-1}$ . The presence of these  $\text{CaCO}_3$  characteristic peaks are also noticeable in the spectrum of bare  $\text{CaO}$  after  $\text{CO}_2$  adsorption (Figure S3, Supporting Information). The bands at 1072 and 858  $\text{cm}^{-1}$  represent symmetric stretching and out-of-plane bending modes of the

carbonate ion, respectively,<sup>41</sup> whereas the peak at 713  $\text{cm}^{-1}$  represents in-plane bending mode of the carbonate ion.<sup>42</sup> Moreover, the broad peak at 1484  $\text{cm}^{-1}$  corresponds to stretching vibrations of C–O bonds, whereas the peaks at 1798 and 3641  $\text{cm}^{-1}$  are assigned to C=O and O–H bonds, respectively.<sup>42</sup>

The SEM images shown in Figure 7a–d reveal the morphology of the adsorbents before and after  $\text{CO}_2$  exposure to  $\text{CO}_2$  at 375 °C. For fresh materials, a relatively dense structure with less degree of agglomeration was found for both materials. Also, the particle size appeared to be uniform in both cases ranging from 100 to 200 nm. After  $\text{CO}_2$  exposure, the materials retained their porous structure and the particles were still well dispersed, although relatively large aggregates formed in the form of aggregated clusters with small cracks on their external surface, as can be seen from Figure 7b,d.

To identify the operating window for adsorption of  $\text{CO}_2$  over K–Ca and Na–Ca double salts, the mass degradation experiments were performed under the flow of  $\text{N}_2$  and 10%

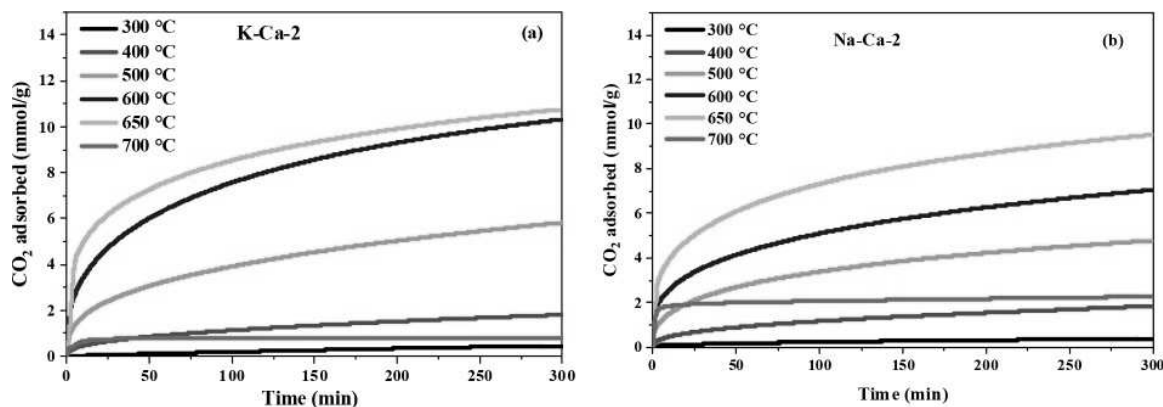


Figure 9.  $\text{CO}_2$  uptake over (a) K-Ca-2 and (b) Na-Ca-2 double salts as a function of temperature.

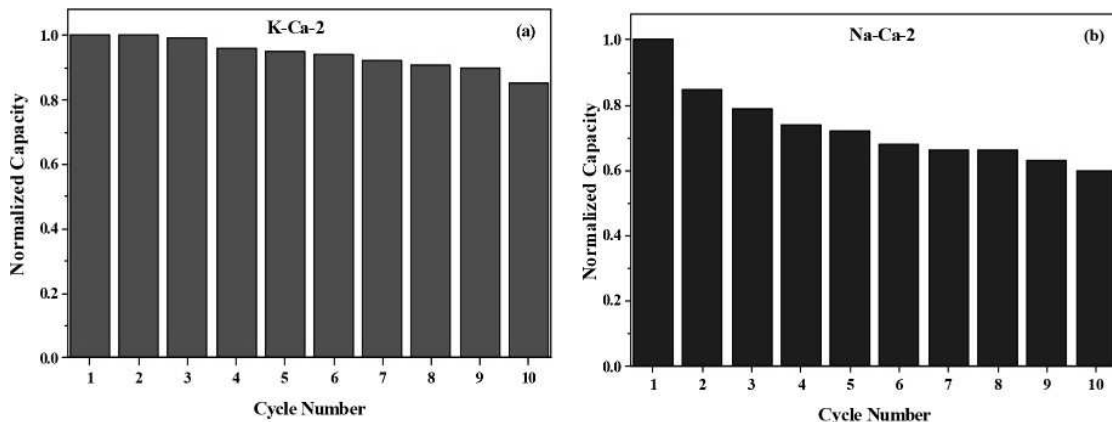


Figure 10. Normalized capacity of (a) K-Ca-2 and (b) Na-Ca-2 over 10 cycles of adsorption and desorption at 375 °C using 10%  $\text{CO}_2/\text{N}_2$ .

$\text{CO}_2/\text{N}_2$  (as simulated flue gas) using TGA. Figure 8a,b shows the weight change of K-Ca-2 and Na-Ca-2 over the temperature range of 100–800 °C. Under  $\text{N}_2$  flow, a significant weight loss (~22.5% for K-Ca and 32% for Na-Ca) was observed at temperatures above 600 °C, whereas under 10%  $\text{CO}_2/\text{N}_2$  gas flow, a  $\text{CO}_2$  adsorption region between 300 and 700 °C was observed, as characterized by the increase in the weight (~12 wt % for K-Ca and 20 wt % for Na-Ca), suggesting the window operation for  $\text{CO}_2$  capture. Above 700 °C, both K-Ca and Na-Ca adsorbents started to lose their capacity as a result of both  $\text{CO}_2$  desorption and materials degradation. Interestingly, Na-Ca-2 retained 82% of its original weight above 700 °C while K-Ca-2 showed 22.5% weight loss under 10%  $\text{CO}_2/\text{N}_2$  flow, similar to its weight loss under pure  $\text{N}_2$ .

The effect of adsorption temperature on adsorption kinetics and  $\text{CO}_2$  capacity of K-Ca-2 and Na-Ca-2 adsorbents is illustrated in Figure 9a,b. It can be noticed that the capacity increased as the temperature was raised from 300 to 650 °C. However, further increase to 700 °C resulted in dramatic capacity loss in both cases, mainly due to the decomposition of the materials, as discussed earlier. The maximum obtained  $\text{CO}_2$  uptakes were found to be 10.7 and 9.5 mmol/g for K-Ca-2 and Na-Ca-2, respectively, which were obtained at 650 °C after 300 min adsorption time. Notably, at higher temperatures, materials exhibited faster sorption kinetics by displaying a sharp increase in  $\text{CO}_2$  uptake at the beginning of the adsorption. For instance, at 650 °C, K-Ca-2 and Na-Ca-2 achieved ~43% of

their equilibrium capacities in the first 10 min of adsorption. A rapid initial uptake followed by slow adsorption over a longer time scale was also reported previously for K-Mg double salts.<sup>18</sup>

To further assess the stability of the K-Ca and Na-Ca double sites, cyclic adsorption measurements were performed using 10%  $\text{CO}_2/\text{N}_2$  at 375 °C. Figure 10a,b shows the  $\text{CO}_2$  capacities over 10 cycles for K-Ca-2 and Na-Ca-2 adsorbents. It is clear from these profiles that both adsorbents experienced a capacity loss over consecutive cycles; however, the loss was more pronounced for Na-Ca double salt. The K-Ca-2 double salt retained 85% of its initial capacity, whereas Na-Ca-2 experienced 37% capacity loss after the 10th cycle. The loss in  $\text{CO}_2$  capture capacity and rapid deactivation of CaO sorbents over multiple cycles is well-known and has been correlated to the sintering of CaO particles under high regeneration temperature.<sup>43,44</sup> For instance, Dean et al.<sup>43</sup> reported a ~40% capacity loss after 50  $\text{CO}_2$  capture-release cycles over CaO adsorbent.<sup>43</sup> Our results indicated that CaO promotion with K and Na positively affects the stability of CaO sorbents, especially in the case of K-Ca. Nonetheless, a much lower drop in capacity was reported for Na-Mg by Lee et al.<sup>33</sup> (only ~1% after seventh cycle) in comparison to Na-Ca (Figure 10b). Such higher capacity loss may be due to the sintering of CaO particles. Another reason could be due to rearrangement of the molten phase of  $\text{Na}_2\text{CO}_3$  in the adsorbent structure during the first cycle. This however requires more investigation to fully understand the cause for deteriorated cyclic capacity of

Na-promoted CaO adsorbents. Moreover, unlike K–Ca, a dramatic CO<sub>2</sub> uptake reduction (~40%) was reported for K–Mg after 10 adsorption/desorption cycles and the authors attributed this drop to the rearrangement of the molten phase of KNO<sub>3</sub> during the first cycle.<sup>18</sup>

## 4. CONCLUSIONS

This work illustrates development and evaluation of a series of inexpensive CaO-based adsorbents promoted by potassium and sodium carbonate salts for use in high temperature CO<sub>2</sub> capture process. The physical, chemical, and morphological properties of the adsorbents were assessed systematically and their CO<sub>2</sub> capture performance was evaluated taking into account the effects of K or Na concentration and adsorption temperature. It was shown that the K- and Na-prompted CaO adsorbents with optimum K/Ca and Na/Ca molar ratios exhibit relatively high capacity, fast kinetics, and good stability (in the case of K–Ca) at high temperatures. Our results highlighted the effectiveness of K–Ca and Na–Ca double salts in adsorption of CO<sub>2</sub> at temperatures above 300 °C. These materials could be used as suitable catalyst supports in the development of hybrid adsorbent-catalyst materials for use in simultaneous capture-conversion process. In that regard, future tasks should focus on improving their relatively low surface area, which could be achieved by supporting them on a high surface area support such as alumina or silica.

## ■ ASSOCIATED CONTENT

### Supporting Information

The Supporting Information is available free of charge on the ACS Publications website at DOI: 10.1021/acs.iecr.7b01587.

Additional materials including Figures S1–S3 as discussed in the text. (PDF)

## ■ AUTHOR INFORMATION

### Corresponding Author

\*E-mail: rezaeif@mst.edu.

### ORCID

Ali A. Rownaghi: 0000-0001-5228-5624

Fateme Rezaei: 0000-0002-4214-4235

### Notes

The authors declare no competing financial interest.

## ■ ACKNOWLEDGMENTS

This work was supported by the University of Missouri Research board (UMRB). The authors acknowledge the Material Research Center (MRC) at Missouri University of Science & Technology for SEM and XRD.

## ■ REFERENCES

- (1) Al-Mamoori, A.; Krishnamurthy, A.; Rownaghi, A. A.; Rezaei, F. Carbon Capture and Utilization Update. *Energy Technol.* **2017**, *5* (6), 834–849.
- (2) Chaffee, A. L.; Knowles, G. P.; Liang, Z.; Zhang, J.; Xiao, P.; Webley, P. A. CO<sub>2</sub> Capture by Adsorption: Materials and Process Development. *Int. J. Greenhouse Gas Control* **2007**, *1* (1), 11–18.
- (3) Rezaei, F.; Webley, P. Structured Adsorbents in Gas Separation Processes. *Sep. Purif. Technol.* **2010**, *70* (3), 243–256.
- (4) Hufton, J. R.; Mayorga, S.; Sircar, S. Sorption-Enhanced Reaction Process for Hydrogen Production. *AICHE J.* **1999**, *45* (2), 248–256.
- (5) Duyar, M. S.; Farrauto, R. J.; Castaldi, M. J.; Yegulalp, T. M. In Situ CO<sub>2</sub> Capture Using CaO/γ-Al<sub>2</sub>O<sub>3</sub> Washcoated Monoliths for

Sorption Enhanced Water Gas Shift Reaction. *Ind. Eng. Chem. Res.* **2014**, *53*, 1064–1072.

(6) Chang, Y.; Chen, Y.; Chang, P.; Chen, S. Synthesis, Characterization, and CO<sub>2</sub> Adsorptive Behavior of Mesoporous AlOOH-Supported Layered Hydroxides. *ChemSusChem* **2012**, *5*, 1249–1257.

(7) Duyar, M. S.; Wang, S.; Arellano-Treviño, M. A.; Farrauto, R. J. CO<sub>2</sub> Utilization with a Novel Dual Function Material (DFM) for Capture and Catalytic Conversion to Synthetic Natural Gas: An Update. *J. CO<sub>2</sub> Util.* **2016**, *15*, 65–71.

(8) Lee, A.; Xiao, G.; Xiao, P.; Joshi, K.; Singh, R.; Webley, P. A. High Temperature Adsorption Materials and Their Performance for Pre-Combustion Capture of Carbon Dioxide. *Energy Procedia* **2011**, *4*, 1199–1206.

(9) Choi, S.; Drese, J. H.; Jones, C. W. Adsorbent Materials for Carbon Dioxide Capture from Large Anthropogenic Point Sources. *ChemSusChem* **2009**, *2* (9), 796–854.

(10) Rownaghi, A. A.; Rezaei, F.; Labreche, Y.; Brennan, P. J.; Johnson, J. R.; Li, S.; Koros, W. J. In Situ Formation of a Monodispersed Spherical Mesoporous Nanosilica – Torlon Hollow-Fiber Composite for Carbon Dioxide Capture. *ChemSusChem* **2015**, *8*, 3439–3450.

(11) Rownaghi, A. A.; Kant, A.; Li, X.; Thakkar, H.; Hajari, A.; He, Y.; Brennan, P. J.; Hosseini, H.; Koros, W. J.; Rezaei, F. Aminosilane-Grafted Zirconia–Titania–Silica Nanoparticles/Torlon Hollow Fiber Composites for CO<sub>2</sub> Capture. *ChemSusChem* **2016**, *9*, 1166–1177.

(12) Thakkar, H. V.; Eastman, S.; Hajari, A.; Rownaghi, A. A.; Knox, J. C.; Rezaei, F. 3D-Printed Zeolite Monoliths for CO<sub>2</sub> Removal from Enclosed Environments. *ACS Appl. Mater. Interfaces* **2016**, *8*, 27753–27761.

(13) Thakkar, H.; Eastman, S.; Al-Mamoori, A.; Hajari, A.; Rownaghi, A. A.; Rezaei, F. Formulation of Aminosilica Adsorbents into 3D-Printed Monoliths and Evaluation of Their CO<sub>2</sub> Capture Performance. *ACS Appl. Mater. Interfaces* **2017**, *9*, 7489–7498.

(14) Rezaei, F.; Mosca, A.; Webley, P.; Hedlund, J.; Xiao, P. Comparison of Traditional and Structured Adsorbents for CO<sub>2</sub> Separation by Vacuum-Swing Adsorption. *Ind. Eng. Chem. Res.* **2010**, *49*, 4832–4841.

(15) Manovic, V.; Anthony, E. J. Lime-Based Sorbents for High-Temperature CO<sub>2</sub> Capture-a Review of Sorbent Modification Methods. *Int. J. Environ. Res. Public Health* **2010**, *7* (8), 3129–3140.

(16) Yong, Z.; Mata, V.; Rodrigues, A. E. Adsorption of Carbon Dioxide at High Temperature-a Review. *Sep. Purif. Technol.* **2002**, *26* (2), 195–205.

(17) Gruene, P.; Belova, A. G.; Yegulalp, T. M.; Farrauto, R. J.; Castaldi, M. J. Dispersed Calcium Oxide as a Reversible and Efficient CO<sub>2</sub>-Sorbent at Intermediate Temperatures. *Ind. Eng. Chem. Res.* **2011**, *50*, 4042–4049.

(18) Lee, H. C.; Kwon, S.; Jeon, S. G.; Lee, K. B.; Hyun, C.; Jae, H.; Chul, H.; Kwon, S.; Goo, S.; Bong, K. Effect of pH-Controlled Synthesis on the Physical Properties and Intermediate-Temperature CO<sub>2</sub> Sorption Behaviors of K–Mg Double Salt-Based Sorbents. *Chem. Eng. J.* **2016**, *294*, 439–446.

(19) Oliveira, E. L. G.; Grande, C. a.; Rodrigues, A. E. CO<sub>2</sub> Sorption on Hydrotalcite and Alkali-Modified (K and Cs) Hydrotalcites at High Temperatures. *Sep. Purif. Technol.* **2008**, *62* (1), 137–147.

(20) Broda, M.; Kierzkowska, A. M.; Müller, C. R. Influence of the Calcination and Carbonation Conditions on the CO<sub>2</sub> Uptake of Synthetic Ca-Based CO<sub>2</sub> Sorbents. *Environ. Sci. Technol.* **2012**, *46* (19), 10849–10856.

(21) Yu, C.; Kuo, H.; Chen, Y. Carbon Dioxide Removal Using Calcium Aluminate Carbonates on Titanate Oxide under Warm-Gas Conditions. *Appl. Energy* **2016**, *162*, 1122–1130.

(22) Wang, Q.; Tay, H. H.; Guo, Z.; Chen, L.; Liu, Y.; Chang, J.; Zhong, Z.; Luo, J.; Borgna, A. Morphology and Composition Controllable Synthesis of Mg-Al-CO<sub>3</sub> Hydrotalcites by Tuning the Synthesis pH and the CO<sub>2</sub> Capture Capacity. *Appl. Clay Sci.* **2012**, *55*, 18–26.

- (23) Wang, Q.; Luo, J.; Zhong, Z.; Borgna, A. CO<sub>2</sub> Capture by Solid Adsorbents and Their Applications: Current Status and New Trends. *Energy Environ. Sci.* **2011**, *4* (1), 42–55.
- (24) Wang, Q.; Wu, Z.; Tay, H. H.; Chen, L.; Liu, Y.; Chang, J.; Zhong, Z.; Luo, J.; Borgna, A. High Temperature Adsorption of CO<sub>2</sub> on Mg-Al Hydrotalcite: Effect of the Charge Compensating Anions and the Synthesis pH. *Catal. Today* **2011**, *164* (1), 198–203.
- (25) Palomares, A.; López-Nieto, J. Reactivity in the Removal of SO<sub>2</sub> and NO<sub>x</sub> on Co/Mg/Al Mixed Oxides Derived from Hydrotalcites. *Appl. Catal., B* **1999**, *20*, 257–266.
- (26) Kim, S.; Jeon, S. G.; Lee, K. B. High-Temperature CO<sub>2</sub> Sorption on Hydrotalcite Having a High Mg/Al Molar Ratio. *ACS Appl. Mater. Interfaces* **2016**, *8* (9), 5763–5767.
- (27) Fang, H.; Kulkarni, A.; Kamakoti, P.; Awati, R.; Ravikovitch, P. I.; Sholl, D. S. Identification of High-CO<sub>2</sub>-Capacity Cationic Zeolites by Accurate Computational Screening. *Chem. Mater.* **2016**, *28*, 3887–3896.
- (28) Hong, S.-H.; Jang, M.-S.; Cho, S. J.; Ahn, W.-S. Chabazite and Zeolite 13X for CO<sub>2</sub> Capture under High Pressure and Moderate Temperature Conditions. *Chem. Commun. (Cambridge, U. K.)* **2014**, *50* (38), 4927–4930.
- (29) Zhang, J.; Singh, R.; Webley, P. A. *Microporous Mesoporous Mater.* **2008**, *111*, 478–487.
- (30) Harada, T.; Hatton, T. A. Colloidal Nanoclusters of MgO Coated with Alkali Metal Nitrates/Nitrites for Rapid, High Capacity CO<sub>2</sub> Capture at Moderate Temperature. *Chem. Mater.* **2015**, *27* (23), 8153–8161.
- (31) Ding, Y.-D.; Song, G.; Liao, Q.; Zhu, X.; Chen, R. Bench Scale Study of CO<sub>2</sub> Adsorption Performance of MgO in the Presence of Water Vapor. *Energy* **2016**, *112*, 101–110.
- (32) Zhang, K.; Li, X. S.; Chen, H.; Singh, P.; King, D. L. Molten Salt Promoting Effect in Double Salt CO<sub>2</sub> Absorbents. *J. Phys. Chem. C* **2016**, *120* (2), 1089–1096.
- (33) Lee, C. H.; Mun, S.; Lee, K. B. Characteristics of Na-Mg Double Salt for High-Temperature CO<sub>2</sub> Sorption. *Chem. Eng. J.* **2014**, *258*, 367–373.
- (34) Lee, C. H.; Kwon, H. J.; Lee, H. C.; Kwon, S.; Jeon, S. G.; Lee, K. B. Effect of pH-Controlled Synthesis on the Physical Properties and Intermediate-Temperature CO<sub>2</sub> Sorption Behaviors of K – Mg Double Salt-Based Sorbents. *Chem. Eng. J.* **2016**, *294*, 439–446.
- (35) Huang, L.; Gao, W.; Harada, T.; Qin, Q.; Zheng, Q.; Hatton, A.; Wang, Q.; Zhang, Y. Alkali Carbonate Molten Salt-Coated CaO with Highly Improved CO<sub>2</sub> Capture Capacity. *Energy Technol.* **2017**, *5*, 1–11.
- (36) Valverde, J. M.; Perejon, A.; Perez-Maqueda, L. A. Enhancement of Fast CO<sub>2</sub> Capture by a Nano-SiO<sub>2</sub>/CaO Composite at Ca-Looping Conditions. *Environ. Sci. Technol.* **2012**, *46* (11), 6401–6408.
- (37) Hu, Y.; Liu, W.; Chen, H.; Zhou, Z.; Wang, W.; Sun, J.; Yang, X.; Li, X.; Xu, M. Screening of Inert Solid Supports for CaO-Based Sorbents for High Temperature CO<sub>2</sub> Capture. *Fuel* **2016**, *181*, 199–206.
- (38) Vu, A. T.; Ho, K.; Jin, S.; Lee, C. H. Double Sodium Salt-Promoted Mesoporous MgO Sorbent with High CO<sub>2</sub> Sorption Capacity at Intermediate Temperatures under Dry and Wet Conditions. *Chem. Eng. J.* **2016**, *291*, 161–173.
- (39) Xiao, G.; Singh, R.; Chaffee, A.; Webley, P. Advanced Adsorbents Based on MgO and K<sub>2</sub>CO<sub>3</sub> for Capture of CO<sub>2</sub> at Elevated Temperatures. *Int. J. Greenhouse Gas Control* **2011**, *5* (4), 634–639.
- (40) Harada, T.; Simeon, F.; Hamad, E. Z.; Hatton, T. A. Alkali Metal Nitrate-Promoted High-Capacity MgO Adsorbents for Regenerable CO<sub>2</sub> Capture at Moderate Temperatures. *Chem. Mater.* **2015**, *27* (6), 1943–1949.
- (41) Sagar, T. V.; Surendar, M.; Padmakar, D.; Parameswaram, G.; Lingaiah, N.; Rao, K. S. R.; Reddy, I. A. K.; Sumana, C.; Prasad, P. S. S. Selectivity Reversal in Oxidative Dehydrogenation of Ethane with CO<sub>2</sub> on CaO–NiO/Al<sub>2</sub>O<sub>3</sub> Catalysts. *Catal. Lett.* **2017**, *147*, 82–89.
- (42) Galván-Ruiz, M.; Hernández, J.; Baños, L.; Noriega-Montes, J.; Rodríguez-García, M. E. Characterization of Calcium Carbonate, Calcium Oxide, and Calcium Hydroxide as Starting Point to the Improvement of Lime for Their Use in Construction. *J. Mater. Civ. Eng.* **2009**, *21* (11), 694–698.
- (43) Dean, C. C.; Blamey, J.; Florin, N. H.; Al-Jeboori, M. J.; Fennell, P. S. The Calcium Looping Cycle for CO<sub>2</sub> Capture from Power Generation, Cement Manufacture and Hydrogen Production. *Chem. Eng. Res. Des.* **2011**, *89* (6), 836–855.
- (44) Hu, Y.; Liu, W.; Sun, J.; Yang, X.; Zhou, Z.; Zhang, Y.; Xu, M. High Temperature CO<sub>2</sub> Capture on Novel Yb<sub>2</sub>O<sub>3</sub>-Supported CaO-Based Sorbents. *Energy Fuels* **2016**, *30* (8), 6606–6613.



(21) BR 102013019137-0 A2



\* B R 1 0 2 0 1 3 0 1 9 1 3 7 A

(22) Data do Depósito: 26/07/2013

(43) Data da Publicação: 25/08/2015

República Federativa do Brasil  
Ministério da Indústria, Comércio Exterior  
e Serviços  
Instituto Nacional da Propriedade Industrial

**(54) Título:** MATERIAL SÓLIDO ABSORVEDORES DE DIÓXIDO DE CARBONO E SUAS PREPARAÇÕES

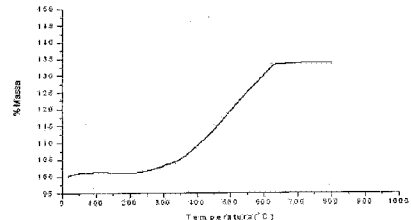
**(51) Int. Cl.:** B01J 20/04; B01D 53/88; B01D 53/14

**(73) Titular(es):** UNIVERSIDADE FEDERAL DE MINAS GERAIS - UFMG, FUNDAÇÃO DE AMPARO À PESQUISA DO ESTADO DE MINAS GERAIS - FAPEMIG

**(72) Inventor(es):** GERALDO MAGELA DE LIMA; ROGÉRIO DE OLIVEIRA

**(85) Data do Início da Fase Nacional:**  
26/07/2013

**(57) Resumo:** MATERIAIS SÓLIDOS ABSORVEDORES DE DIÓXIDO DE CARBONO E SUAS PREPARAÇÕES. A presente invenção descreve o processo de preparação de materiais sólidos para absorção de dióxido de carbono, bem como os produtos obtidos. O processo utiliza-se de misturas ternárias, três compostos sólidos, e misturas binárias, dois compostos sólidos, de áxidos metálicos, hidróxidos e sais, preferencialmente dos hidróxidos de cálcio, de magnésio e de alumínio, óxido de ferro (III) e bicarbonato de sódio, com a finalidade de aumentar a eficiência da captura de dióxido de carbono



## “MATERIAIS SÓLIDOS ABSORVEDORES DE DIÓXIDO DE CARBONO E SUAS PREPARAÇÕES”

A presente invenção descreve o processo de preparação de materiais sólidos para absorção de dióxido de carbono, bem como os produtos obtidos.

5 Neste processo utilizam-se misturas ternárias, três compostos sólidos, e misturas binárias, dois compostos sólidos, de óxidos metálicos, hidróxidos e sais, preferencialmente dos hidróxidos de cálcio, de magnésio e de alumínio, óxido de ferro (III) e bicarbonato de sódio, com a finalidade de aumentar a eficiência da captura de dióxido de carbono.

10 O uso de material (substrato) sólido para a retenção de espécies químicas, em fase de vapor, tem sido amplamente divulgado na literatura. Em geral, a retenção da espécie gasosa ocorre devido a uma reação química entre o material e a referida espécie e, portanto, acarreta uma variação de massa. Esta variação pode ser determinada e usada como um parâmetro de 15 monitoramento da reação. Paralelamente, deve ser levado em conta a eficiência da reação e o gasto de energia quando se avalia a capacidade do material para retenção de uma espécie química.

As fases sólidas, ou seja, os materiais avaliados e escolhidos para a retenção de espécies químicas em correntes gasosas apresentam algumas 20 características peculiares que favorecem a reação entre o sólido e o gás. Os sólidos utilizados possuem estruturas cristalinas, cuja superfície interna dos poros é acessível a uma combinação entre este e a espécie gasosa. Dentre estes materiais os mais utilizados são o Ca(OH)<sub>2</sub>, CaO e MgO (VASCONCELOS, V. et al. Validação experimental de modelos de leitos 25 adsorvedores com zeólitas 5A. *Cerâmica*, v.43, p.281-282, 1997).

Vários trabalhos baseados na retenção de gases em sólido estão sendo feitos, principalmente para diminuição da liberação de gases que causam o Efeito Estufa. Entre os gases que existem naturalmente na atmosfera, aqueles produzidos em excesso geram maiores problemas ambientais: CH<sub>4</sub>, N<sub>2</sub>O, O<sub>3</sub>, 30 SO<sub>3</sub>, SO<sub>2</sub> e o CO<sub>2</sub>, sendo os dois últimos os mais importantes por ser emitidos a partir da queima de combustíveis fósseis, particularmente o carvão para a produção de energia.

A maioria dos estudos atuais, mostra, que se os esforços para conter as emissões de dióxido de carbono não forem ampliados até o final deste século, a concentração desse na atmosfera atingirá 760 ppm, o dobro da atual. Algumas estimativas mostram que na metade deste século a concentração 5 será de 500 ppm. Apenas para comparação, antes da revolução industrial, entre os séculos 18 e 19, os níveis eram de aproximadamente 280 ppm. Atualmente o valor já atinge 380 ppm (ABANADES, J.C. et al. Capture of CO<sub>2</sub> from combustion gases in a fluidized bed of CaO. *Environm. and Energy Eng.*, v.90, p.303-306, 2003; ARESTA, M. et al. Utilization of CO<sub>2</sub> as a chemical 10 feedstock: opportunities and challenges. *Dalton Trans.*, v.28, p.2975-2992, 2007).

De modo a garantir um desenvolvimento sustentável e contribuir para a diminuição do teor de CO<sub>2</sub> na atmosfera, a retenção deste gás num substrato, seja líquido, sólido ou gasoso, é uma alternativa para a diminuição desta 15 espécie química. De acordo com a literatura vários estudos estão sendo feitos na avaliação da retenção, principalmente de CO<sub>2</sub> e SO<sub>3</sub>. Entretanto, pesquisadores ainda não apresentaram uma técnica universal para retenção desses gases em fase sólida.

Assim, pode-se citar como exemplo de estudo o trabalho de Abanades e 20 colaboradores para captura de CO<sub>2</sub> em processo de leito fluidizado de CaO. Foram feitos experimentos para investigar a reação de carbonatação de óxido de cálcio para captura de CO<sub>2</sub> em altas temperaturas. Os resultados mostraram que a eficiência da captura de CO<sub>2</sub> é muito alta, sendo que esta eficiência vai diminuindo com o número de ciclos de carbonatação/calcinação. Como 25 conclusão, ficou estabelecido que o leito fluidizado contendo CaO foi satisfatório para alcançar efetiva eficiência na captura de CO<sub>2</sub> (ABANADES, J.C. et al., 2003).

Outra publicação mostra que os sólidos podem ser usados em larga faixa de temperatura, rejeitos líquidos não são regenerados e os sólidos podem 30 depositar sem inadequada precaução ambiental (HARRISON, D.P. The role of solids in CO<sub>2</sub> capture: A mini review. Department of Chemical Engineering,

Louisiana State University. Disponível em:  
[http://www.researchgate.net/publication/228881342\\_The\\_Role\\_of\\_Solids\\_in\\_CO2\\_Capture\\_A\\_Mini\\_Review?ev=pub\\_cit\\_inc](http://www.researchgate.net/publication/228881342_The_Role_of_Solids_in_CO2_Capture_A_Mini_Review?ev=pub_cit_inc). Acesso em 24 junho 2013).

Alguns autores também estudaram o desempenho de alguns sólidos para absorção cíclica de CO<sub>2</sub>. Os materiais utilizados foram pedra calcária comercial e acetato de cálcio, sendo testada a capacidade de ambos em processos cílicos de carbonatação. A mudança estrutural desses materiais foi determinada por meio de um modelo para avaliação de áreas superficiais chamado de modelo B.E.T (SUN, P. et al. On sorbent performance for cyclic absorption of CO<sub>2</sub>. University of British Columbia. Disponível em: [http://www.docstoc.com/docs/70160164/On-sorbent-performance-for-cyclic-absorption-of-CO2-Ping-Sun1\\_-C](http://www.docstoc.com/docs/70160164/On-sorbent-performance-for-cyclic-absorption-of-CO2-Ping-Sun1_-C). Acesso em: 23 junho 2013).

Alguns pesquisadores citam a retenção do CO<sub>2</sub> em substratos naturais (SONG, C. CO<sub>2</sub> conversion and utilization: an overview. In: SONG, C.; GAFFNEY, A.M.; FUJIMOTO, K. CO<sub>2</sub> conversion and utilization. Washington: *American Chemical Society*, 2002. p. 2-30; STEINBERG, M. CO<sub>2</sub> mitigation and fuel production. In: Song, C.; GAFFNEY, A.M.; FUJIMOTO, K., CO<sub>2</sub> conversion and utilization. Washington: *American Chemical Society*, 2002. p.31-38).

Já a tecnologia de captura e armazenamento de carbono (CCS) envolve a captura do CO<sub>2</sub> em grandes fontes estacionárias (centrais termoelétricas, cimenteiras, refinarias, etc.), e o seu transporte por gasoduto ou navio até um local de armazenamento, em que o CO<sub>2</sub> é injetado a grandes profundidades (> 800m) em formações geológicas de características apropriadas e que garantam a retenção do CO<sub>2</sub> durante milhões de anos.

A tecnologia CCS tem por objetivo combater as alterações climáticas através da redução em mais de 90% das emissões de CO<sub>2</sub> de grandes instalações industriais (KTejo, Estudo de viabilidade da captura de CO<sub>2</sub> na central termoelétrica do PEGO <http://www.ktejo.cge.uevora.pt/wp-content/uploads/2009/10/Brochura-KTEJO.pdf>).

Por outro lado, existem três procedimentos para redução das emissões de carbono antropogênico:

- (1) promoção da eficiência energética, produzindo menos CO<sub>2</sub> por unidade de emprego de energia na indústria, no transporte e em setores residenciais;
- (2) descarbonização do fornecimento de energia por meio da utilização de fontes de energia renovável ou alternativa; e,
- 5       (3) remoção ou captura de CO<sub>2</sub> de correntes de resíduos para subsequente armazenamento, ou seja, sequestro de carbono. As duas primeiras alternativas oferecem menores custos, embora apresentem impactos limitados. A remoção e sequestro é a única alternativa que permite o uso continuado de combustíveis fósseis, ainda que de alto custo, é uma forma viável de reduzir as
- 10      concentrações de CO<sub>2</sub> (SUSLICK, S.B.; RAVAGNANI G., A. T.F.S. Modelo dinâmico de sequestro geológico de CO<sub>2</sub> em reservatórios de petróleo. *Revista Brasileira de Geociências*, p.39–60, 2008).

As técnicas utilizadas para sequestro de carbono devem ser rentáveis e competitivas, fornecer armazenamento estável e seguro em longo prazo e

15      serem aceitáveis ambientalmente. A tecnologia de sequestro de CO<sub>2</sub> pode ser utilizada sem a necessidade de mudanças drástica na infraestrutura de fornecimento de energia em diversos países. O CO<sub>2</sub> capturado deve ser armazenado, com a garantia de que não seja posteriormente emitido para a atmosfera. As várias opções de armazenamento devem ser examinadas

20      minuciosamente em relação aos custos, e principalmente, segurança e potenciais efeitos ambientais. Assim sendo, vários são os aspectos que devem ser considerados:

- (1) o processo de armazenamento de CO<sub>2</sub> necessita ser menos prejudicial ao ambiente que a liberação contínua do gás;
- 25      (2) o período de armazenamento deve ser longo, preferencialmente de centenas a milhares de anos;
- (3) o risco de acidentes deve ser minimizado; e,
- (4) o tipo de armazenamento não deve violar quaisquer leis ou regulamentos nacionais ou internacionais.

30      Os caminhos ideais de sequestro de CO<sub>2</sub> são aqueles que oferecem maiores capacidades de armazenamento aliadas ao baixo custo. Estas características podem ser obtidas em operações de recuperação avançada de

óleo, por exemplo. A existência de reservatórios naturais de CO<sub>2</sub> prova que, sob circunstâncias favoráveis, este gás pode ser armazenado por centenas de anos ou mais (HOLLOWAY, S. Underground Sequestration of Carbon Dioxide - A Viable Greenhouse Gas Mitigation Option. *Energy*, v.30, n.11-12, p.2318-5 2333, 2005).

A fim de demonstrar a relevância do processo e a complexidade da absorção de gases produzidos em sistemas de combustão ou presentes em ambientes fechados, alguns documentos de patente são exemplificados no estado da técnica.

10 Existem algumas tecnologias que foram propostas no intuito de absorver gases tóxicos em ambientes fechados, como por exemplo, submarinos e aparelhos de respiração com refluxo de gases anestésicos.

Para a purificação do ar em submarinos (absorção de CO<sub>2</sub>) o documento GB190603570 (Winand, P.; "Process for the Elimination of Carbon Dioxide from 15 the Gaseous Combustion Products of Combustion Engines", 1906) descreve uma mistura absorvente de amônia com óxido de sódio ou óxido de potássio, sendo que estes são produzidos durante a geração do comburente O<sub>2</sub>; em motores de combustão interna que são destinados à propulsão de submarinos. Relacionado ainda à atmosfera de submarinos, a patente US2545194 (Colburn, 20 A. P.; Dodge, B.; "Adsorption process for removal of carbon dioxide from the atmosphere of a submarine", 1951) descreve a utilização apenas de óxido de lítio (Li<sub>2</sub>O) para absorção de CO<sub>2</sub>, pois uma quantidade menor de massa é suficiente para a manutenção da qualidade do ar para a tripulação. Com o desenvolvimento de tecnologias para a exploração espacial, a absorção de 25 CO<sub>2</sub> em ambientes fechados assume uma posição de elevada relevância, como é demonstrado pela patente US7326280 (Hrycak, M. B.; Mckenna, D. B.; "Enhanced carbon dioxide adsorbent", 2005), aplicada em sistemas de purificação de naves (foguetes) e estações espaciais com a utilização do óxido de lítio.

30 A aplicação em larga escala de processos de absorção de dióxido de carbono em ambientes fechados pode ser demonstrada pela patente US5087597 (Orlando, L. et al.; "Carbon dioxide adsorbent and method for

producing the adsorbent", 1992) com a descrição de uma mistura à base de polialcoxissilano, sílica, alumina e óxido de ferro, que é empregada na absorção de CO<sub>2</sub> presente em contêineres para transporte de materiais susceptíveis à decomposição por ambiente ácido ou para o transporte de animais.

Outra aplicação de grande importância corresponde à absorção de CO<sub>2</sub> em aparelhos de anestesia gasosa. Estes aparelhos devem apresentar um sistema para a absorção do CO<sub>2</sub> expirado pelo paciente; entretanto, os materiais absorventes não podem reagir com as substâncias anestésicas, como ocorre em sistemas de absorção de compostos por óxidos de metais alcalinos. Neste caso, o documento PI9713138 (Armstrong, J. R.; Murray, J.; "Absorvente de dióxido de carbono para uso em anestesiologia, e, processo de preparação do mesmo", 1997) propôs a substituição da cal soldada por uma mistura de hidróxido de cálcio, gesso e alumínio e um agente higroscópico (cloreto de cálcio). Semelhantemente, o documento RU2152251 (Imanenkov, S. I. et al.; "Method of synthesis of carbon dioxide adsorbent", 2000) descreve a utilização de uma mistura de hidróxido de cálcio e carbonato de potássio para absorção de CO<sub>2</sub> em aparelhos respiratórios.

Para aplicações industriais os processos de absorção podem ser realizados de formas mais diversificadas, como, por exemplo, a patente PI0306705 (Johannes, B. T. et al.; "Process for removing carbon dioxide from gas mixtures", 2004) que mostra o emprego de uma mistura composta por água, sulfolano e uma amina secundária ou terciária derivada da etanolamina. O processo de absorção é realizado através da pulverização da solução absorvente contra o fluxo de gás contendo CO<sub>2</sub>, H<sub>2</sub>S e/ou CO<sub>2</sub>. O processo descrito deve ser realizado preferencialmente a uma temperatura entre 50°C e 90°C.

Para a absorção de CO<sub>2</sub> em fluxos de gases, à temperatura ambiente ou aproximadamente até 100°C, diversos pedidos de patente podem ser encontradas descrevendo a utilização de zeólitas em aparelhos específicos, como no pedido US5531808 (Ojo, A. F.; Fitch, F.R; Buelow, M.; "Removal of carbon dioxide from gas streams", 1996) onde se utiliza a zeólita-X. Já no

documento EP0173501 (Keith, P. G.; "Process for removing carbon dioxide from gas mixtures", 1986) utiliza-se a zeólita-A. Os processos de absorção de CO<sub>2</sub> através de zeólitas são limitados pela faixa de temperatura, devido à fraca interação que a zeólita apresenta com o CO<sub>2</sub> absorvido. Para temperaturas 5 mais elevadas, em que a absorção de CO<sub>2</sub> será efetuada, deve-se utilizar material que não sofra decomposição térmica e que, preferencialmente, seja ativado pelo aumento da temperatura. Outro exemplo é descrito no documento PI0003340, que relata a preparação de uma mistura composta por óxido de magnésio e um carbonato de metal alcalino (Mayorga, S. G. et al.; 10 "Adsorventes de dióxido de carbono contendo óxido de magnésio adequado para uso sob altas temperaturas e processo de sua fabricação", 2000). Essa mistura absorve CO<sub>2</sub> em uma faixa de temperatura entre 300°C e 550°C.

Além dos métodos de absorção descritos nos documentos supracitados, o documento US2008086938 (Hazlebeck, D. A.; Dunlop, E. H.; "Photosynthetic 15 carbon dioxide sequestration and pollution abatement", 2008) descreve a utilização do CO<sub>2</sub> produzido em plantas industriais para ser injetado em biodigestores contendo algas, que através do processo de fotossíntese realizam a biossíntese de óleos combustíveis de interesse industrial.

Alguns métodos paliativos para impedir a liberação de dióxido de carbono na atmosfera também podem ser encontrados, como, por exemplo, o documento AU2008100189 (Jonnes, I.S. F.; "Sequestration of carbon in sinking water", 2008), que sugere um método para a realização de depósitos de CO<sub>2</sub> em profundezas oceânicas, entre 3.000 a 4.000 metros, aproximadamente. Nesta patente descreve-se uma tecnologia na qual o dióxido de carbono é 20 sequestrado e injetado no mar numa profundidade acima de 3000 metros. Além disto, sugere-se ainda que óxido de Fe(III) seja adicionado ao processo de forma a aumentar a quantidade de fitoplanctons, que irá processar o CO<sub>2</sub>, o que difere substancialmente da tecnologia proposta neste documento.

Todos os documentos supracitados não se assemelham com a 25 tecnologia ora descrita.

Por outro lado, o documento PI0903159-6 e o certificado de adição C10903159-6 (Belchior, J. C. et al.; "Materiais cerâmicos para absorção de

gases ácidos, processo de preparação dos mesmos e processo para a absorção e regeneração de CO<sub>2</sub>", 2009, 2010, respectivamente) descrevem o processo de preparação de cerâmicas para absorção de gases ácidos, agravantes do efeito estufa, que são liberados em sistemas de combustão, ou 5 que estão presentes em ambientes fechados. Em relação ao dióxido de carbono, alvo principal da presente invenção, é descrito um processo de absorção, transporte, processamento e transformação do gás em outros produtos. O processo utiliza materiais cerâmicos preparados através da mistura sólida de um ou mais óxidos metálicos, com um ou mais agentes aglomerantes 10 e um agente expansivo. O produto gerado pode ser processado e o sistema absorvente, regenerado. O dióxido de carbono obtido no processamento pode ser empregado como gás carbônico analítico ou comercial, carbamatos diversos e carbonato de amônio.

A principal diferença da tecnologia apresentada nos pedidos 15 supracitados em relação à tecnologia proposta no presente pedido é a utilização do bicarbonato de sódio como um dos reagentes. O bicarbonato tem a finalidade de gerar poros na cerâmica depois de aquecida, pela liberação de CO<sub>2</sub> em atmosfera de gás inerte. Após esse aquecimento o material é resfriado e novamente aquecido numa atmosfera de CO<sub>2</sub> onde é absorvido pela 20 cerâmica ocupando os poros deixado pela liberação do CO<sub>2</sub> proveniente do NaHCO<sub>3</sub>. Assim, o material aqui descrito, mais poroso, funciona como um absorvedor de CO<sub>2</sub> com maior eficiência.

Importante frisar que o processo para absorver CO<sub>2</sub>, aqui descrito 25 apresenta uma eficiência de aproximadamente 50% superior ao relatado no pedido de patente PI0903159-6.

A tecnologia para captura CO<sub>2</sub> ora proposta é constituída de materiais de baixo custo como Ca(OH)<sub>2</sub>, Al(OH)<sub>3</sub>, Fe<sub>2</sub>O<sub>3</sub> e NaHCO<sub>3</sub>, onde o custo é de aproximadamente US\$ 250.00/tonelada, incluindo materiais, absorção e processo de pelotização. O custo total estimado está resumido na Tabela 1.

30 **Tabela 1:** Custo estimado por Kwh para as etapas de preparação da cerâmica, objeto da presente invenção.

Etapas	Energia (Kwh) *1Kwh = US\$ 0,20	Custo (US\$)
Material		186,00
Processo de pelotização	60	12,00
Absorção	84	16,80
Total		214,80

O processo de preparação de cerâmicas proposto pela tecnologia é simples e envolve a reutilização do material, por pelo menos 10 vezes, o que indica alto potencial de captura de dióxido de carbono por um mesmo material. Trata-se de um processo viável financeiramente, alcança níveis consideráveis de eficiência e que é relevante frente a outras tecnologias já conhecidas.

### DESCRIÇÃO DAS FIGURAS

A **Figura 1** apresenta a curva termogravimétrica do Ca(OH)<sub>2</sub> na presença de CO<sub>2</sub>.

A **Figura 2** mostra a curva termogravimétrica das misturas ternárias na presença de CO<sub>2</sub>.

A **Figura 3** representa o fluxograma das misturas ternárias preparadas.

A **Figura 4** representa o fluxograma das misturas binárias preparadas.

A **Figura 5** representa o gráfico da resistência mecânica versus misturas ternárias.

As **Figuras 6, 7 e 8** mostram os difratogramas de raios X dos materiais Al2, Fe2 e Mg2, respectivamente, antes do tratamento térmico.

As **Figuras 9, 10 e 11** apresentam os difratogramas de raios X dos materiais Al2, Fe2 e Mg2, respectivamente, após o tratamento térmico realizado até 1000°C.

### DESCRIÇÃO DETALHADA DA INVENÇÃO

A presente invenção descreve um material sólido na forma de misturas sólidas, binárias (contendo dois componentes) ou ternárias (contendo 3 componentes) para a absorção de dióxido de carbono, seu processo de preparação e uso. Tais misturas sólidas são compostas por um ou mais

agentes absorventes, selecionados do grupo compreendendo um ou mais óxidos de metais alcalinos terrosos, um ou mais hidróxidos de metais alcalinos ou óxidos de metais de transição, preferencialmente hidróxido de cálcio (Ca(OH)<sub>2</sub>) (80% e 90%p/p), agentes aglomerantes, preferencialmente, hidróxido de magnésio (Mg(OH)<sub>2</sub>) (5%, 10%, 15% e 20% p/p)), de alumínio (Al(OH)<sub>3</sub>) (5%, 10%, 15% e 20%p/p)) e óxido de ferro (III) e como agente gerador de poros, bicarbonato de sódio (NaHCO<sub>3</sub> (5%, 10%, 15% e 20%p/p)), formando misturas ternárias sólidas e misturas binárias sólidas que são apresentadas nas figuras 3 e 4. As misturas destes componentes devem ser feitas em meio aquoso para que o sólido final adquira uma consistência adequada.

Após a completa homogeneização dos componentes, a mistura é mantida em repouso por um período de 2 a 48 horas.

Para a eliminação do excesso de água a mistura pode ou não ser levada a uma estufa com aquecimento até 60°C. Após essa etapa o material é aquecido rigorosamente (entre 200°C e 800°C) por um período de 1 hora, o que garante a eliminação de interferentes no material absorvente. Este aquecimento deve ocorrer na ausência de fluxo de ar ou oxigênio, ou seja, em uma câmara fechada ou com a ausência de gases ácidos, que poderiam ser absorvidos durante a síntese do material.

Por outro lado, o material sólido pode ser modelado em forma de esferas. Essas podem ser confeccionadas utilizando um disco pelotizador, onde a mistura foi preparada utilizando um moinho de bola, com a finalidade de homogeneizá-la. Após a homogeneização a mistura é colocada no disco pelotizador que foi acionado e girando a uma velocidade de 10 rpm. Durante esse processo água foi borrifada para facilitar a aglomeração e modelagem das esferas. Ao atingir o tamanho desejado, o disco foi estacionado e as esferas retiradas.

Assim, as diferentes composições - binárias e ternárias - mostradas nas figuras 3 e 4 têm a propriedade de absorver dióxido de carbono após o tratamento térmico em diferentes temperaturas que podem variar de 25°C a 950°C, com um rendimento de cerca de 50% em relação ao pedido de patente PI0903159-6. Portanto, a tecnologia proposta pode ser aplicada para

descontaminação de ambientes fechados a temperatura ambiente (aproximadamente 25°C), purificação de fluxos de gás e absorção de gases de rejeito industrial em temperaturas entre 100°C e 950°C.

Ademais, a capacidade destes materiais em capturar CO<sub>2</sub> foi avaliada 5 utilizando um aparelho de termogravimetria com um fluxo desse gás a 30 mL min<sup>-1</sup>, a uma razão de aquecimento de 10°C/min até 1000°C. Al(OH)<sub>3</sub>, Fe<sub>2</sub>O<sub>3</sub> ou Mg(OH)<sub>2</sub> foram utilizados como agentes aglomerantes com uma concentração de até 15% (p/p) e NaHCO<sub>3</sub>, 15% (p/p), foi utilizado afim de aumentar a porosidade das esferas através de sua decomposição, formando Na<sub>2</sub>CO<sub>3</sub> e 10 CO<sub>2</sub>, ou através do rearranjo estrutural das fases presentes.

A invenção pode ser melhor compreendida através dos seguintes exemplos, não limitantes.

#### **EXEMPLO 1. Preparação dos materiais absorventes e suas capacidades de capturar CO<sub>2</sub>**

##### **15 A) Preparação dos materiais, composições e modelagem em esferas**

A mistura dos componentes foi feita no estado sólido e a água foi adicionada gradativamente até que o material adquirisse consistência desejada. O material foi pelotizado em tamanhos (1 a 10 mm) diversos e deixado ao ar livre, ou não, por até 48 horas.

##### **20 A.1) Preparação das amostras contendo hidróxido de alumínio**

Para a preparação de Al1 (80%:5%:15%), foram medidos 4 kg de Ca(OH)<sub>2</sub>, 0,25 kg de Al(OH)<sub>3</sub> e 0,75kg de NaHCO<sub>3</sub> e colocados num moinho de bola para homogeneizar a mistura e, posteriormente, colocado no disco pelotizador, onde a água é adicionada para facilitar a aglomeração do material.

25 Em seguida, o material foi deixado em repouso, por até 48 horas e, depois, calcinado em uma mufla com razão de aquecimento de 5°C/min até atingir a temperatura de 1000°C, em atmosfera dinâmica de ar e mantida nessa temperatura durante 60 minutos.

As amostras ((Al2(80%:10%:10%) e Al3(80%:15%:5%)) e foram feitas 30 utilizando o mesmo procedimento para a amostra Al1 observando as devidas proporções.

### **A.2) Preparação das amostras contendo óxido de ferro(III)**

Para a preparação de Fe1(80%:5%:15%), foram medidos 4 kg de Ca(OH)<sub>2</sub>, 0,25 kg de Fe<sub>2</sub>O<sub>3</sub> e 0,75kg de NaHCO<sub>3</sub> e colocados num moinho de bola para homogeneizar a mistura e, posteriormente, colocado no disco pelotizador, onde a água é adicionada para facilitar a aglomeração do material.

5 Em seguida, o material foi deixado em repouso, por até 48 horas e, depois, calcinado em uma mufla com razão de aquecimento de 5°C/min até atingir a temperatura de 1000°C, em atmosfera dinâmica de ar e mantida nessa temperatura durante 60 minutos.

10 As amostras (Fe<sub>2</sub>(80%:10%:10%) e Fe3(80%:15%:5%)) foram feitas utilizando o mesmo procedimento para amostra Fe1 observando as devidas proporções.

### **A.3) Preparação das amostras contendo hidróxido de magnésio**

Para a preparação de Mg1(80%:5%:15%), foram medidos 4 kg de Ca(OH)<sub>2</sub>, 0,25 kg de Mg(OH)<sub>2</sub> e 0,75kg de NaHCO<sub>3</sub> e colocados num moinho de bola para homogeneizar a mistura e posteriormente é colocado no disco pelotizador, onde a água é adicionada para facilitar a aglomeração do material.

15 Em seguida, o material foi deixado em repouso, por até 48 horas e, depois, calcinado em uma mufla com razão de aquecimento de 5°C/min até atingir a temperatura de 1000°C, em atmosfera dinâmica de ar e mantida nessa

20 temperatura durante 60 minutos.

As amostras ((Mg2(80%:10%:10%) e Mg3(80%:15%:5%)) foram feitas utilizando o mesmo procedimento para amostra Mg1 observando as devidas proporções.

25 Na preparação dos novos materiais absorventes, o Ca(OH)<sub>2</sub> foi usado como base uma vez que como mostrado na figura 1, este material apresenta maior capacidade de capturar CO<sub>2</sub> entre os materiais testados após o prévio tratamento térmico a 1000°C por 1 hora.

30 Nas figuras 3 e 4 (fluxogramas) estão apresentados os grupos de materiais absorventes preparados, com as proporções em massa definidas para toda a faixa que cada conjunto de componente possibilita a absorção do dióxido de carbono.

Todos os novos materiais apresentaram capacidade de capturar CO<sub>2</sub>, sendo esse comportamento mais evidente nas misturas Al1 a Al3 e Mg1 a Mg3 a altas temperaturas (maiores que 800°C) e para Fe1 a Fe3 a baixas temperaturas (aproximadamente 300°C). Isto pode ser observado na figura 2 5 pela comparação entre Al2, Fe2, Mg2 e Ca(OH)<sub>2</sub> puro.

#### A.4) Modelagem em esferas

Os materiais, em forma de esferas foram confeccionados por meio de um disco pelotizador. As misturas foram preparadas utilizando um moinho de bola, com a finalidade de homogeneizá-las. Após a homogeneização a mistura 10 foi colocada no disco pelotizador que foi acionado e girando a uma velocidade de 10 rpm. Durante esse processo água foi borrifada para facilitar a aglomeração e modelagem das esferas. Ao atingir o tamanho desejado, o disco foi estacionado e as esferas, retiradas.

#### B) Estudo da capacidade de captura de CO<sub>2</sub>

##### 15 B.1) Método de diferença de massa

Para verificar a capacidade de absorção de CO<sub>2</sub>, as amostras Al2 (Ca(OH)<sub>2</sub>:Al(OH)<sub>3</sub>:NaHCO<sub>3</sub>, 80%:10%:10%), Fe<sub>2</sub>(Ca(OH)<sub>2</sub>):Fe<sub>2</sub>O<sub>3</sub>:NaHCO<sub>3</sub>, 80%:10%:10%) e Mg2 (Ca(OH)<sub>2</sub>:Mg(OH)<sub>2</sub>:NaHCO<sub>3</sub>, 80%:10%:10%) (Figura 3), foram colocadas, separadamente, em uma mufla, com uma razão de aquecimento 5°C/min até a 1000°C, em atmosfera dinâmica de ar e mantida 20 nessa temperatura durante 40 minutos. Posteriormente, a mistura foi resfriada e a massa perdida foi medida. Logo após, foi colocada em atmosfera de CO<sub>2</sub>, em um forno tubular horizontal com uma rampa de 60 minutos (razão de aquecimento 20°C/min) até atingir a temperatura de 1000°C e mantida por 30 25 minutos nesta temperatura. Após esta etapa o material foi resfriado e, então, novamente medida a sua massa.

Os dados obtidos para captura de CO<sub>2</sub> pelos materiais Al2, Fe2 e Mg2 pelo método da diferença de massa estão relatados na tabela 2.

30 **Tabela 2.** Resultados obtidos através da reação entre a cerâmica e o CO<sub>2</sub> usando a diferença de massa.

Composição da mistura	Massa inicial das amostras (g)	Massa tratadas a 1000°C (g)	Massa após absorção de CO <sub>2</sub> (g)	% de absorção CO <sub>2</sub>
Al2	0,99	0,57	0,92	61,2
Fe2	1,07	0,76	1,11	46,5
Mg2	1,12	0,66	1,07	61,8

Os três materiais utilizados como exemplos apresentaram capacidade de absorver CO<sub>2</sub>, sendo importante ressaltar que os Al2 e Mg2 apresentam a capacidade de reter cerca de 60% p/p de CO<sub>2</sub> em relação à massa inicial do material tratado termicamente.

## 5 B.2) Método da Termogravimetria

O método da termogravimetria foi utilizado a fim de se validar os resultados obtidos no experimento anterior (item B.1), além de permitir um controle mais rigoroso do fluxo de gás e da temperatura, por serem controlados pelo aparelho.

10 As mesmas misturas ternárias e misturas binárias testadas anteriormente e misturas binárias foram colocadas, separadamente, no aparelho de termogravimetria. Primeiramente, tratadas a temperatura de 1000°C, em gás argônio por 1 hora, resfriadas e, logo em seguida, o gás é trocado para CO<sub>2</sub> que é aquecido juntamento com a amostra até 1000°C; 15 depois, no próprio aparelho foram calculadas as massas adquiridas pelas amostras.

Os dados obtidos para captura de CO<sub>2</sub> pelos materiais Al2, Fe2 e Mg2 pelo método da termogravimetria estão relatados na tabela 3.

20 **Tabela 3– Resultados obtidos através da reação entre as misturas ternárias e o CO<sub>2</sub> usando termogravimetria.**

Composição da mistura	Massa inicial das amostras (mg)	Massa tratadas a 1000°C em (mg)	Massa após absorção de CO <sub>2</sub> (mg)	% de absorção CO <sub>2</sub>
Al2	19,692	9,704	15,371	58,4
Fe2	24,852	14,414	20,147	39,8
Mg2	18,604	10,874	17,235	58,5

Nestes experimentos, os três materiais utilizados como exemplos apresentaram capacidade de absorver CO<sub>2</sub>, sendo que os valores obtidos para a porcentagem em massa de CO<sub>2</sub> absorvida pelas misturas ternárias, nesta situação, são similares ao do método da diferença de massa.

## 5 EXEMPLO 2. Estudo da resistência mecânica dos materiais

A resistência mecânica dos materiais absorventes preparados foi obtida e comparada com o do Ca(OH)<sub>2</sub> puro, cujo valor deste é de 46N. Verificou-se que algumas misturas ternárias apresentaram maiores valores de resistência mecânica que Ca(OH)<sub>2</sub> puro, como pode ser observado através da figura 5.

10 O uso de Mg(OH)<sub>2</sub> e Al(OH)<sub>3</sub> como agente aglomerante aumentou a resistência mecânica das misturas ternárias e binárias em relação ao Ca(OH)<sub>2</sub> puro. Isto é importante, pois possibilita que o material permaneça estruturado após os ciclos absorção e dessorção de CO<sub>2</sub>.

## EXEMPLO 3. Difratogramas dos materiais

15 As amostras, em forma de esferas, contendo as misturas ternárias (Al2, Fe2 e Mg2) foram analisadas separadamente, antes do tratamento térmico e apresentaram os difratogramas mostrados nas figuras 6, 7 e 8. A identificação da fase cristalina foi obtida por comparação dos difratogramas de raios X das amostras analisadas com o banco de dados PDF2 do ICC – International  
20 Center for Diffraction Data/JCPDS-Joint Committee on Powder Diffraction Standards.

Nos difratogramas, após tratamento térmico (Figuras 9, 10 e 11), para as esferas Al2, Fe2 e Mg2, respectivamente, observou-se uma mistura de Ca(OH)<sub>2</sub> e CaCO<sub>3</sub>, nas fases portlandita, forma cristalina do hidróxido de cálcio  
25 e calcita.

Para garantir a decomposição do CaCO<sub>3</sub> presente foi feita uma calcinação a temperatura de 1000°C, durante uma hora. Durante esse processo ocorreu também a decomposição do hidróxido de cálcio.

A diminuição das porcentagens de CaCO<sub>3</sub> e Ca(OH)<sub>2</sub>, foi verificada pelo  
30 difração de raios X em comparação com as mesmas amostras antes do

tratamento térmico (Figuras 6 a 8) e após o tratamento térmico (Figuras 9 a 11).

Ademais, verificou-se a formação dos óxidos de cálcio em todas as amostras e uma mistura de óxidos entre óxido de cálcio e os agentes aglomerantes ( $\text{Al}_2\text{O}_3$  e  $\text{MgO}$ ).

5

## REIVINDICAÇÕES

1. Material sólido para absorção de dióxido de carbono, caracterizado por compreender agentes absorventes e estes serem um ou mais óxidos de metais alcalinos terrosos, um ou mais hidróxidos de metais alcalinos ou óxidos de metais de transição, preferencialmente o hidróxido de cálcio e, agentes aglomerantes e estes serem, preferencialmente, hidróxido de magnésio, hidróxido de alumínio e óxido de ferro (III), associados ao bicarbonato de sódio, como agente gerador de poros.

2. Material sólido para absorção de dióxido de carbono, de acordo com a reivindicação 1, caracterizado pelas concentrações (p/p) dos reagentes sólidos compreenderem:  $\text{Ca}(\text{OH})_2$  (80%, 90%),  $\text{Mg}(\text{OH})_2$  (5%, 10%, 15% e 20%),  $\text{Al}(\text{OH})_3$  (5%, 10%, 15% e 20%) e  $\text{NaHCO}_3$  (5%, 10%, 15% e 20%).

3. Processo para preparação de material sólido para absorção de dióxido de carbono, caracterizado por compreender as seguintes etapas:

- a) Mistura dos componentes sólidos: agentes absorventes, agentes aglomerantes, e agente gerador de poros, em água suficiente para aglomerar os componentes;
- b) Homogeneização da mistura e repouso, por um período entre 2 a 20 horas;
- c) Aquecimento ou não da mistura a uma temperatura até 60°C, por um período de 1 hora;
- d) Resfriamento; e,
- e) Novo aquecimento da mistura a uma temperatura de até 1000°C, por 1 hora, em ausência de ar ou oxigênio.

4. Processo para preparação de material sólido para absorção de dióxido de carbono, de acordo com a etapa "a" da reivindicação 3, caracterizado pelos agentes absorventes compreenderem um ou mais óxidos de metais alcalinos terrosos, um ou mais hidróxidos de metais alcalinos ou

óxidos de metais de transição, preferencialmente o hidróxido de cálcio, nas concentrações 80% e 90%p/p.

5. **Processo para preparação de material sólido para absorção de dióxido de carbono, de acordo com a etapa “a” da reivindicação 3, caracterizado pelos agentes aglomerante compreenderem, preferencialmente, hidróxido de magnésio, hidróxido de alumínio e óxido de ferro (III), nas concentrações 5%, 10% e 15%p/p.**

6. **Processo para preparação de material sólido para absorção de dióxido de carbono, de acordo com a etapa “a” da reivindicação 3, caracterizado pelo agente gerador de poros ser bicarbonato de sódio, nas concentrações 5%, 10% e 15%p/p.**

7. **Processo para a preparação de material sólido para absorção de dióxido de carbono, de acordo com a etapa “e” da reivindicação 3, caracterizado pelo aquecimento da mistura ocorrer na presença de argônio, nitrogênio ou na ausência de fluxo de ar.**

8. **Processo para preparação de material sólido para absorção de dióxido de carbono, de acordo com a reivindicação 3, caracterizado pelo material poder ser moldado em formatos específicos na etapa posterior à homogeneização e pelotizado por granulometrias variadas.**

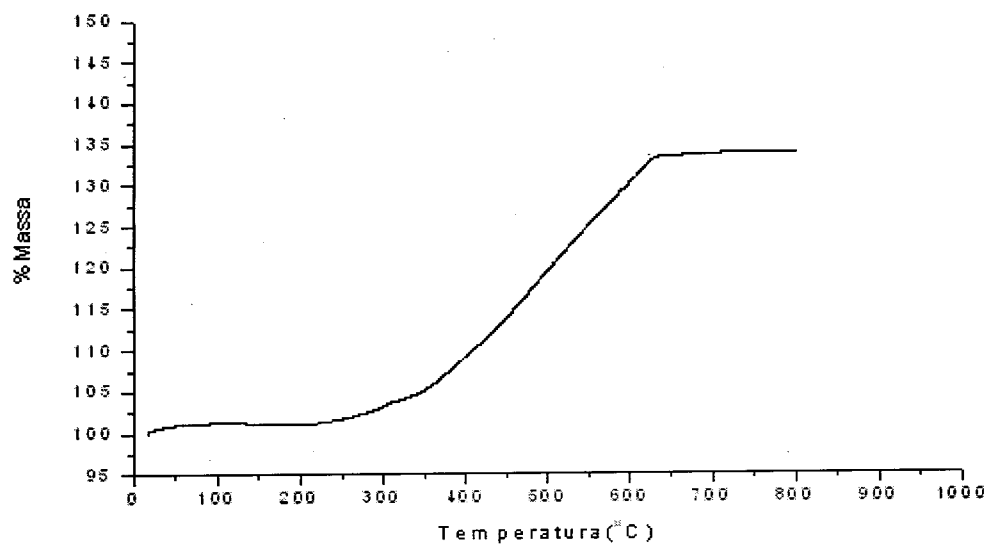
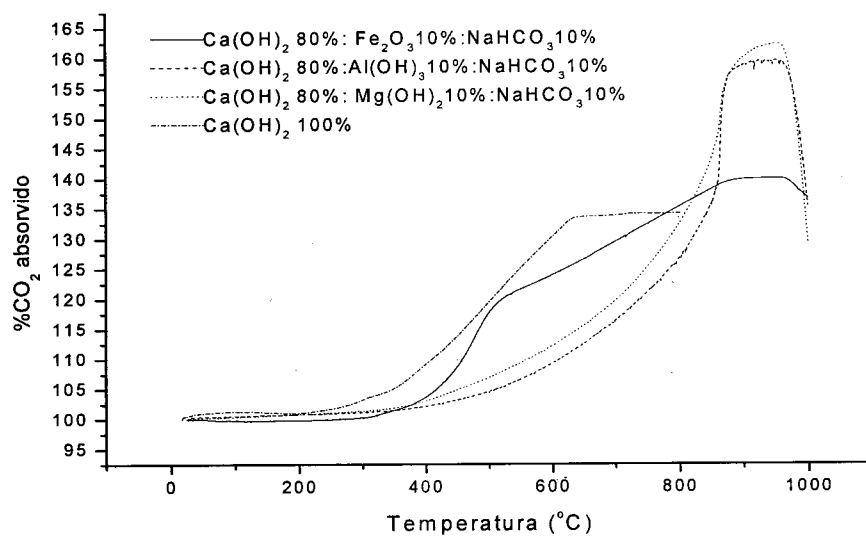
20 9. **Processo para absorção de CO<sub>2</sub>, caracterizado por compreender as seguintes etapas:**

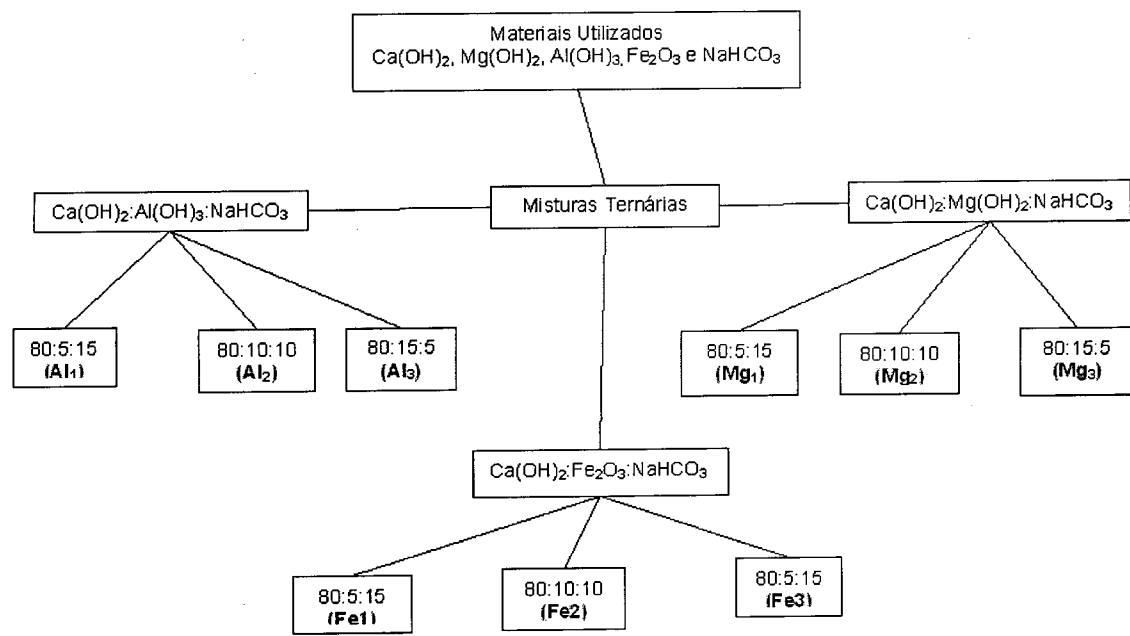
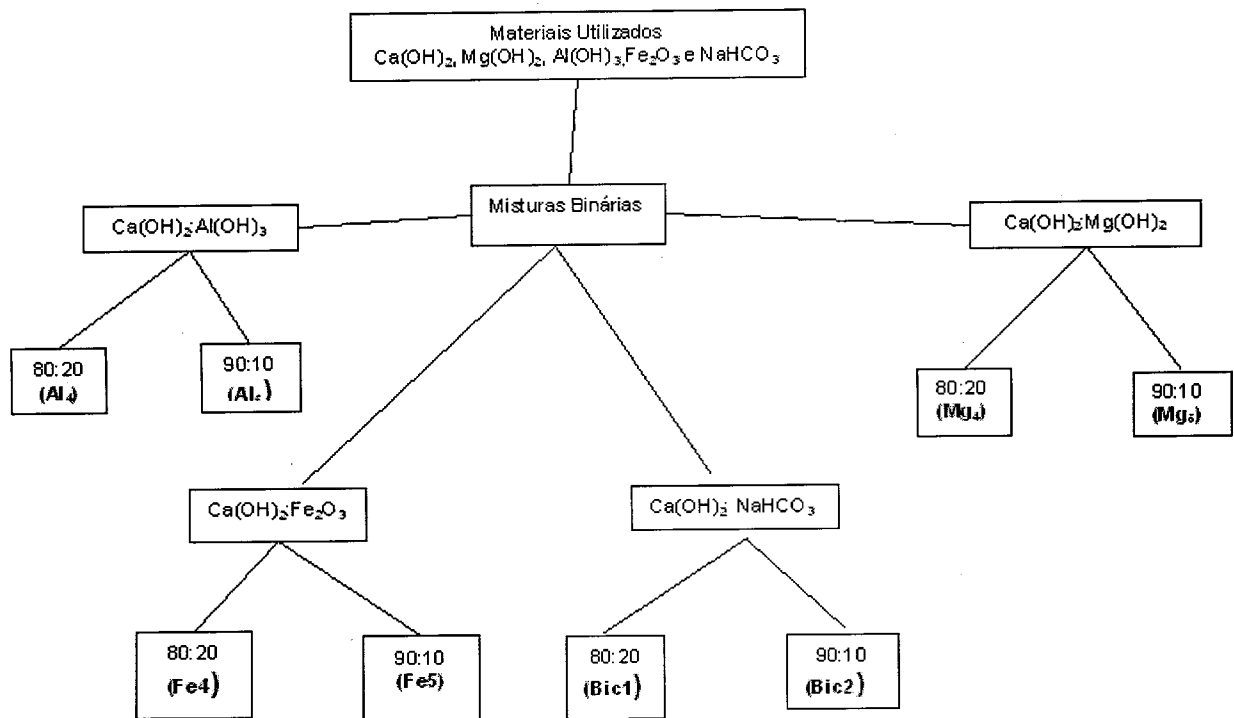
- a) Preparação do material absorvente, conforme definido nas reivindicações 1 a 7;
- b) Exposição do material absorvente ao fluxo do CO<sub>2</sub>;
- c) Decomposição térmica dos carbonatos formados para regeneração do CO<sub>2</sub>; e,
- d) Condução do CO<sub>2</sub> liberado aos sistemas de processamento de interesse industrial.

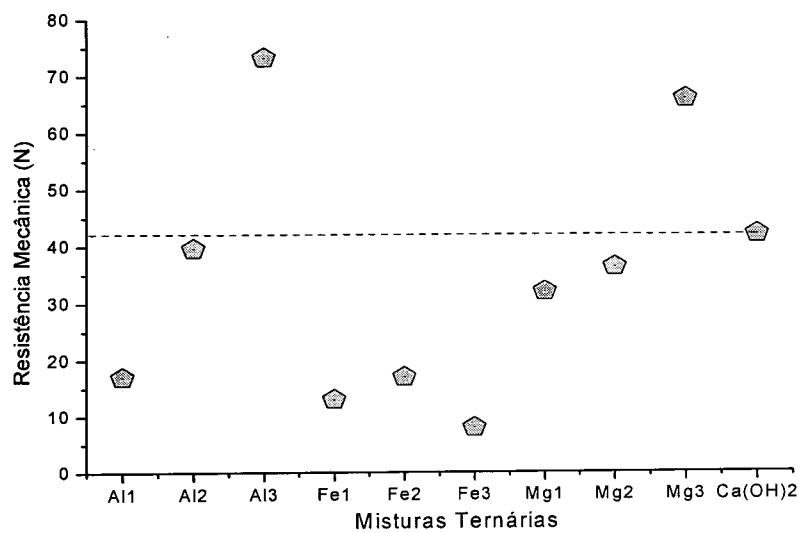
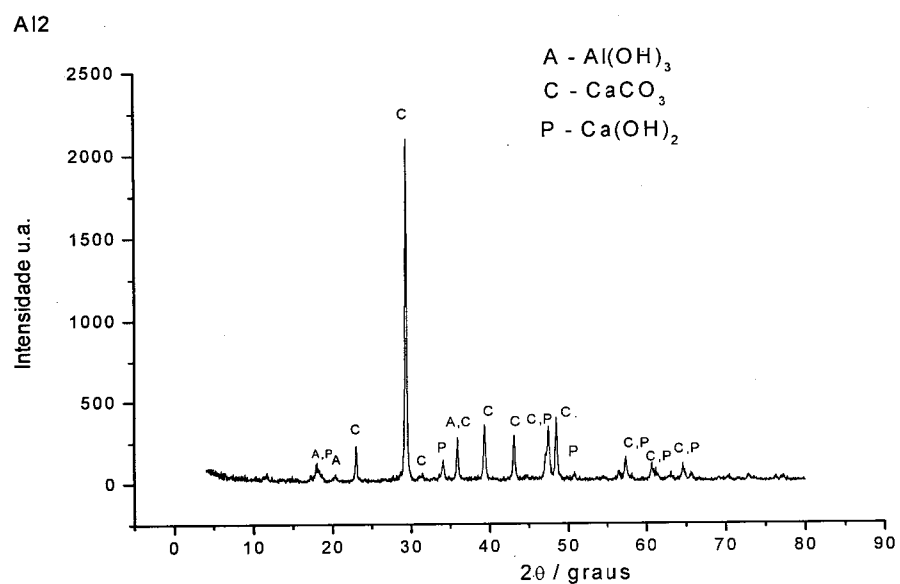
**10. Processo para absorção de CO<sub>2</sub>, de acordo com a etapa “b” da reivindicação 9, caracterizado pelo fluxo do gás CO<sub>2</sub> apresentar uma temperatura entre 50°C e 1000°C.**

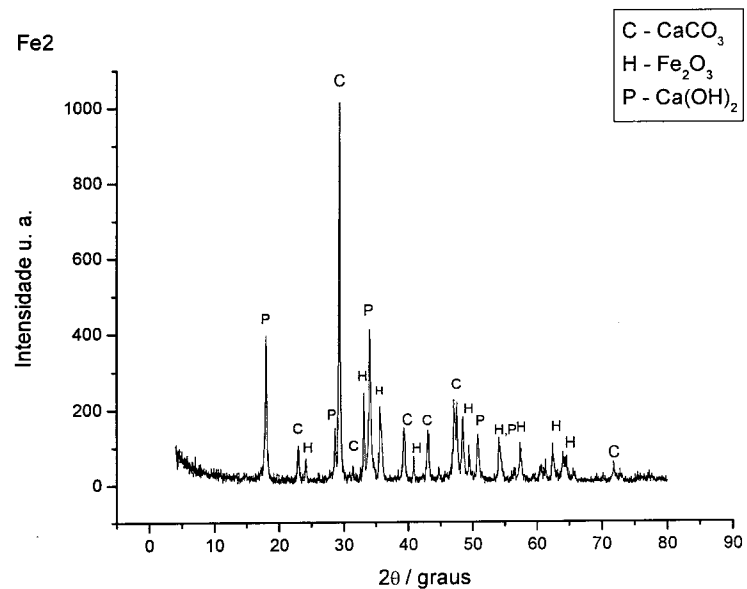
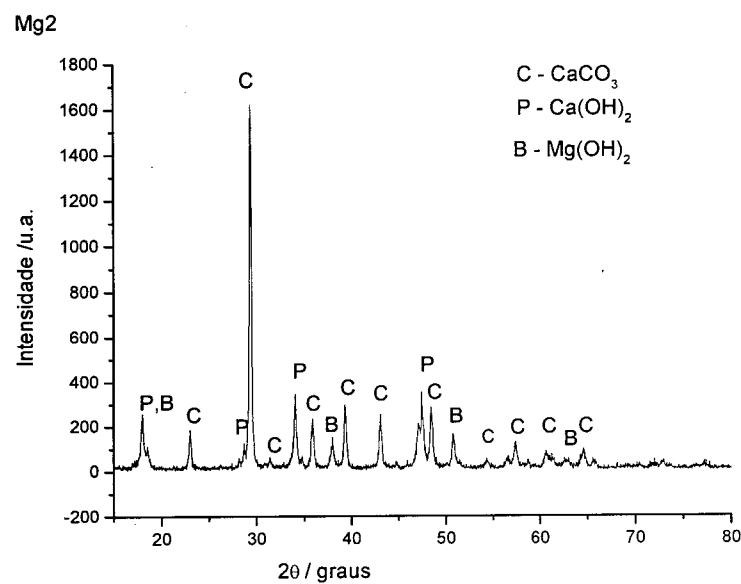
**11. Processo para absorção de CO<sub>2</sub>, de acordo com a etapa “c” da 5 reivindicação 9, caracterizado pela decomposição térmica dos carbonatos formados ocorrer em uma temperatura entre 900 e 1000°C.**

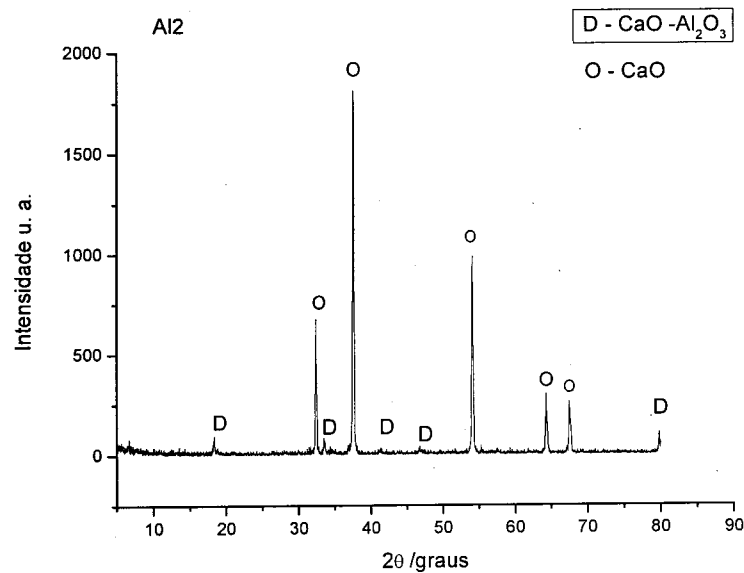
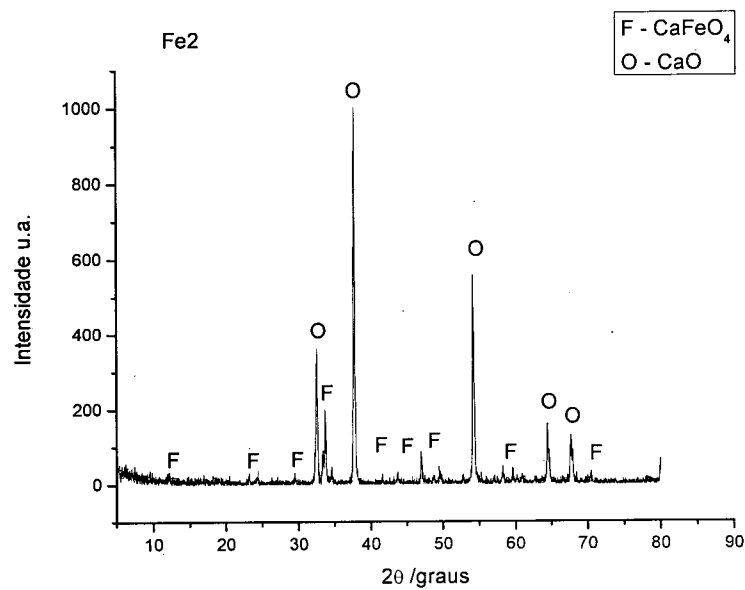
**12. Uso do material sólido, caracterizado por ser na absorção de dióxido de carbono em sistemas de exaustão com temperatura do fluido entre 50 e 1000°C.**

**FIGURAS****Figura 1****Figura 2**

**Figura 3****Figura 4**

**Figura 5****Figura 6**

**Figura 7****Figura 8**

**Figura 9****Figura 10**

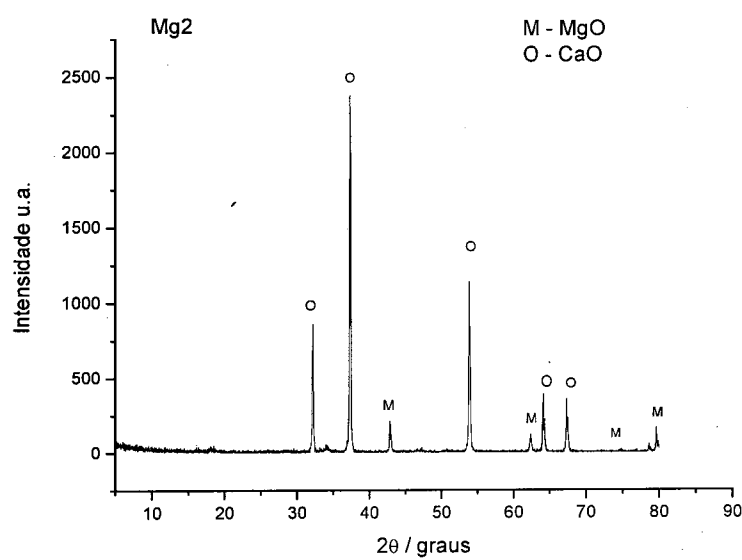


**Figura 11**

**RESUMO****“MATERIAIS SÓLIDOS ABSORVEDORES DE DIÓXIDO DE CARBONO E SUAS PREPARAÇÕES”**

A presente invenção descreve o processo de preparação de materiais sólidos para absorção de dióxido de carbono, bem como os produtos obtidos. O processo utiliza-se de misturas ternárias, três compostos sólidos, e misturas binárias, dois compostos sólidos, de óxidos metálicos, hidróxidos e sais, preferencialmente dos hidróxidos de cálcio, de magnésio e de alumínio, óxido de ferro (III) e bicarbonato de sódio, com a finalidade de aumentar a eficiência da captura de dióxido de carbono.

**Espacenet****Bibliographic data: KR20110047302 (A) — 2011-05-09****CO<sub>2</sub> SORBENT AND MANUFACTURING METHOD THEREOF****Inventor(s):****Applicant(s):**

**Classification:** - **international:** *B01D53/14; B01J20/04; B01J20/08; C01B32/50*  
- **cooperative:** *B01D53/02 (KR); B01J20/043 (KR); B01J20/08 (KR); B01D2257/504 (KR); Y02A50/2342 (EP); Y02C10/06 (EP); Y02P20/152 (EP)*

**Application number:** KR20090103878 20091030      Global Dossier

**Priority number(s):** KR20090103878 20091030

**Also published as:** KR101155303 (B1)

**Abstract of KR20110047302 (A)**

**PURPOSE:** A carbon dioxide absorbent for exhaust gas and a producing method thereof are provided to effectively collect carbon dioxide using an absorption reactor, and to easily recycle the carbon dioxide using a regeneration reactor. **CONSTITUTION:** A carbon dioxide absorbent for exhaust gas contains a solid material formed with 5~70wt% of active component, 5~70wt% of supporter, 5~70wt% of inorganic binder, and 5~60wt% of regenerating agent. The active component is a compound capable of converted into alkali metal, alkaline-earth metal carbonate, bicarbonate, or carbonate. The supporter is alumina. The inorganic binder is a cement material, a clay material, or a ceramic material. The regenerating agent is the titania dioxide, zirconia dioxide, or hydrotalcite.



# Patent Translate

Powered by EPO and Google

## Notice

This translation is machine-generated. It cannot be guaranteed that it is intelligible, accurate, complete, reliable or fit for specific purposes. Critical decisions, such as commercially relevant or financial decisions, should not be based on machine-translation output.

## DESCRIPTION KR20110047302

Carbon dioxide absorber for flue gas and its manufacturing method {CO<sub>2</sub> SORBENT AND MANUFACTURING METHOD THEREOF}

The present invention relates to a carbon dioxide absorbent for flue gas and a method for manufacturing the same, and more particularly, to a carbon dioxide absorbent for flue gas and a method of manufacturing the same that can be repeatedly used in the capture and regeneration of carbon dioxide.

Carbon dioxide is one of the major substances that cause the greenhouse effect, which is known to have the greatest impact on global warming due to the increase in atmospheric emissions due to the continuous increase in fossil fuels. Therefore, the problem of global warming cannot be overcome without controlling the emission of carbon dioxide. There are various methods for removing carbon dioxide from flue gas generated by the combustion of fossil fuels, such as wet chemical absorption, absorption, membrane separation, and low temperature cooling separation. However, these methods have a high recovery cost or are difficult to apply to power plants or large industries. Dry CO<sub>2</sub> capture technology is an efficient way to remove carbon dioxide from flue gas. This method uses a solid as an absorbent instead of the liquid solvent used in wet chemical cleaning. That is, the active ingredient and carbon dioxide in the solid absorbent form carbonate or bicarbonate by the chemical reaction in the absorption reactor to capture the carbon dioxide contained in the exhaust gas, and the absorbent absorbed carbon dioxide is regenerated by additional heat in the regeneration reactor and is repeated again. It can be used as a technology. Dry regeneration absorption technology is a low cost material, can be recycled and used repeatedly. In addition, it is a field capable of sustained growth compared to other technologies in many aspects such as design flexibility, eco-friendliness, low energy regeneration, and high efficiency carbon dioxide absorption (absorption and reactivity). Conventional patents related to the dry regeneration absorption technology include US Patent US7314847B1, US Patent US6908497B1, Japanese Patent Application Publication JP2007-090208A, US Patent Publication US20070072769A1, and the like. The above patents mainly relate to absorbents having the active ingredient in the support or to the active ingredient itself, and are not suitable for application to the process of collecting and separating carbon dioxide while the solid absorbent particles move continuously between the two reactors for absorption and regeneration. Therefore, it is inefficient in collecting and separating carbon dioxide.

The object of the present invention is to solve the above-mentioned problems, and to effectively collect in the flue gas temperature range before discharging carbon dioxide into the atmosphere, and to be easily regenerated by an additional heat source, continuous absorption and regeneration between the two reactors. The present invention provides a carbon dioxide absorbent for flue gas and a method for manufacturing the same, which can be repeatedly used while moving to reduce the CO<sub>2</sub> capture cost. In order to achieve the above object, the exhaust gas carbon dioxide absorbent according to the present invention, in the carbon dioxide absorbent for exhaust gas to collect the carbon dioxide contained in the exhaust gas, the solid raw material constituting the absorbent is 5 to 70% by weight of the active ingredient, 5 ~ 70% by weight of the support, 5-70% by weight of the inorganic binder and 5-70% by weight of the regeneration enhancer. In addition, the method for producing a carbon dioxide absorbent for flue gas according to the present invention comprises the steps of preparing a slurry using the solid raw material, drying the prepared slurry in a spray dryer to prepare a first absorbent, and dry firing the first manufactured absorbent Preparing a final absorbent. According to the carbon dioxide absorbent for flue gas according to the present invention and a method for manufacturing the same, physical properties such as spherical shape, average particle size and size distribution, filling density, and wear resistance are satisfied as conditions of the absorbent required in the process, and CO<sub>2</sub> Excellent absorption and regeneration performance. In addition, since mass production is easy and low cost is generated, there is an advantage in that CO<sub>2</sub> of large-scale emission sources such as power plants, steelmaking, and refinery industries can be collected at low cost. In addition, the absorption reaction (50 ~ 110 °C) and regeneration (100 ~ 200 °C) in the exhaust gas temperature range does not require an additional heat source can be solved both problems of cost reduction and efficient use of energy at the same time have.

Hereinafter, preferred embodiments of the present invention will be described in detail with reference to the accompanying drawings. The solid raw material constituting the carbon dioxide absorbent for flue gas according to the present invention comprises an active ingredient, a support, an inorganic binder, and a regeneration enhancer. The active ingredient is a substance that selectively reacts with carbon dioxide to efficiently collect and separate carbon dioxide from a gas stream. Such materials include alkali metals, alkaline earth metal carbonates, bicarbonates or components which can be converted to such carbonates, belonging to groups 1 and 2 of the periodic table. The active ingredient comprises 5 to 70% by weight of the total solid raw material, preferably 10 to 50% by weight. The purity of the active ingredient is preferably at least 98%. The support is a material having a large specific surface area so that the active ingredient is well distributed in the absorbent particles, thereby increasing the utility of the active ingredient and adsorbing or absorbing carbon dioxide or water required for the reaction. As such a material, alumina having a large specific surface area is used, which accounts for 5 to 70% by weight of the total solid raw material, and preferably 5 to 50% by weight. The alumina used at this time has an Al<sub>2</sub>O<sub>3</sub> content of 99.8% and a specific surface area of 150 m<sup>2</sup> / g or 250 m<sup>2</sup> / g. The inorganic binder is a substance that gives strength to the absorbent by binding the active ingredient and the support. Inorganic binders include cements such as calcium silicate and calcium aluminate, clays such as bentonite and kaolin, ceramics such as alumina sol, silica sol, and boehmite. These inorganic binders comprise 5 to 70% by weight of the total solid raw material, preferably 10 to 50% by weight. The regeneration enhancer is a material that facilitates regeneration so that the absorption and regeneration reactions can be repeatedly performed without a decrease in reactivity due to repeated use of the absorbent. Regeneration enhancers include titania (TiO<sub>2</sub>), zirconia dioxide (ZrO<sub>2</sub>), and hydrotalcite consisting of magnesium and alumina. Such regeneration accelerators comprise 5 to 70% by weight of the total solid material, preferably 5 to 50% by weight.

In the process of preparing the carbon dioxide absorbent for flue gas according to the present invention, an additive is required to impart plasticity and dispersibility in the process of mixing a solid raw material with water as a solvent. That is, in the process of preparing the slurry, the solid raw material is well dispersed to produce a stable and flowable slurry, and an additive is required to maintain the shape of the spray-dried molded particles. Organic additives added for this purpose include dispersants, antifoaming agents and organic binders. In addition, a pH adjuster for adjusting the pH concentration of the slurry is added. The dispersant is used to prevent the particles from agglomerating during the grinding process. That is, when the raw material particles are pulverized and become fine powder particles in the process of pulverizing to control the particle size of the solid raw material constituting the absorbent, the particles may be agglomerated with each other. The use of is essential. Dispersants include anionic dispersants, cationic dispersants, amphoteric dispersants, nonionic dispersants, or a combination thereof. Anionic dispersants include polycarboxylic acids, polycarboxylic acid amines, polycarboxylic acid amine salts, polycarboxylic acid soda salts, and the like. Such anionic dispersants account for 0.1 to 10% by weight relative to the total solid raw materials. Nonionic dispersants include fluorine-based surfactants (Fluorsurfactant), accounting for 0.01 ~ 0.3% by weight relative to the total solid raw materials. The antifoaming agent is used to remove bubbles in the slurry to which the dispersing agent and the organic binder are applied, and a metal soap-based and polyester-based nonionic surfactant is used. These defoamers account for 0.01 to 0.2% by weight of the total solid raw materials. The organic binder is added during slurry production to impart plasticity and fluidity of the slurry and ultimately maintain the shape of the spray-dried solid absorbent particles, thereby facilitating handling of the particles before drying and firing. As the organic binder, polyvinyl alcohol-based, polyglycol-based, methyl cellulose or combinations thereof may be used. The organic binder accounts for 0.5 to 5% by weight of the total solid raw materials.

Hereinafter, the manufacturing process of the carbon dioxide absorbent for exhaust gas according to the present invention will be described in detail. 1 is a process chart showing a manufacturing process of the carbon dioxide absorbent for exhaust gas according to the present invention. In order to prepare a carbon dioxide absorbent for exhaust gas according to the present invention, a process of preparing a slurry by mixing a solid raw material in water, pulverizing and dispersing the mixture (S10), the process of primary molding the absorbent by spray drying the prepared slurry (S20), And drying and firing the molded absorbent particles to prepare a final absorbent (S30). The absorbent thus prepared absorbs CO<sub>2</sub> in the flue gas temperature range (50-100 ° C.) through an absorption reactor and is regenerated and reused by an additional heat source at 100-200 ° C. through a regeneration reactor. 2 is a flowchart illustrating a process of preparing a slurry in detail. After precisely weighing each raw material according to its composition, distilled water corresponding to the concentration of the slurry to be prepared (weight ratio of solid raw material to liquid water) is placed in a suitable container (S11). At this time, a dispersing agent and an antifoamer can be added. Subsequently, an active substance such as potassium carbonate is first completely dissolved, and then a support, an inorganic binder, and a regeneration accelerator are added and mixed (S12). In this process, a dispersant or antifoaming agent may be added to impart fluidity of the slurry mixed with the solid raw materials and to facilitate mixing of the raw materials. In addition, the concentration of the slurry can be adjusted with water to prevent the use of excess dispersant, the concentration of the mixed slurry is preferably 20 to 50% by weight. By adding the raw materials or by stirring using a stirrer in a completely added state, the raw materials are evenly mixed (S13). There is no particular limitation on the stirrer, but a mechanical stirrer, a homogenizer, an ultrasonic homogenizer, a high shear blender, a double helix mixer, etc. are mainly used. It can be optionally used depending on the amount of raw material to be added.

To disperse the particles of the solid raw materials included in the mixed slurry to 1 μm or less and to homogeneously disperse the pulverized particles, an additional dispersing agent and an antifoaming agent may be used, and a stable slurry may be prepared using a pH adjuster. have. When the inputted raw materials are mixed as described above, the raw materials are crushed and homogenized using a grinder (S14). At this time, the grinding method is a large grinding effect and wet milling (Wet milling) method is used in order to solve problems such as blowing of particles during dry grinding. The mill used for grinding the solid raw materials includes a roller mill, a ball mill, an attrition mill, a planer mill or a bead mill. When grinding and

homogenizing using a high energy bead mill in the grinder, the filling amount of the bead (Bead) is preferably 60 to 80% based on the volume of the grinding vessel. Beads, which are grinding media, use Yttrium stabilized zirconia beads which are excellent in strength and stability. The size of the ball is preferably in the range of 0.3 to 1.25 mm. In the grinding process, the size of the solid raw material particles included in the slurry is controlled to 1  $\mu\text{m}$  or less and comminution or homogenizing two or more times to prepare a homogeneous slurry. During the grinding process, the flow of the slurry is adjusted by adding a dispersant and an antifoaming agent so that the slurry can be transported through a pump for the next grinding. Meanwhile, the organic binder is added before final grinding so that the slurry is uniformly mixed. The slurry which has been pulverized and homogenized is made of a dispersant, an antifoaming agent, or additional water to adjust the characteristics of the slurry such as concentration and viscosity, followed by a vacuum sieving process. Etc.) are removed (S15). 3 is a process chart showing a process of forming a water absorbent by spray drying the prepared slurry.

After the foreign matter contained in the slurry is removed, it is transferred to a container for spray drying (S21), and then sprayed into the spray dryer through a pump (S22). The viscosity of the slurry transferable to the pump is not limited, but may be sprayed to 300 cP or more. In the spray dryer, the flowable slurry is shaped into spherical solid absorbent particles. Operation conditions of the spray dryer is such that the particle size distribution of the absorbent is 30 ~ 400  $\mu\text{m}$ . Factors affecting the shape, particle size and distribution of the absorbent particles, the structure of the absorbent include the concentration and viscosity of the slurry, the degree of dispersion, the injection pressure and amount of the slurry, the drying capacity and temperature of the spray dryer. These parameters depend on the spray dryer's structure and spray type. The spray dryer is not particularly limited, but may be manufactured to be spray dried in a countercurrent manner using a pressure nozzle. That is, in order to increase the residence time of the particles sprayed in the dryer in order to increase the average particle of the absorbent in the spray dryer to 60 ~ 180  $\mu\text{m}$  counter counter type (Centrifugal Pressure Nozzle) installed in the lower part of the dryer (Counter Current Fountain Configuration Spraying method is available. Preferred spray dryer operating conditions are injection pressure 5 ~ 15kg /  $\text{cm}^2$ , inner diameter of the pressurized nozzle 0.5 ~ 1.2mm, dryer inlet temperature 260 ~ 300 ° C, dryer outlet temperature 110 ~ 130 ° C. 4 is a process chart showing a process of preparing a final absorbent by drying and baking the molded absorbent. Absorbent spherically shaped in the spray dryer is dried for 2 hours or more in a reflux dryer in an air atmosphere of 110 ~ 150 ° C (S31). The dried absorbent is heated in an air atmosphere at a temperature increase rate in the range of 2-5 ° C / min and maintained at the final firing temperature in the range of 350-1000 ° C for at least 2 hours (S32). The final absorbents to meet the requirements of the process, spherical shape, particle size 60 ~ 180  $\mu\text{m}$ , particle distribution 30 ~ 400  $\mu\text{m}$ , packing density 0.6g / cc or more, CO<sub>2</sub> absorption ability 3% by weight or more, regeneration performance 70% or more, wear resistance is 30% or less, and regeneration performance is 70% or more.

Hereinafter, various features according to the present invention will be described in detail by way of examples. Example 1 In this example, 20 to 50% by weight of potassium carbonate (K<sub>2</sub>CO<sub>3</sub>) or potassium bicarbonate (KHCO<sub>3</sub>) as an active ingredient in a total of 8 kg of solid raw materials, and 20 to 50% by weight of gamma alumina ( $\gamma$ -Al<sub>2</sub>O<sub>3</sub>) as a support Calcium silicate, Bentonite, Pseudo-bohemite as inorganic binder, 15 ~ 20 wt%, Titania (TiO<sub>2</sub>), Zirconia dioxide (TiO<sub>2</sub>), Hydrotalcite (Hydrotalcite) 5 to 20% by weight of the absorbent was prepared as a composition ratio. A mixed slurry was prepared by sequentially adding the raw materials to water while stirring so that the concentration of the solid raw material included in the slurry was 25 to 40% by weight. At this time, the dispersant was added before the raw material for easy mixing and dispersion of the raw material, or in a small amount depending on the viscosity of the mixed slurry, the degree of stirring in the sequential loading of the raw material. The antifoaming agent was added in small amounts depending on the degree of bubbles generated after dispersing agent or stirring the slurry. The mixed slurry was sufficiently stirred for 10 minutes or more at a speed of 10,000-25,000 rpm using a double spiral stirrer to prevent sedimentation of particles having a relatively large specific gravity or large sizes among solid raw materials. The mixed slurry was prepared by pulverizing and homogenizing the solid raw material particles using a high energy bead mill two or more times. At this time, an additional water, a dispersant, an antifoaming agent, and an organic amine for pH adjustment were added to control the properties of the slurry, such as the viscosity of the slurry, the concentration of the solid raw material, and the pH. Polyethylglycol (PEG) was added as an organic binder in an amount of 1 to 3% by weight based on the total solids, and was added before final grinding to disperse homogeneously in the slurry. The final slurry obtained through the characteristics control of the slurry as described above was vacuum sieved to remove foreign substances that may be introduced during the manufacturing process. The slurry from which foreign substances were removed was spray dried by adjusting the concentration to 27 to 38 wt%.

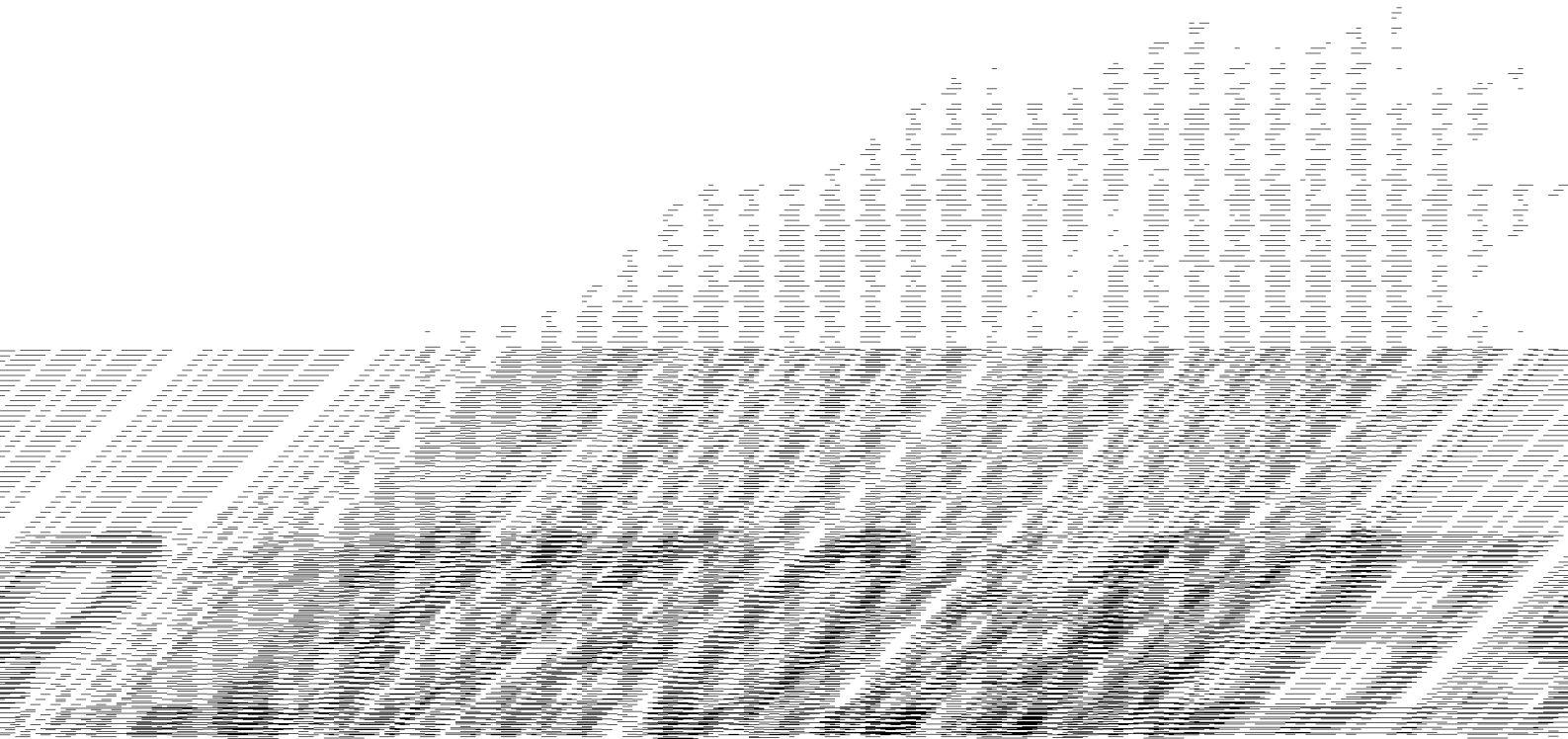
The molded absorbent particles are dried at 120 ° C for at least 2 hours in an air atmosphere dryer, and then heated at a heating rate of 2-5 ° C / min to a final firing temperature of 500 to 650 ° C in a furnace. The final absorbent was prepared by maintaining at least 2 hours at temperature. In order to effectively remove the organic additives and the organic binder added during the slurry manufacturing process, each one hour was maintained at 200 ° C, 400 ° C and 500 ° C before reaching the final firing temperature. Thus prepared absorbents are designated as A, B, C, D, E, F, G, H according to the composition of the active ingredient, support, binder and regeneration enhancer. Table-1 below shows the composition and manufacturing characteristics of the absorbent including the regeneration enhancer. <Table 1> Solid Absorbent Manufacturing Characteristics Solid Absorbent Absorbent A Absorbent B Absorbent C Absorbent D Absorbent E Absorbent F Absorbent G Absorbent H Active ingredient (K<sub>2</sub>CO<sub>3</sub>), Weight% 353535354040-Absorbent (KHCO<sub>3</sub>), Weight% ---- -3535 support ( $\gamma$ -Alumina, VGL-15), weight% 4333434333-4343 support ( $\gamma$ -Alumina, VGL-25), weight% ----- 23-Inorganic binder (Calcium silicate), weight% 77577777 Inorganic Binder (Bentonite), Weight% 55555555 Inorganic Binder (Similar Boehmite), Weight% 55555555 Regeneration Enhancer (TiO<sub>2</sub>), Weight% 5107-10205-Regeneration Enhancer (ZrO<sub>2</sub>), Weight% --- 5-5 Regeneration Enhancer (hydrotalcite), Weight% -5 ----- Total solid raw material, Weight% 100 100 100 100 100 100 100 Nonionic dispersant, Weight% 0.01 to 0.1 Anionic dispersant, Weight% 0.1 to 3 Antifoaming agent, Weight% 0.01 to 0.1 Organic binder, weight% 1.0

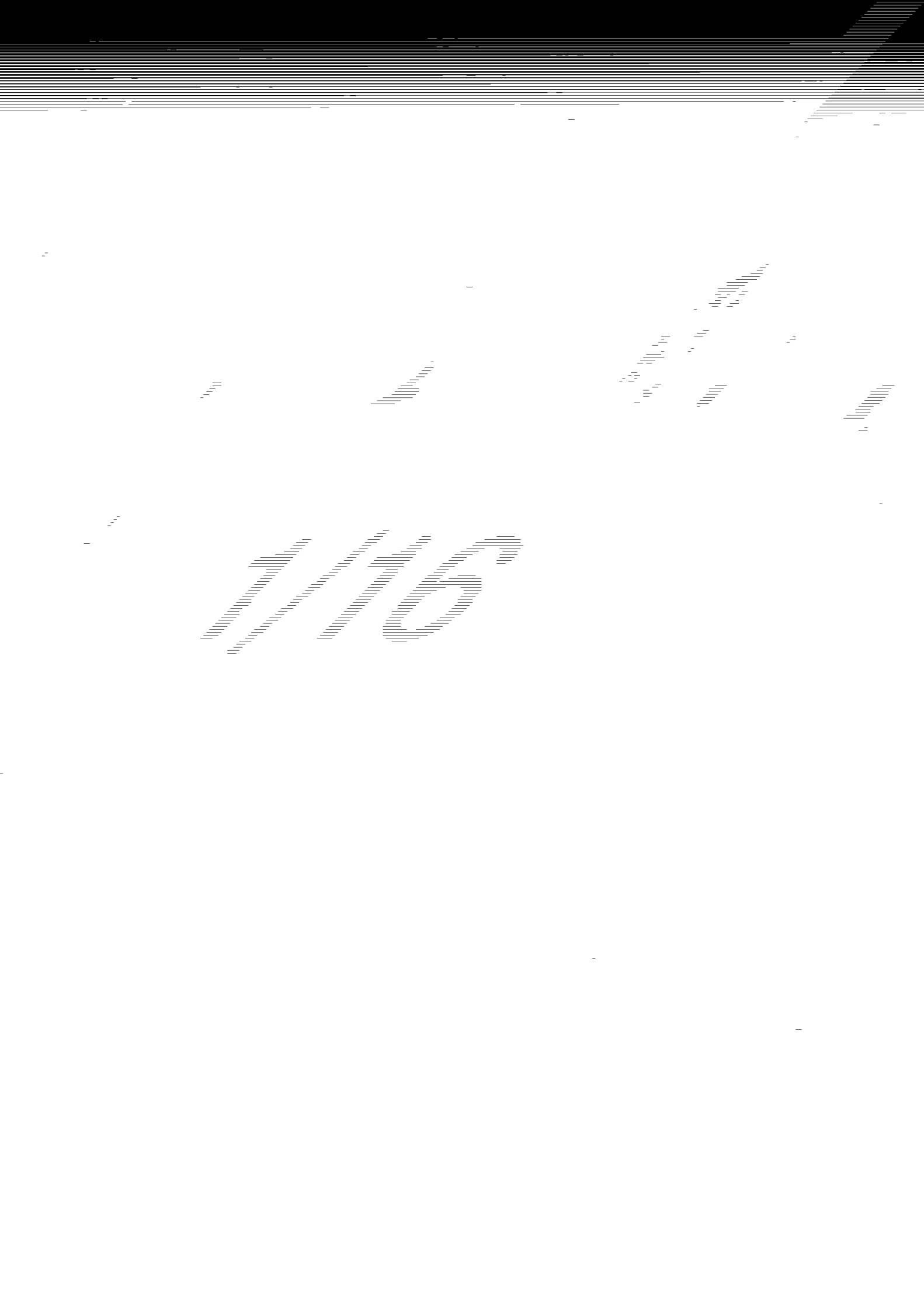
to 5.0 slurry concentration, weight% 32.530.137.4933.9731.8230.727.4930.92 slurry pH11.911.411.0910.7810.9810.868.838.75pH regulator (organic amine), weight%-0.130.13--0.130. 13 viscosity, cP650036,5001,8531,7102,8001,1801,4301,790 Shows a summary of the physical properties and response characteristics of the absorber A ~ H prepared as described above.

The shape of the particles was determined using the naked eye, an industrial microscope or an electron scanning microscope (SEM), and the average particle and particle size distribution of the absorbent were measured according to the standard method ASTM E-11. At this time, 10g of the absorbent sample was sieved for 30 minutes in a sieve shaker (Seive shaker) and the average particle size and size distribution was calculated according to the calculation method presented. Tadensity of the absorbent was measured according to the apparatus and method presented in the standard ASTM D 4164-88. Specific surface area and pore volume of the absorbent were used by Quantachrome Multi BET surface area meter and Hg porosity meter, respectively. Attrition resistance of the absorbent molded by the spray drying method was measured in accordance with the test method and the procedure presented in the specification using a 3-hole attrition tester manufactured in accordance with ASTM D5757-95. The Attrition Index (AI), calculated according to the method proposed by STM, is a fraction of the initial sample volume (50 g), which is collected by the wear from the wear tube for 5 hours at a flow rate of 10 liters per minute (10 liters per minute). It is shown. One of the important indicators of the (fluidized bed or high velocity fluidized bed) process is that less than 30% is preferred for the (fluidized bed) process. The absorption and regeneration reactions, which are the reaction characteristics of the absorbents A to H prepared in this example, were measured by thermogravimetric analysis. The weight and total flow rate of the sample used were 10 mg and 60 ml / min, respectively. CO<sub>2</sub> absorption reaction was measured at 70 ° C, regeneration reaction was carried out at 140 ° C. The reaction gas was a replica of the flue gas of a coal-fired power plant. The composition of the gas consisted of 14.4% of carbon dioxide, 5.4% of oxygen, 10% of water as steam, and 70.2% of nitrogen. Nitrogen was used as the regeneration gas. Absorption and regeneration of absorbents were carried out at least 1.5 cycles (absorption-regeneration-absorption) to evaluate the first and second CO<sub>2</sub> absorption capacity of the absorbent and the ratio of the second absorption capacity to the first absorption capacity. Is expressed as a percentage.

The wear index (AI) expressed in wear resistance indicates that the smaller the value, the higher the wear strength. Here, the utilization rate is a percentage of the CO<sub>2</sub> absorption capacity measured relative to the theoretical CO<sub>2</sub> absorption capacity of each absorbent is an indicator of the utilization of the active ingredient contained in each absorbent. A photograph showing that the shape of the solid absorbent presented in this example is spherical is shown in FIG. 5. <Table 2> Physical and CO<sub>2</sub> Reaction Properties of Each Sorbentsorbents ABCDEFGH Shapessssssssss BETd, m<sup>2</sup> / g394444731-6432Hg porosity,% 6345665354-7465Ale,% 0.50.20.10.40.40.04128.94 TGA CO<sub>2</sub> absorption capacity, weight% 1st6.145.666.958.936.748.045.843.972st4.614.955.897.045.435.604.093.98 Regeneration,% 75888579817070 Final firing temperature, ° C 550 500 500 500 500 550 550 In order to evaluate CO<sub>2</sub> absorption and regeneration after firing at 550 ° C for solid absorbents A and F molded by the spray drying method in the above example, A absorbent was subjected to a 2-cycle (absorption-regeneration repeated) test. F absorbents were subjected to a 6 cycle (absorption-regeneration repeated) test. The absorption and regeneration results of the A and F absorbers are shown in FIGS. 6 and 7. As shown in the figure, it can be seen that A and F absorbers do not significantly change the weight increase due to the CO<sub>2</sub> absorption capacity and the weight loss due to the regeneration reaction even after repeated absorption and regeneration reactions. As shown in the above examples, the present invention has shown that it is possible to directly use a solid absorbent including a regeneration enhancer in a dry CO<sub>2</sub> capture process using a spray drying technique. In particular, the solid absorbent according to the embodiment of the present invention, spherical shape, particle size 60 ~ 180μm, particle distribution 30 ~ 400μm, packing density 0.6g / cc or more, CO<sub>2</sub> absorption ability 3% by weight or more, regeneration performance 70 It can be seen that not only satisfies all the physical properties required in the process with more than%, less than 30% of abrasion resistance, and more than 70% of regeneration performance, as well as excellent CO<sub>2</sub> absorption ability and regeneration.

Such a solid absorbent according to an embodiment of the present invention has the advantage that it is possible to collect CO<sub>2</sub> of large-scale emission sources such as power plants, steelmaking, oil refining industry at low cost because it is easy to mass production and low cost. In addition, since it can be operated in the exhaust gas temperature range of 200 ° C or less, a separate heat source supply is not required, thereby solving both problems of cost reduction and efficient energy use. As described above, the present invention has been described based on the preferred embodiments, but the present invention is not limited to the specific embodiments, and can be changed within the scope described in the claims by those skilled in the art. have.





2025

2007





A decorative horizontal border consisting of a series of parallel diagonal lines forming a zigzag pattern.

42/65

1

2

3

4

5

6

7





2020

1

2

3

4

5

2020

6



—  
—  
—  
—

—  
—  
—  
—

—  
—  
—  
—

—  
—  
—  
—

2266

—

—

— —

— — — — —

1

2

3

4

2020

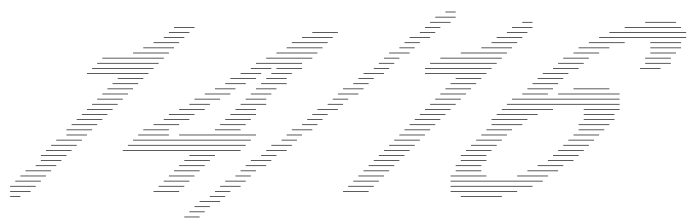
5

100

100

100

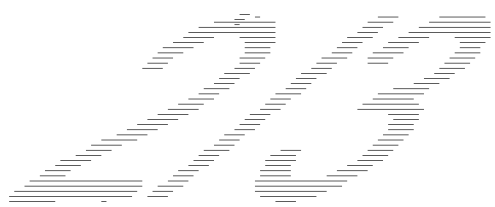
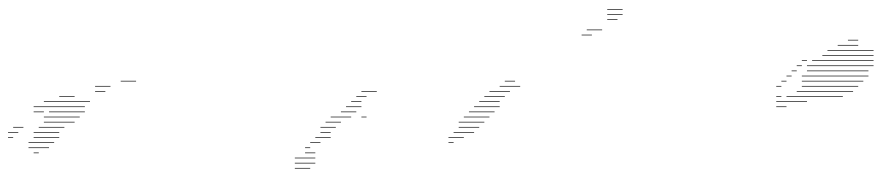
100

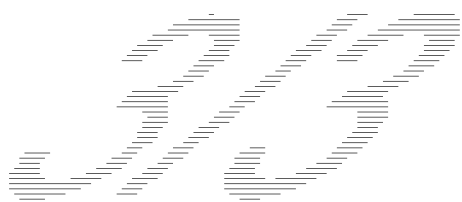
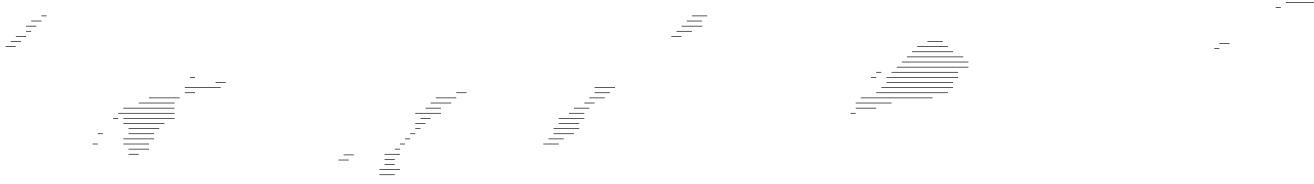


2000

2020







—

—

—

—

—

1

2

3

4

5

6

7

8

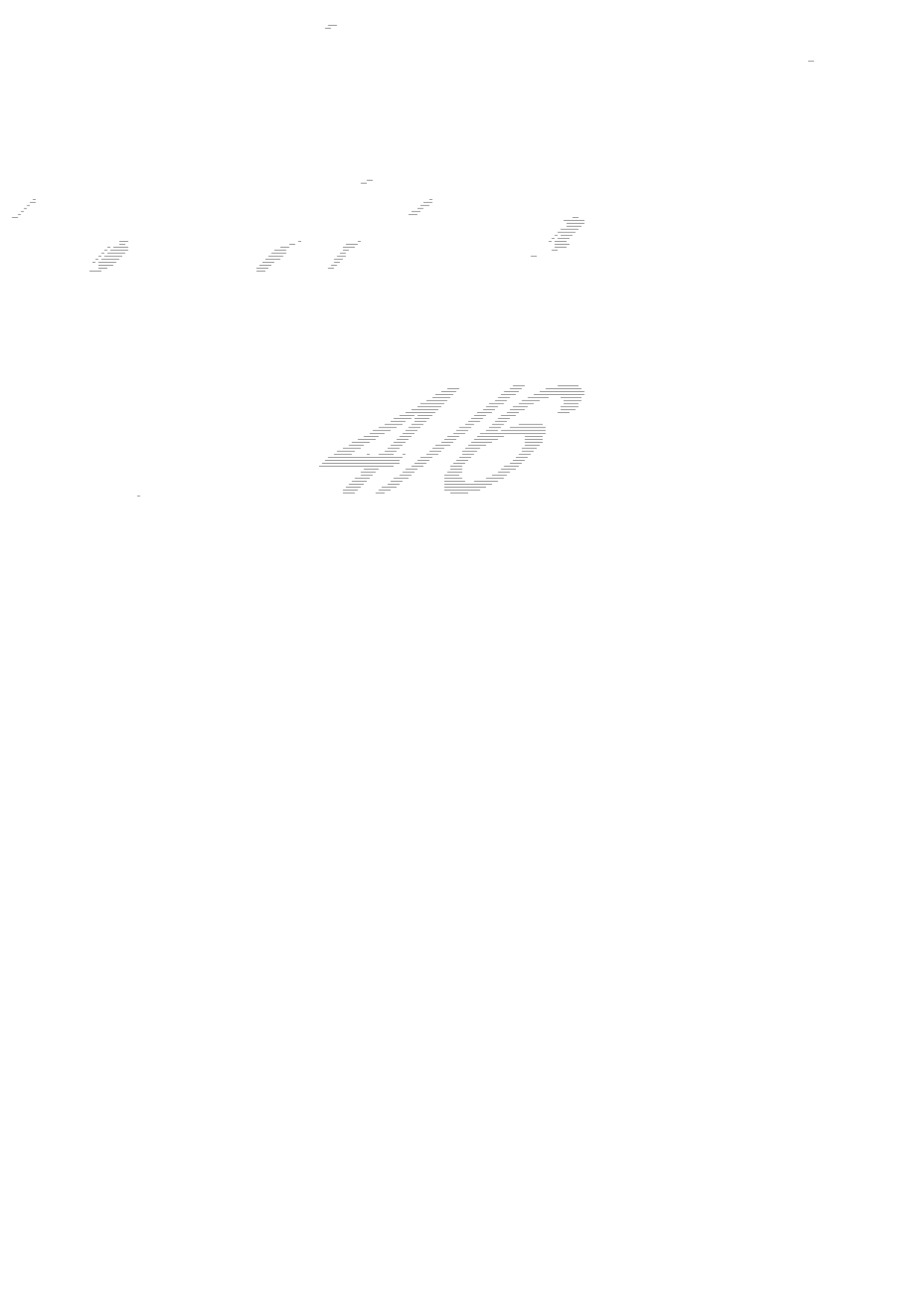
9

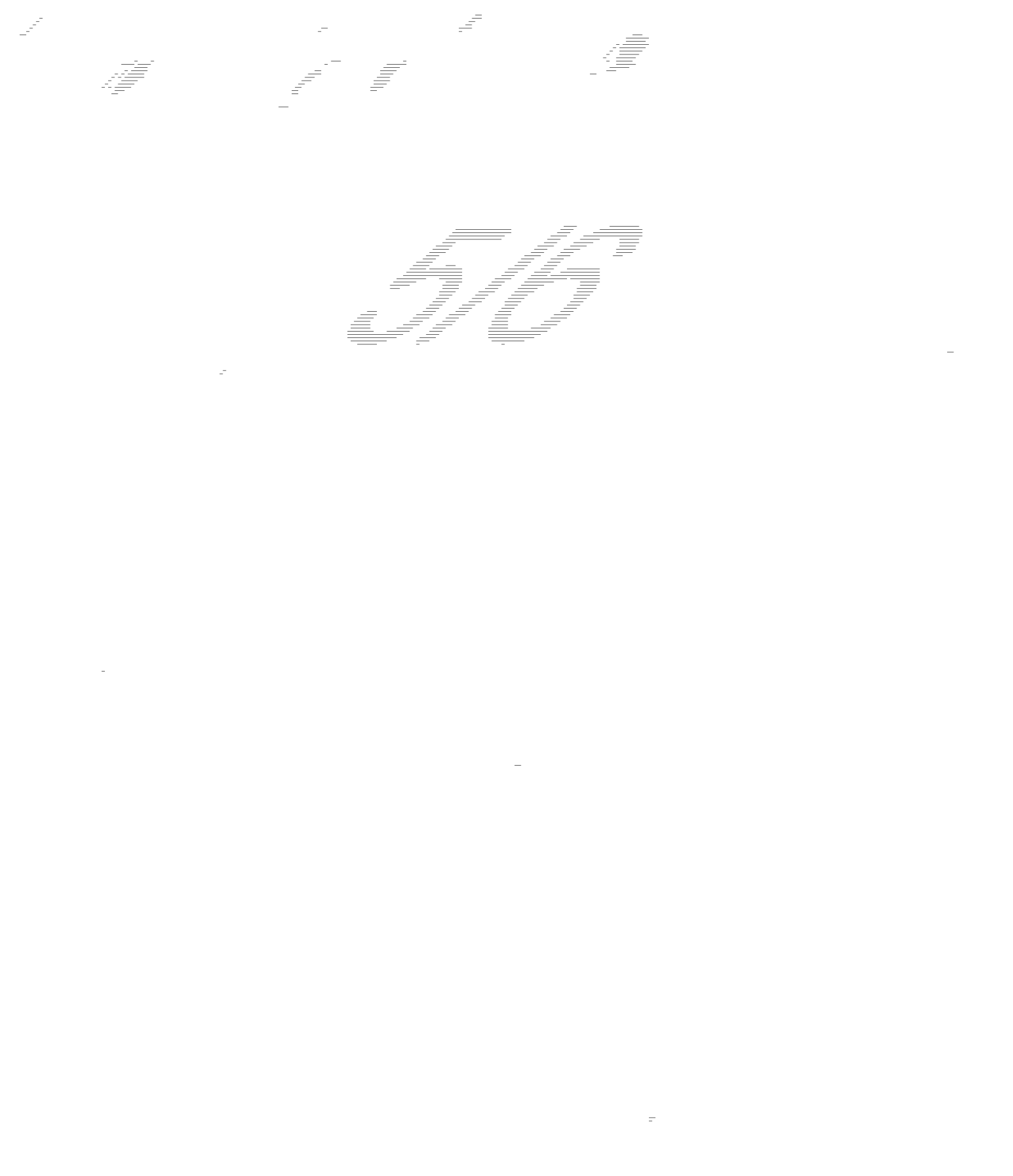
26

26

26

26





1



2



1



